UNIVERSITY OF CALIFORNIA SAN DIEGO

Development of the painted white urchin, *Lytechinus pictus*, as a genetically enabled model to address impacts of chemical exposure on the larval immune response

A dissertation submitted in partial satisfaction of the requirements for
the degree Doctor of Philosophy

in

Marine Biology

by

Katherine T. Nesbit

Committee in charge:

Amro Hamdoun, Chair
Lena Gerwick
Deirdre Lyons
Bradley Moore
Victor Nizet

2022

The dissertation of Katherine T. Nesbit is approved, and it is acceptable in quality and form for publication on microfilm and electronically.

University of California San Diego

2022

DEDICATION

To my family for their unwavering support. Especially my parents, Dorothy and Phillip, for always believing in me and teaching me the strength and tenacity required to accomplish my goals. Also, to my siblings: my brother Mark, for setting an example of navigating science that made research seem less intimidating; and to my twin sister, Veronica, for uplifting me and reminding me to acknowledge and celebrate my accomplishments – no matter how big or small.

To my mentors, past and present. In particular Dr. Elaine Seaver who was my first mentor in science. You took a chance on a plucky undergraduate who knew nothing of life in the lab; but those early experience with your group learning about *Capitella* were formative, and I am so grateful to you for opening my eyes to the fascinating field of developmental biology. My next mentor, Dr. Andrew (Andy) E. Christie, also played a crucial role in my scientific pursuits. As my Honors program mentor, you were candid with your guidance (even when I was no longer a trainee in the lab) and helped me to consider opportunities that I wouldn't have pursued otherwise – including pursuing my Masters degree at University of North Carolina Wilmington. I also owe much thanks to my Masters mentor, Dr. Robert (Bob) Roer. You struck the perfect balance of instruction and independence, and made the transition to graduate school as smooth as possible. My time as your student helped me to understand more about my interests in biology for the long-haul, and prepared me for the challenges I would face as a doctoral student. And of course, to my doctoral advisor, Dr. Amro Hamdoun. My tenure in the lab has taught me so much, it's honestly hard to know where to start. Thank you for seeing my potential and pushing me beyond what I thought my capabilities and contributions could be. Thank you as well for your compassion during the inevitable struggles. Thanks for challenging me to think both broadly, and

deeply about problems in biology, and for offering me the flexibility and freedom to pursue my interests in the lab. Good mentorship doesn't force a mold for a student or stuff them into a predetermined track. Rather, it encourages mentees to develop their own form and set their own course. Your commitment to tailoring mentorship styles to individual strengths and weaknesses has helped immensely in my shaping of this journey. I also want to thank Dr. Victor Vacquier for your gentle guidance and understanding along the way. I will never forget my first week in the lab. You stopped by my office, sat down and took the time to simply ask how I was doing – but *really* how I was doing. Your consideration for the well-being of students, and wealth of knowledge on all-things-sea-urchin is invaluable and I am so glad we've overlapped.

I also want to thank my partner, Erick, for your encouragement and support. You've seen every stage of my academic career thus far. Your belief in me throughout this endeavor has been a pillar of strength when the going got tough. Thank you for accompanying me on this wild expedition.

To my sweet, gentle, and joyful puppy Iver. Love you, ya little fuzz-butt!

EPIGRAPH

"It is the best kept secret in science. We never tell people what fun we are having."

~ Elizabeth Blackburn, Nobel Prize in Physiology or Medicine (2009) ~

TABLE OF CONTENTS

LIST OF FIGURES

LIST OF TABLES

Chapter 3

Chapter 4

Chapter 5

ACKNOWLEDGEMENTS

I would like to acknowledge Professor Amro Hamdoun for his support as the chair of my dissertation committee Similarly, I would also like to acknowledge Drs. Deirdre Lyons, Lena Gerwick, Victor Nizet, and Bradley Moore for their guidance and participation as members of my dissertation committee.

I would also like to acknowledge the members of the Hamdoun Lab (past, and present whom overlapped with me during my tenure from 2016-2021). Science is collaborative by nature, and the support shared among this group of talented, intelligent, and creative people has been instrumental to the completion of this work.

Chapter 2, in full, is a reprint of the material as it appears in Developmental Dynamics 2021. Nesbit KT and Hamdoun A. The dissertation author is the primary investigator and author of this paper.

Chapter 3, in part, is a reprint of material as it appears in Genome Biology and Evolution (2021). Warner JF, Lord J, Schreiter SA, Nesbit KT, Hamdoun A, and Lyons DC. The dissertation author is a co-author of this paper. Additional portions of Chapter 3 have been submitted for publication in PLOS Biology (2021). Espinoza JA, Vyas H, Schrankel CS, Mitchell K, Nesbit KT, Jackson E, and Hamdoun A. The dissertation author is a coauthor of this paper.

Chapter 4 is currently being prepared for submission for publication. Nesbit KT and Hamdoun A. The dissertation author is the primary investigator and author of this material.

Chapter 5, is unpublished with coauthors. Chang N, Le KP, Nesbit KT and Hamdoun A. The dissertation author will be a co-author of this material.

VITA

EDUCATION

2014 Bachelor of Science with High Honors. Marine Biology. University of Hawai'i at Mānoa. Honolulu, HI.

2016 Master of Science. Marine Biology. University of North Carolina Wilmington. Wilmington, NC.

2022 Doctor of Philosophy. Marine Biology. Scripps Institution of Oceanography, University of California San Diego. San Diego, CA.

PUBLICATIONS

Warner JF, Lord J, Schreiter SA, **Nesbit KT**, Hamdoun A, Lyons DC. (2021). High contiguity genome assembly of the painted sea urchin Lytechinus pictus, a genetically enabled model system for cell biology and embryonic development. *Genome Biology and Evolution*. 13(4), evab061.

Nesbit KT, Wolfe WH, Mullane KK, Chamberlain EJ, Saberski E, Rasina BA, Jones-Cervantes SA. (2021). SCOPE (Scripps Community Outreach for Public Education): A volunteer STEM outreach program connecting communities to research at Scripps Institution of Oceanography. *Connected Science Learning. Accepted*.

Nesbit KT and Hamdoun A. (2020) Embryo, larval and juvenile staging of Lytechinus pictus from fertilization through sexual maturation. *Developmental Dynamics*. 249(11): 1334-1346.

Nesbit KT, Fleming, T, Batzel G, Pouv A, Rosenblatt H, Pace D, Hamdoun A, Lyons D. (2019). The painted sea urchin, Lytechinus pictus, as a genetically-enabled developmental model. In, K. Folts and Hamdoun A (Eds.) Echinoderms: Experimental Approaches Methods in Cell Biology: Academic Press: Elsevier v150.

Hamdoun A, Schrankel CS, **Nesbit KT**, Espinoza JE. Sea urchins as Lab Animals for Reproductive and Developmental Biology. (2018). In: MK Skinner (Ed.), Encyclopedia of Reproduction, vol. VI, pp. 696-703. Academic Press: Elsevier.

Nesbit KT, and Roer RD (2016). Silicification of the medial tooth in the blue crab Callinectes sapidus. *Journal of Morphology*. 277(12): 1648-1660.

Nesbit, KT and Christie, AE (2014). Identification of the molecular components of a *Tigriopus californicus* (Crustacea, Copepoda) circadian clock. *Comp. Biochem. Physiol. Part D Genomics Proteomics*. 12:16-44.

Christie, AE, Fontanilla, TM, **Nesbit, KT**, Lenz, PH (2013). Prediction of the protein components of a putative *Calanus finmarchicus* (Crustacea, Copepoda) circadian signaling system using de novo assembled transcriptome. *Comp. Biochem. Physiol. Part D Genomics Proteomics*. 8(3):165-193

SELECTED FUNDING AWARDS DURING DISSERTATION PERIOD

April 2020 **Scholarship:** Association for Women in Science (AWIS) – San Diego Chapter 2020 Scholarship Award for Doctoral Students.

Aug. 2019 **Academic Fellowship:** National Institutes of Health (NIH) Diversity Supplement. National award for students from backgrounds traditionally underrepresented in STEM fields. This award funds doctoral students' research as a supplement to a parent grant.

July 2018 **Scholarship:** Hispanic Scholarship Fund (HSF). National competitive award for students with Hispanic heritage to obtain college and graduate degrees, with emphasis on STEM programs.

March 2018 **Scholarship:** Offer of MBL Support. Marine Biological Laboratory at Woods Hole, University of Chicago. Funds covered the full cost of attendance to the Summer 2018 "Embryology: Concepts and Techniques in Modern Developmental Biology" course at MBL Woods Hole. (06/2018-07/2018)

Aug. 2017 **Academic Fellowship:** H. William Menard Memorial Fund. Scripps Institution of Oceanography, University of California San Diego. Funds cover tuition and fees to help support graduate student researchers. (08/2017)

Jan 2017 **Academic Fellowship:** Scripps Fellowship. Scripps Institution of Oceanography, University of California San Diego. Departmental predoctoral support award. (01/2017 - 06/2017)

Aug. 2016 **Academic Fellowship:** Cody Fellowship. Scripps Institution of Oceanography, University of California San Diego. Departmental predoctoral support award. (08/2016-12/2016

TEACHING and LEADERSHIP EXPERIENCE DURING DISSERTATION

2019 **Teaching Assistant – SIO139**
(01/2019 – 06/2019) University of California – San Diego, Scripps Institution of Oceanography, La Jolla, CA.

- Led review sections and assisted students with scientific writing exercises, laboratory exercises using R, and research presentation skills in the undergraduate course SIO 139 entitled "Current Research in Marine Biology"

2017 **Teaching Assistant – SIO189**
(08/2018 – 12/2017) University of California – San Diego, Scripps Institution of Oceanography, La Jolla, CA.

- Led discussion and review sections for the undergraduate SIO189 course on Pollution, Environment, and Health. Graded exams and assignments, corresponded with students on course material.

2017 **Coordinator, Scripps Community Outreach for Public Education (SCOPE)**
(08/2017-present) Scripps Institution of Oceanography, La Jolla, CA.

- Plan logistics for educational activities for community groups through SCOPE. Activities include on campus visits, such as tours of research facilities, and off campus activities, such as guest speaker requests. Audiences originate from the local San Diego area, to international groups.
- Organize and lead volunteer activities including volunteer appreciation events, and volunteer tour-training sessions.
- Design guides for volunteers and other STEM outreach activity materials to supplement classroom education for visiting educators.

WEB-BASED PUBLICATIONS and MEDIA COVERAGE DURING DISSERTATION

May 2021 **Student Spotlight.** Scripps Institution of Oceanography: UC San Diego initiative to highlight the important contributions to research and education made by graduate and professional students. Link: https://grad.ucsd.edu/student-life/student-spotlights/sio/katherine-nesbit.html

Nov. 2020 **Womengineered**. Science communication social media account (Instagram) highlight featuring women in science, and discussing equity, diversity, and inclusion in STEM with a focus on women's issues. Link: https://www.instagram.com/p/CHvmzD9DWdV/

Nov. 2020 **Journal Cover**. Developmental Dynamics. Data from Nesbit and Hamdoun 2020 (see publications above) earned the cover image for this issue of the journal.

Oct. 2020 **SeatheScience.** Science communication social media account (Instagram) submission post featuring early career scientists and other earth and ocean science topics. Link: https://www.instagram.com/p/CF21hoUhvMd/

Oct. 2020 **Echinobase**. Authored the "About" page information and images for *Lytechinus pictus* hosted on the community resource portal for echinoderm biologists. Link: http://legacy.echinobase.org/Echinobase/LpAbout

Oct. 2020 **Latinx and Hispanic Excellence at Scripps**. News feature composed in recognition of Latinx Heritage Month featuring members of the Scripps

community with Latinx and/or Hispanic backgrounds. Link: https://scripps.ucsd.edu/news/recognizing-latinx-and-hispanic-excellence-scripps

Aug. 2020 **Developmental staging poster**. Collaboration utilizing data from Nesbit and Hamdoun 2020 (see publications above) was used to generate an updated and publicly available developmental staging series poster for the sea urchin model system as part of the journal's free staging series posters. Link: https://anatomypubs.onlinelibrary.wiley.com/hub/journal/10970177/homepage/custom_designed_page_a3.htm

July 2018 **Photo Contest Winner**. Ocean Conservancy. Category – Underwater Wonders. Annual photo contest with submissions from artists around the globe. Contest winners have their images features in the annual calendar, proceeds of which go towards ocean conservation. Link: https://beautifulnow.is/discover/impact/award-winning-photos-from-ocean-conservancy-photo-contest-will-move-you-to-take-action

Jan. 2018 **Innovate 8: Students explore oceanography and climatology**. News feature on CBS San Diego featuring the SCOPE program. Link: https://www.cbs8.com/article/news/local/outreach/innovate8/innovate-8-students-explore-oceanography-and-climatology/509-bcd3096d-e622-4e9e-a7bd-840474177021

Oct. 2016 **Photo of the Week**. A star of the sea. Baby urchin cultured by grad student. Scripps News highlight featuring *Lytechinus pictus* cultured in the lab through metamorphosis by the dissertation author. Link: https://scripps.ucsd.edu/news/photo-week-star-sea

ABSTRACT OF THE DISSERTATION

Development of the painted white urchin, *Lytechinus pictus*, as a genetically enabled model to address impacts of chemical exposure on the larval immune response

by

Katherine T. Nesbit

Doctor of Philosophy in Marine Biology

University of California San Diego 2022

Professor Amro Hamdoun, Chair

Embryos develop in dynamic environments and are subject to myriad stressors – both biotic and abiotic. Among those stressors are encounters with pathogens and toxic molecules. The systems for sensing and responding to the environment include a robust suite of molecular machinery that protects the cell, and a heterogeneous population of immune cells that mount coordinated responses. Establishing a whole-animal echinoderm embryo model to address

embryo-environment interactions and how stressors influence such systems is the focus of this dissertation work.

Accomplishing this task began with identifying a need for a sea urchin model species that grew more rapidly that other commonly used echinoderms, and establishing a comparable developmental staging scheme and culturing practices for rearing animals in the lab. The painted white urchin, *Lytechinus pictus*, was a clear choice for the optimal model.

Generating molecular tools was also essential, and yielded a fully sequenced genome with chromosomal resolution and transcriptomic tools pooled across developmental stages. To assess the quality of these molecular resources I annotated the suite of ATP-binding cassette transporters (ABCs). ABCs are expressed in, and play important roles in handling of toxic molecules as well as in the differentiation and migration of, immune cells.

In addition to the ABCs, I combed the genome for other components involved in immunity – including cytokines, transcription factors, enzymes, effectors, and signal mediators. This suite of annotations establishes a foundation of potential targets of exposure in the immune system. From there, I challenged sea urchin larvae with bacterial infection and characterized the first phenotypic responses of an echinoderm model of immunosuppression.

The outcome of this research is a series of tools and resources that open doors for future investigation. With a reliable, dose-dependent model of immunosuppression and complimentary molecular tools in a rapidly developing echinoderm species, it is now possible to address the influence of toxic molecules on whole-animal immune responses. It is also possible to investigate how early life exposures alter later life health or the health of subsequent generations. Finally, we can begin to tease apart the cross-talk of developmental and protective systems in the embryo contributing to environmental sensing and signaling.

CHAPTER 1

Introduction

1.1 Outline of Dissertation

The motivating question behind my dissertation work asks – how do embryos interact with their environment? Development is a dynamic process that can be influenced by many different biotic and abiotic stressors, singularly and (more often) in combination. Abiotic stressors include challenges regulating pH, light and UV exposure, temperature, oxidizers, mechanical forces, osmoregulation and salt content, and encounters with toxic molecules. Biotic stressors include competition with members of the same or different species, and challenges from pathogens or other disease agents. Of particular interest to my work are exposures to toxic molecules and encounters with pathogens, as well as the interactions between these two stressors on the overall health of an organism.

Much of biological research relies on the utilization of model organisms that are best-suited to particular questions. The traditional models in biology are mouse, zebrafish, chick, frog, the nematode worm *C. elegans*, fruit fly, and then plants like the thale cress, *Arabidopsis*, and single celled organisms including yeast and bacteria. One unifying advantage of these traditional models is that they are all genetically enabled. However, these model systems are primarily terrestrial, and none are marine, despite marine organisms providing a lot of important contributions to modern biological research. Marine models are particularly well-suited to studying embryo-environment interactions. In particular, sea urchins which are broadcast spawners and produce millions of orphan embryos that develop in the water column.

I began looking at the painted white urchin, *Lytechinus pictus* with the idea in mind that this species would be a suitable model for better understanding embryo-environment interactions. The eggs and embryos of this species are stunningly beautiful, and their pace of development is twice as fast as the development of the purple sea urchin, which is one of the

most widespread species used in sea urchin research. I began creating a developmental timeline and updating culturing methods for rearing the larvae through settlement. The previous descriptions of *L. pictus* development and culturing practices by Ralph T. Hinegardner[1-4] were a solid foundation to build from. However, this work was more than 50 years old and largely overlooked in favor of work in other species such as *S. purpuratus* and *Lytechinus variegatus* that had genomic resources available. Thus, I sought to update the developmental staging and culturing practices. This work is summarized in Chapter 2. The ultimate goal in mind with this work was to aid efforts to generate inbred or transgenic lines of sea urchin, which Hinegardner had originally theorized *L. pictus* would be suitable for, and which the urchin research community has lacked as an important tool.

Budding from the updates on culturing and developmental staging in *L. pictus*, molecular resources for this species were in development. This included sequencing of a pooled developmental transcriptome[5] from egg to 2 day old plutei and generation of a genome[6]. These data would significantly impact the utility of *L. pictus* as a model organism. To validate the quality and completeness of the newly generated genomic resources, I began identifying the ABC transporters in *L. pictus*. This expanded to annotations of other transporters from the solute carrier protein (SLCs) superfamily as part of a small molecule transport system that plays a critical role in environmental sensing and signaling. The data from these efforts is summarized in Chapter 3. The ABCB1a candidate I identified in this work became the main target for CRISPR-mediated knockout in *L. pictus* as part of a lab-wide effort to generate a knockout animal line.

While sifting through the genome for ABCs, my continued interest in their functional roles led to another exciting direction for my research. While reading a review[7] on cell migration and multidrug resistance in metastatic cancers a figure struck me as familiar. The figure modeled

the putative effect of MRP4/5 (ABCC4/5) on tumor cell migration. In this model, MRP4/5 inhibition impacted downstream cAMP gradients and PKA activity resulting in increased migratory abilities of cancerous cells[8]. I remember commenting that the modeled metastatic cancer cell(s) expressed ABCC5 just like the migratory larval pigment cells (PCs), and asking whether chemicals inhibiting ABCC5 might alter migratory abilities of PCs in the urchin. This question is what ultimately led to the work detailed in Chapter 4 which ties together perspectives in developmental biology, immunology, and toxicology to understand the role that drug exposure plays in overall maintenance of organismal health and lays a foundation for making predictions about the influence of other toxic exposures on immune functions.

In order to set the stage for the collective body of work presented in this dissertation, the remainder of this chapter introduces brief primers in key topic areas relevant for the data discussed in Chapters 2-4.

1.2 Relevant Topics Areas

1.2.1 The sea urchin embryo model

Sea urchins are part of a group of organisms called echinoderms, stemming from the Greek roots *echinos* meaning 'spiny' and *derma* meaning 'skin'. There are five classes of echinoderms: Ophiuroids – brittle stars, Asteroids – sea stars, Crinoids – feather stars, Holothuroids – sea cucumbers, and Echinoids – sea urchins and sand dollars. These classes represent over 7,000 extant species[9]. Echinoderms are deuterostomes, and their early embryonic development is remarkably similar to the early development of mammals and other vertebrates. Sea urchins have a biphasic life history, during which the planktonic, bilaterally symmetrical embryonic and larval stages[10] mature and metamorphose[2] into the benthic adult body plan with pentaradial symmetry. This group of animals has captivated biologists for over 100 years, and

the study of sea urchin embryos specifically has contributed a number of significant insights that have been foundational for our understanding of development, cell specification and differentiation, inheritance, and even genetics and molecular biology[11].

There are several favorable traits of the urchin embryo system that were central to its initial selection and continued persistence as a model[12]. Firstly, is the matter of convenience. Early studies in the late 1800s in experimental embryology and development relied on materials that were easily at-hand. Adult sea urchins can be readily collected from coastal waters around the world. Due to the reliable access to adult animals, there is an abundance of gametic material as well since sea urchins have high fecundity as broadcast spawners and release millions of eggs or sperm at a time. Another advantage is that the egg is fertilized externally in a simple dish of sea water, and the resulting embryos develop rapidly and synchronously. Moreover, the embryos are transparent (especially in comparison to other embryological models such as the heavily pigmented and/or yolky eggs and embryos of the African clawed frog *Xenopus*, zebrafish *Danio rerio*, and chick *Gallus gallus*) enabling visualization of key developmental and cellular events.

Since its beginnings as a developmental model, the study of urchin development has lent to the advancement of cellular and molecular biology. For example, sea urchin histones were the first protein coding eukaryotic genes cloned[13]. Urchins were also used in the Nobel prize-winning discovery of cyclin proteins which regulate the cell cycle[14]. Among other topics of interest that are particularly well-suited for study in the urchin and other echinoderm models are the genetic and cellular control of embryonic territories and the construction of a well-defined gene regulatory network[15], the role of genetic variation in physiological resilience[16], comparative evolutionary studies among urchins and other echinoderm species[17-19], as well as the mechanisms

which enable the embryo to interface with the environment including protective machinery[20-23] to defend against pathogens and environmental stressors.

1.2.2 ATP-binding cassette transporters

ATP-binding cassette transporters (ABCs) are transmembrane proteins found in all kingdoms of life, from bacteria to humans. There are eight major subfamilies of ABC transporters in sea urchin[22,23], and seven represented in mammals[24]. In the purple urchin, the best described subfamilies are the B-, C-, and G-subfamilies. Although the general number of genes within each subfamily is similar across organisms, several families are expanded in the echinoderms, most notably the ABCC subfamily[25].

There are a variety of ligands that can be bound and translocated by ABC transporters. By utilizing energy from the hydrolysis of ATP, ABCs are able to move ligands across a membrane. Their ligands include cyclic nucleotides, inflammatory mediators such as leukotrienes, prostaglandins and other lipids, metals, sterols, ions, and a number of foreign (or xenobiotic) molecules including pharmaceutical drugs like chemotherapeutics[24,26-28]. There is often overlapping substrate specificity among the transporters from the multidrug resistance groups (ABC -B, -C, and -G subfamilies). The promiscuity of many of these transporters, and the fact that many of their natural ligands are exogenous molecules supports the well-accepted idea that these proteins play essential protective roles for the cell. There are also a number of non-protective roles that these proteins serve. Additional well-studied roles for these proteins include ion regulation[29], developmental signaling[30], cell migration[31], antigen presentation[32], and in humans, mutations or misregulation in these genes are associated with disease[26,33-36].

1.2.2 Immunity in the sea urchin

Understanding disease and the pathways involved in protection against infection is critical for maintaining health. The immune system is the primary defense and must have robust communication and

sensing mechanisms to detect microbial invasion or other potentially dangerous foreign bodies. The discovery of phagocytosis, the process by which a cell engulfs another cell or particle, was actually first discovered in the sea star larvae by Nobel laureate Elie Metchnikoff[37]. Referred to as the father of innate immunity, this work set the stage for our understanding of how immune cells in humans, like macrophages, neutrophils, and dendritic cells, aid in pathogen clearance.

The sea urchin immune system is an innate, compliment-like network of interacting cell types[38,39]. Despite the lack of adaptive immunity features, there are a number of important genetic components of immunity that are shared between urchins and mammals[40,41]. Interestingly, the larval and adult immune systems are not identical, each containing unique cell types, or differing in the repertoire and expression levels of immune receptors and effector molecules[39,42]. Here, we expand on the current knowledge base of the larval immune system as an elegant infection model involving coordinated cellular responses to pathogenic bacteria. The larval immune system is composed of five distinct cell types: ameboid cells, filapodial cells, ovoid cells, globular cells, and pigment cells[38]. The focus of this work will be on the pigment cells, which arise from the differentiation of a population of aboral secondary mesenchymal cells (SMCs) at approximately 24 hours post-fertilization (hpf) in *S. purpuratus*[43]. The remaining immune cells types are collectively referred to as blastocoelar cells, whose precursors are oral SMCs which differentiate at approximately 48 hpf in *S. purpuratus*[44].

Pigment cells (PCs) contain granules of an autofluorescent naphthoquinone called echinochrome A, which gives these cells their characteristic red color and also has antimicrobial properties[45]. PCs express a number of unique marker genes including a polyketide synthase (PKS), an ABC transporter (ABCC5a), and immune-related genes like a thioester containing protein (tecp2) and a scavenger receptor protein (SRCR142)[42]. Moreover, these cells undergo dramatic cell shape changes and have dynamic migratory behaviors upon immune activation.

When the larvae are fed cells of the opportunistic pathogenic bacteria *Vibrio diazotrophicus*, a coordinate immune response is mounted. The gut epithelium becomes inflamed and the gut lumen shrinks. PCs, which are normally embedded in the ectoderm in beautiful stellate conformations, become rounded and migrate through the blastocoel. Activated PCs will interact with other immune cell types and congregate at the gut as part of this dose-dependent and reversible immune response[42]. Alongside the conspicuous phenotypic changes are dynamic changes in immune gene regulation throughout the course of infection. PC specific gene changes include the upregulation of SRCR142, and the up-then-down regulation of tecp2. Other dynamic transcriptional changes include the downregulation of a macrophage inhibitory factor (*mif7*), downregulation of the perforin-like marker (*macpfA2*), and upregulation of an echinoderm specific immune effector (*185*/*333*)[42].

The PCs, in coordination with the other immune cell types protect the larvae against infection in a microbially rich environment. As free-swimming planktonic larvae, these animals are not subjected to singular stressors. The immune system of the urchin serves as an indicator of environmental stressors[46]. Biotic stressors such as infection, and abiotic stressors like temperature and pH change as well as exposure to toxic molecules in the environment (both microbially and/or anthropogenically sourced) are likely encountered simultaneously. Combinatorial challenges to health are understudied, despite being more representative of the environment that animals and human interact with every day. This raises the question of how toxic exposures may impact the immune system – by sensitizing an organism, altering resistance and recovery to immune challenges.

1.2.3 Environmental pollution and early life exposures

All organisms interact with a complex and dynamic environment that presents repeated challenges for environmental sensing and response. Among these challenges are the risks of exposure to

harmful chemical substances. Exposures come from a variety of environmental sources, but can be broadly classified into two major categories: 1) anthropogenically produced toxicants, and 2) naturally synthesized toxins. Anthropogenic toxicants contaminate the environment and include heavy metals (e.g., mercury), plastics and plasticizing chemicals (e.g., phthalates), pharmaceutical drugs, flame retardants (e.g., polybrominated diphenyl ethers or PBDE), and pesticides (e.g., DDT). Naturally produced toxins include products from plants and animals (e.g., tetrodotoxin), algae (e.g., domoic acid, saxitoxin, and microcystins), and bacteria (e.g., anthrax, apoptosis inducing proteins). The focus of this work is primarily on the influence of anthropogenically sourced chemicals that enter the environment and have consequences for organismal and human health.

Early life exposures to environmental toxicants negatively impact adult and fetal health[47,48]. In particular, developmental exposures are linked to disruption of neurological function[49,50], endocrine disruption and estrogenic effects[51-54], decreased reproductive function[55], interference of cellular transport[56], and immunotoxicity[57-60].

The diversity of negative health outcomes and the influence of exposure parameters (ex. duration and dosing) highlights a need for a more complete understanding of exposure risks and the molecular underpinning that are impacted. To tackle these questions, robust experimental systems are needed to untangle the complex consequences of toxicant exposure on cellular and organismal health, especially in developmental contexts for embryos in dynamic environments.

1.3 REFERENCES

1. Cameron RA, Hinegardner RT. Initiation of metamorphosis in laboratory cultured sea urchins. *The Biological Bulletin*. 1974;146(3):335-342.

2. Cameron RA, Hinegardner R. Early events in sea urchin metamorphosis, description and analysis. *Journal of Morphology*. 1978;157(1):21-31.

3. Hinegardner RT. Growth and development of the laboratory cultured sea urchin. *The Biological Bulletin*. 1969;137(3):465-475.

4. Hinegardner RT. Morphology and genetics of sea-urchin development. *American Zoologist*. 1975:679-689.

5. Nesbit KT, Fleming T, Batzel G, Pouv A, Rosenblatt HD, Pace DA, Hamdoun A, Lyons DC. The painted sea urchin, Lytechinus pictus, as a genetically-enabled developmental model. *Methods Cell Biol*. 2019;150:105-123. https://doi.org10.1016/bs.mcb.2018.11.010.

6. Warner JF, Lord JW, Schreiter SA, Nesbit KT, Hamdoun A, Lyons DC. Chromosomal-level genome assembly of the painted sea urchin Lytechinus pictus, a genetically enabled model system for cell biology and embryonic development. *Genome Biology and Evolution*. 2021.

7. Kryczka J, Boncela J. Cell Migration Related to MDR—Another Impediment to Effective Chemotherapy? *Molecules*. 2018;23(2):331.

8. Sinha C, Ren A, Arora K, Moon CS, Yarlagadda S, Woodrooffe K, Lin S, Schuetz JD, Ziady AG, Naren AP . PKA and actin play critical roles as downstream effectors in MRP4-mediated regulation of fibroblast migration. *Cellular signalling*. 2015;27(7):1345-1355.

9. Brusca RC, Brusca GJ. *Invertebrates*. Basingstoke; 2003.

10. Smith MM, Cruz Smith L, Cameron RA, Urry LA. The larval stages of the sea urchin, Strongylocentrotus purpuratus. *Journal of Morphology*. 2008;269(6):713-733.

11. Ernst SG. Offerings from an urchin. *Developmental biology*. 2011;358(2):285-294.

12. Hamdoun A, Schrankel CS, Nesbit KT, Espinoza JA. Sea Urchins as Lab Animals for Reproductive and Developmental Biology. 2018.

13. Kedes LH, Chang AC, Houseman D, Cohen SN. Isolation of histone genes from unfractionated sea urchin DNA by subculture cloning in E. coli. *Nature*. 1975;255(5509):533-538.

14. Evans T, Rosenthal ET, Youngblom J, Distel D, Hunt T. Cyclin: a protein specified by maternal mRNA in sea urchin eggs that is destroyed at each cleavage division. *Cell*. 1983;33(2):389-396.

15. Oliveri P, Davidson EH. Gene regulatory network controlling embryonic specification in the sea urchin. *Current opinion in genetics & development*. 2004;14(4):351-360.

16. Pespeni MH, Sanford E, Gaylord B, Hill TM, Hosfelt JD, Jaris HK, LaVigne M, Lenz EA, Russell AD, Young MK, Palumbi SR. Evolutionary change during experimental ocean acidification. *Proceedings of the National Academy of Sciences*. 2013;110(17):6937-6942.

17. Cary GA, Hinman VF. Echinoderm development and evolution in the post-genomic era. *Developmental biology*. 2017;427(2):203-211.

18. Hinman VF, Davidson EH. Evolutionary plasticity of developmental gene regulatory network architecture. *Proceedings of the National Academy of Sciences*. 2007;104(49):19404-19409.

19. McCauley BS, Weideman EP, Hinman VF. A conserved gene regulatory network subcircuit drives different developmental fates in the vegetal pole of highly divergent echinoderm embryos. *Developmental biology*. 2010;340(2):200-208.

20. Gökirmak T, Campanale JP, Shipp LE, Moy GW, Tao H, Hamdoun A. Localization and substrate selectivity of sea urchin multidrug (MDR) efflux transporters. *Journal of Biological Chemistry*. 2012;287(52):43876-43883.

21. Gökirmak T, Shipp LE, Campanale JP, Nicklisch SC, Hamdoun A. Transport in technicolor: Mapping ATP□binding cassette transporters in sea urchin embryos. *Molecular reproduction and development*. 2014;81(9):778-793.

22. Goldstone J, Hamdoun A, Cole BJ, Howard-Ashby M, Nebert DW, Scally M, Dean M, Epel D, Hahn ME, Stegeman JJ. The chemical defensome: environmental sensing and response genes in the Strongylocentrotus purpuratus genome. *Developmental biology*. 2006;300(1):366-384.

23. Shipp LE, Hamdoun A. ATP□binding cassette (ABC) transporter expression and localization in sea urchin development. *Developmental Dynamics*. 2012;241(6):1111-1124.

24. Schinkel AH, Jonker JW. Mammalian drug efflux transporters of the ATP binding cassette (ABC) family: an overview. *Advanced drug delivery reviews*. 2012;64:138-153.

25. Gökirmak T, Campanale JP, Reitzel AM, Shipp LE, Moy GW, Hamdoun A. Functional diversification of sea urchin ABCC1 (MRP1) by alternative splicing. *American Journal of Physiology-Cell Physiology*. 2016;310(11):C911-C920.

26. Dean M. The human ATP-binding cassette (ABC) transporter superfamily. 2002.

27. Dean M, Annilo T. Evolution of the ATP-binding cassette (ABC) transporter superfamily in vertebrates. *Annu Rev Genomics Hum Genet*. 2005;6:123-142.

28. Kathawala RJ, Gupta P, Ashby Jr CR, Chen Z-S. The modulation of ABC transporter-mediated multidrug resistance in cancer: a review of the past decade. *Drug resistance updates*. 2015;18:1-17.

29. Bryan J, Muñoz A, Zhang X, Düfer M, Drews G, Krippeit-Drews P, Aguilar-Bryan L . ABCC8 and ABCC9: ABC transporters that regulate K+ channels. *Pflügers Archiv-European Journal of Physiology*. 2007;453(5):703-718.

30. Petrášek J, Friml J. Auxin transport routes in plant development. *Development*. 2009;136(16):2675-2688.

31. Kassmer SH, Rodriguez D, Langenbacher AD, Bui C, De Tomaso AW. Migration of germline progenitor cells is directed by sphingosine-1-phosphate signalling in a basal chordate. *Nature communications*. 2015;6(1):1-10.

32. Schumacher T, Kantesaria DV, Heemels MT, Ashton-Rickardt PG, Shepherd JC, Fruh K, Yang Y, Peterson PA, Tonegawa S, Ploegh HL . Peptide length and sequence specificity of the mouse TAP1/TAP2 translocator. *The Journal of experimental medicine*. 1994;179(2):533-540.

33. Borst P, Elferink RO. Mammalian ABC transporters in health and disease. *Annual review of biochemistry*. 2002;71(1):537-592.

34. Gottesman MM, Ambudkar SV. Overview: ABC transporters and human disease. *Journal of bioenergetics and biomembranes*. 2001;33(6):453-458.

35. Silverton L, Dean M, Moitra K. Variation and evolution of the ABC transporter genes ABCB1, ABCC1, ABCG2, ABCG5 and ABCG8: implication for pharmacogenetics and disease. *Drug metabolism and drug interactions*. 2011;26(4):169.

36. Tarling EJ, de Aguiar Vallim TQ, Edwards PA. Role of ABC transporters in lipid transport and human disease. *Trends in Endocrinology & Metabolism*. 2013;24(7):342-350.

37. Metchnikoff E. *Untersuchungen über die intracelluläre Verdauung bei wirbellosen Thieren*. A. Hölder; 1883.

38. Smith LC, Rast JP, Brockton V, Terwilliger DP, Nair SV, Buckley KM, Majeske AJ . The sea urchin immune system. *Invertebrate Survival Journal*. 2006;3(1):25-39.

39. Hirano M. Echinoderm immunity: is the larval immune system immature? *Immunology and Cell Biology*. 2016;94(9):809.

40. Pancer Z, Rast JP, Davidson EH. Origins of immunity: transcription factors and homologues of effector genes of the vertebrate immune system expressed in sea urchin coelomocytes. *Immunogenetics*. 1999;49(9):773-786.

41. Buckley KM, Ho ECH, Hibino T, Schrankel CS, Schuh NW, Wang G, Rast JP . IL17 factors are early regulators in the gut epithelium during inflammatory response to Vibrio in the sea urchin larva. *Elife*. 2017;6:e23481.

42. Ho EC, Buckley KM, Schrankel CS, Schuh NW, Hibino T, Solek CM, Bae K, Wang G, Rast JP . Perturbation of gut bacteria induces a coordinated cellular immune response in the purple sea urchin larva. *Immunology and cell biology*. 2016;94(9):861-874.

43. Gibson AW, Burke RD. The origin of pigment cells in embryos of the sea urchin Strongylocentrotus purpuratus. *Developmental biology*. 1985;107(2):414-419.

44. Tamboline CR, Burke RD. Secondary mesenchyme of the sea urchin embryo: ontogeny of blastocoelar cells. *Journal of Experimental Zoology*. 1992;262(1):51-60.

45. Smith VJ, Desbois AP, Dyrynda EA. Conventional and unconventional antimicrobials from fish, marine invertebrates and micro-algae. *Marine drugs*. 2010;8(4):1213-1262.

46. Pinsino A, Matranga V. Sea urchin immune cells as sentinels of environmental stress. *Developmental & Comparative Immunology*. 2015;49(1):198-205.

47. Perera F, Herbstman J. Prenatal environmental exposures, epigenetics, and disease. *Reproductive toxicology*. 2011;31(3):363-373.

48. Landrigan PJ, Fuller R, Acosta NJ, Adeyi O, Arnold R, Baldé AB, Bertollini R, Bose-O'Reilly S, Boufford JI, Breysse PN, Chiles T. The Lancet Commission on pollution and health. *The lancet*. 2018;391(10119):462-512.

49. Mariussen E. Neurotoxic effects of perfluoroalkylated compounds: mechanisms of action and environmental relevance. *Archives of toxicology*. 2012;86(9):1349-1367.

50. Senanayake N, Karalliedde L. Neurotoxic effects of organohosphorus insecticides. *New England Journal of Medicine*. 1987;316(13):761-763.

51. Kahn LG, Philippat C, Nakayama SF, Slama R, Trasande L. Endocrine-disrupting chemicals: Implications for human health. *The Lancet Diabetes & Endocrinology*. 2020;8(8):703-718.

52. Roepke TA, Snyder MJ, Cherr GN. Estradiol and endocrine disrupting compounds adversely affect development of sea urchin embryos at environmentally relevant concentrations. *Aquatic Toxicology*. 2005;71(2):155-173.

53. Sifakis S, Androutsopoulos VP, Tsatsakis AM, Spandidos DA. Human exposure to endocrine disrupting chemicals: effects on the male and female reproductive systems. *Environmental toxicology and pharmacology*. 2017;51:56-70.

54. Yilmaz B, Terekeci H, Sandal S, Kelestimur F. Endocrine disrupting chemicals: exposure, effects on human health, mechanism of action, models for testing and strategies for prevention. *Reviews in endocrine and metabolic disorders*. 2020;21(1):127-147.

55. Recio□Vega R, Ocampo□Gómez G, Borja□Aburto VH, Moran□Martínez J, Cebrian□Garcia ME. Organophosphorus pesticide exposure decreases sperm quality: association between sperm parameters and urinary pesticide levels. *Journal of applied toxicology*. 2008;28(5):674-680.

56. Nicklisch SC, Rees SD, McGrath AP, Gökirmak T, Bonito LT, Vermeer LM, Cregger C, Loewen G, Sandin S, Chang G, Hamdoun A . Global marine pollutants inhibit P-glycoprotein: Environmental levels, inhibitory effects, and cocrystal structure. *Science advances*. 2016;2(4):e1600001.

57. Leijs MM, Koppe JG, Olie K, Aalderen WMv, Voogt Pd, Tusscher GWt. Effects of dioxins, PCBs, and PBDEs on immunology and hematology in adolescents. *Environmental science & technology*. 2009;43(20):7946-7951.

58. Selgrade MK. Immunotoxicity—The risk is real. *Toxicological Sciences*. 2007;100(2):328-332.

59. Galloway TS, Depledge MH. Immunotoxicity in invertebrates: measurement and ecotoxicological relevance. *Ecotoxicology*. 2001;10(1):5-23.

60. Galloway T, Handy R. Immunotoxicity of organophosphorous pesticides. *Ecotoxicology*. 2003;12(1):345-363.

CHAPTER 2

Embryo, larval, and juvenile staging of *Lytechinus pictus* from fertilization through sexual maturation

2.1 ABSTRACT

Sea urchin embryos have been used for more than a century in the study of fertilization and early development. However, several of the species used, such as *Strongylocentrotus purpuratus*, are wild-caught and have long generation times making them suboptimal for genetic, transgenerational studies. This chapter presents an overview of the development of a rapidly developing echinoderm species, *Lytechinus pictus,* from fertilization through sexual maturation. When grown at room temperature (20°C) embryos complete the first cell cycle in 90 minutes, followed by subsequent cleavages every 45 minutes, leading to hatching at 9 hours post-fertilization (hpf). The swimming embryos gastrulate from 12-36 hpf and produce the cells which subsequently give rise to the larval skeleton and immunocytes. Larvae begin to feed at 2 days and metamorphose by 3 weeks. Juveniles reach sexual maturity at 4-6 months of age, depending on individual growth rate. This staging scheme lays a foundation for future studies in *L. pictus,* which share many of the attractive features of other urchins but have the key advantage of rapid development to sexual maturation. This is significant for multigenerational and genetic studies newly enabled by CRISPR-CAS mediated gene editing.

2.2 INTRODUCTION

The diversity of animal form and function within the oceans provides a rich platform for biological discovery. Many marine organisms – including annelids[1], choanoflagellates[2], cnidarians[3], copepods[4], diatoms[5], echinoderms[6], oysters[7], sponges[8], and tunicates[9] among others – have been used in the lab, leading to a long history of significant contributions coming from marine organisms[10-17]. Echinoderms in general, and the sea urchin in particular, have played a foundational role in experimental embryology. Each female releases millions of eggs in a single spawning, fertilization occurs externally, eggs and embryos are large and relatively transparent, and development is rapid and synchronous in little more than a dish of sea water. In addition,

mRNAs, guide RNAs, morpholinos, proteins, and small molecule reporters can be easily delivered into the egg by microinjection[6], facilitating the manipulation of developmental pathways.

The most frequently used urchin species is the purple sea urchin, *Strongylocentrotus purpuratus*. Several other species including *Lytechinus variegatus, Paracentrotus lividus*, and *Hemicentrotus pulcherrimus* are also used where they are more readily available. The genome of *S. purpuratus* was first of these to be published[18] and the resulting resource[19] has greatly contributed to the utilization of this species. However, there remain major limitations to the widely used echinoderm species in modern cell and developmental biology. Perhaps the most significant of these is their limited utility in multigenerational genetic studies, namely due to their long generation times. In the case of *S. purpuratus* the generation time is at least 11 months[20,21], and perhaps as long as two years for robust reproduction[20], making the generation of genetic lines a difficult prospect.

Lytechinus pictus (aka the white or painted urchin) is an attractive alternative to *S. purpuratus*. These urchins share most of the advantages of other urchins but, unlike species such as *S. purpuratus, L. pictus* have relatively short generation times of 4-8 months[22,23]. In addition, they can be cultured at room temperature (20-22°C) and the adults have small body sizes (~1-4 cm test diameter). This rapid development and smaller adult size make the establishment of genetic lines (inbred and transgenic) an attainable goal.

L. pictus is native to the East Pacific Ocean, with a geographic range spanning from Central California to Cedros Island, Mexico[24]. This species is approximately 40 million years diverged from *S. purpuratus*, and >200 million years separated from sea urchins of the genus *Arabacia* and the sand dollar *Dendraster excentricus*[25-27]. *L. pictus* is an abundant urchin species

and has been reported to live on sandy-bottoms and in sea grass bays, as well as in and around kelp beds at depths between 2 m - 300 m[28]. Originally thought to be a distinct species from *Lytechinus anamesus*, cross-fertilization between *L. pictus* and *L. anamesus*[29], and later molecular evidence from mitochondrial DNA and bindin[24], indicates that these are one species. In the laboratory, *L. pictus* live between 7-9 years, and grow to approximately 4 cm test diameter[23].

Prior work on culturing of *L. pictus* laid a foundation for generating a standard staging scheme for this species[22,23]. However, a gap in what is known is a detailed description of embryogenesis and larval morphogenesis useful for staging embryos. Here we provide updated and detailed imaging of a developmental staging scheme for *L. pictus* including key developmental events in embryogenesis such as early cleavage, blastula stages, gastrulation, as well as summaries of later larval development, and post-metamorphic life history. We aimed to compare our staging scheme with the timing of development in *S. purpuratus* to assist in comparability across species. This staging scheme will help standardize work across labs and help establish spatial and temporal maps of major developmental events.

2.3 RESULTS

Early cleavage stages

L. pictus eggs (Fig. 2.1A) average 110 μm in diameter and form a conspicuous fertilization envelope (Fig. 2.1B) following the initiation of the cortical reaction at fertilization[30] and coinciding with changes in the electrical potential of the egg[31]. At 20°C, the first cell cycle takes 1.5 hours (Fig. 2.1C) and two subsequent symmetric cleavages (Fig. 2.1D, E) occur in the following 45-minute intervals (2.25 and 3 hpf). The fourth division, which forms the 16-cell embryo (Fig. 2.1F), occurs at 3.75 hpf and is the first asymmetric cell division, giving rise to four

macromeres and four smaller micromeres in early cleavage. Division of all the cells except the micromeres occurs next, at 4.5 hpf, yielding a 28-cell stage embryo (Fig. 2.1G). The fifth cleavage gives rise to four micromeres and four small micromeres. The micromeres ultimately give rise to the primary mesenchyme cells which form the larval skeleton while the small micromeres are presumed to directly or indirectly contribute to formation of the germ line[32]. Small micromeres of *L. pictus* have reduced efflux transport activity[33] which can be used to selectively load these cells with small molecule fluorescent substrates of transporters. By 5.75 hpf, the embryo is at the 60-cell stage (Fig. 2.1H) and at this stage, septate cell junctions are beginning to form[34], which help segregate the contents of the blastocoel from the external environment.

Expansion of the blastocoel and gastrulation

The cavity between cells of the early embryo expands quite dramatically between the fifth and tenth cleavages, and between 6.5-7.5 hpf the embryo is in the early blastula stages (Fig. 2.2A-B). The opening to the blastocoel is visible and a cluster of small micromeres, which have divided to a total of 8 cells, reside at the vegetal pole of the embryo (Fig. 2.2B, white arrow). The cavity of the blastocoel is more pronounced and changes in the morphology of the layer of cells from more rounded to an intermediate shape are apparent.

By 8 hpf the embryo is a mature blastula (Fig. 2.2C) with cell shapes more akin to a regularly spaced, columnar epithelium. Nuclei are slightly closer to the basolateral membrane, and the vegetal pole cluster of small micromeres becomes more difficult to resolve. The blastulae are ciliated at this stage and spin within the envelope, eventually hatching by 9 hpf (Fig. 2.2D). At this stage the cells at the vegetal pole will begin to thicken, forming a mesenchyme blastula stage embryo (Fig. 2.2E) by 12 hpf. Signs of delamination and the ingression of a population of

cells, the primary mesenchyme cells (PMCs) which give rise to skeletogenic cells[35,36] (Fig. 2.2F, white arrow), is evident by 15 hpf in *L. pictus*. This classic epithelial-mesenchymal transition ends the blastula phases and marks the subsequent onset of gastrulation.

Gastrulation of the embryo occurs in two main phases - primary and secondary invagination. Primary invagination is initiated following PMC ingression, when the thickened vegetal plate bends inward. This process is assisted in part by cues from bottle cells[37,38] and micromeres[39]. The majority of PMC ingression at the vegetal pole (Fig. 2.3A) is completed by 17 hpf. Bending of the vegetal plate characteristic of primary invagination, and the arrangement of ingressed PMCs into an ordered ring (Fig. 2.3B) begins at 18 hpf and is complete by 20 hpf. After primary invagination, a slight pause occurs before the pronounced elongation of the archenteron. At around 24 hpf, secondary invagination is underway and the archenteron has begun to extend through the blastocoel; secondary mesenchyme cells (SMCs), which give rise to muscle and immune cell types such as pigment cells, are evident in the blastocoel and at the tip of the archenteron at this mid-gastrula phase (Fig. 2.3C). The SMCs have long filopodia which are easily visible halfway through gastrulation. These filopodia extend towards the animal pole and can interact with surrounding cells[40] and provide one platform for cellular communication. The subset of SMCs that will further differentiate into pigment cells are migrating through the blastocoel to later embed into the ectoderm. There are also distinct arrangements of PMCs into the triradiate skeleton. By late gastrulation (Fig. 2.3D), at 30 hpf, the archenteron has crossed the space of the blastocoel and the arrangements of skeletogenic cells are clear and they have begun to form skeletal rods branching out from the origins of the triradiate (Fig. 2.3D, white arrow). The primordial germ cells (PGCs) are presumed to migrate to the left and right coelomic pouches during later gastrulation and into the prism stage (Fig. 2.3F, white arrows).

By 38 hpf embryos are at the late prism stage (Fig. 2.3F) and mineralization of skeletal rods is apparent, while the archenteron has a more pronounced bend towards the oral side of the animal indicating it is nearly ready to fuse with the ectoderm to form the mouth. Compartmentalization and functional patterning of the larval gut is ongoing throughout gastrulation, though morphologically the gut is still very simple until later in development when it differentiates further into the tripartite fore-, mid-, and hindgut.

Larval development

The first larval stage of *L. pictus* is the pluteus stage (Fig. 2.3F) which occurs by 2 days post-fertilization (dpf). At this time the larvae have three distinct gut compartments, the esophagus, stomach, and intestine (corresponding to the former fore- mid- and hindgut)[41]. Larvae at 2 days will begin to filter feed phytoplankton such as *Rhodamonas lens* from the surrounding water. The larvae also have a population of conspicuous immunocytes termed pigment cells which contain granules of the autofluorescent pigment echinochrome (Fig. 2.3F, insets). Subsequent larval development in sea urchins is divided up into stages based on the progression of key morphological features, such as the acquisition of additional pairs of arms, extension and differentiation of the left and right coeloms, formation of epaulettes and the vestibule, and elaboration of the rudiment structures[42]. Additional staging schemes detailing later larval development, focus primarily on the maturation of the rudiment with special attention to skeletal features and tissue organization of juvenile structures[43].

In *L. pictus*, the majority of larvae are all developmentally at Stage I (Fig 2.4A-I) at 3dpf. During Stage I feeding is evidenced by the red digestive remnants of *Rhodamonas* in the stomach. Between Stage I and Stage II (Fig. 2.4A-II), there is thickening of the tissue that eventually forms the oral hood (white arrow, Fig. 2.4A-II). The left and right coeloms extend

along the stomach of the larva. The extension of the left and right posterodorsal arms during Stage III larvae (Fig. 2.4A-III, yellow arrow) is apparent at 7 dpf. In *L. pictus* there is further elaboration of the oral hood and it extends to overhang the mouth. The tissue that forms the left and right preoral arms is not yet fully extended. There is mineralization of the skeletal rods that support the posterodorsal pair of arms, and evidence of invagination of the vestibule on the left side of the larva (Fig. 2.4A-III, white arrow). The tissue which forms the vestibule folds inward towards the gut, where it will eventually meet the coelomic structures on the left side of the larva (Fig. 2.4B-III, yellow dashed line).

As the posterodorsal arms continue to extend, initiation of the development of rudiment structures occurs, marking a Stage IV larva (Fig. 2.4A-IV, white arrow). The early rudiment appears as a crescent-shaped structure adjacent to the gut (Fig. 2.4B-IV, yellow dashed line). Cells that originally migrated to the left coelomic pouch during embryogenesis contribute to the rudiment, which matures into the body of the juvenile animal at metamorphosis. The completion of extension of the preoral arms is evident in a Stage V larva (Fig. 2.4A-V, yellow arrow) which occurs between 10-12 dpf in *L. pictus*. The rudiment elaborates and organizes folds of tissue into a pentagonal disc (Fig. 2.4B-V, yellow dashed line) as the larva develops into Stage V (Fig. 2.4A-V, white arrow).

As the rudiment matures, three pedicellariae are formed which will be carried through metamorphosis (Fig. 2.4A-V, grey arrows). These structures persist in a Stage VI larva (Fig. 2.4A-VI) and precede the state known as competency at 3 weeks post-fertilization (wpf). At the final stage (Stage VII) the larva contains a mature rudiment with 5 tube feet and mineralized spines that are tucked away within the larval body. The rudiment sits adjacent to the gut, and when the larvae are ready to undergo metamorphosis, the gut turns a greenish color and the

tissue acquires a scaled or textured appearance. Tube feet within the rudiment will extend and emerge from the larval body. The larvae bend the arms to the side and attach to the benthos during metamorphosis, allowing the body of the juvenile to emerge from the larva and an extensive tissue reorganization occurs[44,45] which includes shedding of skeletal rods and resorption of larval arm tissue.

Juvenile development to adulthood

At 24 hours post-metamorphosis (hpm) the newly settled juvenile (Fig. 2.5A) has 5 tube feet and 20 walking spines. The body of the animal typically contains a pale yellowish-green pigmented swirl, and sometimes remnants of larval tissue can be observed. This pigmented section, and the overall main body of the juvenile is freckled with red pigment cells retained from the larva. The pedicellariae from the larva are also retained. In newly metamorphosed animals, there are also 10 additional juvenile spines that are located on the aboral side. As juveniles continue to grow, they feed on diatoms and biofilms after formation of the teeth between 4-5 days post-metamorphosis (dpm). They will continue to develop additional tube feet and walking spines, the plates that form the test will start to fuse, and the structure of the anal plate becomes more apparent. By 4-months post-metamorphosis, the animal has a white to orange-ish appearance. The pigment cells that were once observed following metamorphosis are no longer visible. The animals eventually acquire a purple pigmentation at the base of the spines during their post-metamorphic growth period.

At four months, the range of body sizes for animals in our hands is between 1-15 mm in diameter, with growth rate post-metamorphosis being highly variable even among siblings reared under identical conditions. Although sexual maturation appears a function of both age and size,

we have been able to most consistently spawn animals that are 9-10 mm diameter, consistent with previous reports[23].

2.4 DISCUSSION

Towards a unified echinoderm development staging scheme.

This paper provides an initial staging scheme for *L. pictus*. Knowing the precise timing of specification and differentiation of important cell populations is essential to being able to manipulate the embryo and provide a common language for discussion of development. Perhaps the most well-recognized standardized staging schemes come from *Xenopus*[46-48], zebrafish[49], and chick[50]. Each of these vertebrate models has unique advantages and improved accessibility for studying specific processes in development such as nervous system development, regeneration, or formation of limb buds. Expanding on the available standardized staging schemes to include invertebrates helps to query processes less easily accessed in vertebrates. In the case of sea urchins these include fertilization, early cell divisions and gastrulation to name a few.

There have been numerous descriptions of the morphologies of other echinoderms including members of the genera *Arabacia*[51], *Echinus*[52], and *Strongylocentrotus*[53-55]. Of these, *S. purpuratus* is arguably the species with the most detailed descriptions of early cleavages, and later larval development from feeding stages through metamorphosis[42,43]. However, many of the existing descriptions are fragmentary, and do not capture all of development through the life cycle. Thus, there is need for standardized staging schemes spanning the entire life cycle, such as the one presented here.

Here we have shown that, like other echinoderms, the early stages of development in *L. pictus* occur rapidly and synchronously. There are limited morphological differences of *L. pictus* in comparison to *S. purpuratus*, the key divergence focuses on timing of important developmental structures and processes. The first asymmetric cleavage, forming the micromeres,

occurs by 3.5 hpf, small micromeres form by 5.75 hpf, and hatching happens in 9 hours. By comparison, it takes *S. purpuratus* 2-2.5 hours for the first cell division, 6.5 hours to reach the first asymmetric division forming the micromeres, and 27 hours to hatch from the fertilization envelope when cultured at 12°C[56]. Thus, experiments pertaining to early development can be completed in the course of a single day in *L. pictus*.

Progression through the larval period for *L. pictus* also occurs more rapidly and follows the progression of major events and development of core morphological structures that is observed in *S. purpuratus,* but in half the time. For example, feeding for *L. pictus* begins by 2 days, whereas feeding of *S. purpuratus* occurs at 4 days[42]. The extension of the left and right posterodorsal arms during Stage III larvae is apparent at 7 dpf. In *S. purpuratus* this stage is achieved at the earliest 18 dpf, but can take as long as 28 days[42]. The completion of extension of the preoral arms is evident in a Stage V larva between 10-12 dpf in *L. pictus*. To reach an equivalent stage in *S. purpuratus* takes 25-35 days[42]. Metamorphosis of *L. pictus* occurs at 21 days, compared to between 40-80 days in *S. purpuratus*[42,56] .

Echinoderms with similar developmental tempos include the Panamanian populations of *L. variegatus,* which have generation times, on the order of 6-8 months[57], comparable to *L. pictus*. *Temnopleurus reevesii* can also achieve maturity between 6-10 months[58], making its generation time relatively comparable to *L. pictus* under optimal conditions. Those working with *Paracentrotus lividus* have started to compile similar staging schemes[59] and that species may also have comparable generation times of approximately 5 months to earliest gamete production[28]. However, the prevalence of *L. pictus* on the West Coast of the United States, the optical transparency of their eggs, the ability to culture at room temperature (20°C), and the smaller adult body sizes all lend to preference for this species in our hands.

2.5 CONCLUSIONS

Historical and future contributions from research in L. pictus

There have already been a number of important contributions from *L. pictus*, most notably in the study of fertilization and early embryogenesis. For example, activation of *L. pictus* and *S. purpuratus* eggs with ionophores, and the resulting observations of respiration and protein synthesis provided evidence that egg activation was independent of extracellular ions and dependent on the release of intracellular calcium[31,60]. The dynamics of the endoplasmic reticulum (ER) membrane at fertilization was first described in the eggs of *L. pictus*[61]. Some of the first promoters studied in sea urchins were the metal-responsive elements and regions upstream of *metallothionein* (*MT1*) in *L. pictus*[62,63]. Sea urchins, including *L. pictus*, were widely used in the early studies of mRNA translation and protein synthesis in early development[64-66]. This included the early work of Nemer and colleagues demonstrating that a diverse array of mRNAs stored in the egg of *L. pictus* encode the newly synthesized proteins of the early embryo[67]. *L. pictus* were also used in landmark studies on the cell cycle showing changes in calcium concentration during migration of the pronuclei, the breakdown of the nuclear envelope, during the transition between metaphase and anaphase, as well as during cleavage[68].

Gene editing has now become widespread in marine organisms including sea urchins[69-73]. During this "CRISPR era"[74-76] the ability to rear juveniles, generate lines[58] and investigate later life developmental impacts resulting from early events in embryogenesis is going to be of increasing importance. The comparatively short generation time of *L. pictus* enables opportunities to create inbred lines of animals with reduced variability and stable genetic backgrounds for manipulation. The growing collection of community resources for working with *L. pictus* also make targeted molecular and genetic studies achievable. This includes a

transcriptome and fully sequenced genome (745MB) that will soon be publicly available[77]. This would provide a pathway to target ubiquitous genes in specific cell types, or to study longer-term consequences of the environment through action on development. Understanding of ecological and evolutionary development of *L. pictus* could strengthen our understanding of the processes that control development across echinoderms.

2.6 METHODS

Culturing of Larvae

Adult animals were spawned by injection of 100-150 µL of 0.55 M KCl through the peristomal membrane. Females were inverted and kept submerged in filtered sea water (FSW) during spawning, and sperm was collected undiluted and kept at 15°C until use. Eggs were washed 6-10 times with FSW and visually examined for quality before fertilization. Eggs were fertilized using 2-3 drops of a fresh sperm dilution (2 µL semen into 40 mL FSW). Eggs were checked for fertilization success, where only batches of eggs with >98% successful fertilization were used. Embryos were grown with agitation at room temperature (20°C) as previously described[77]. Briefly, embryos were grown in FSW at a concentration of 1 embryo per mL until hatching from the fertilization envelope. Upon hatching, embryos were further diluted to a concentration of 1 embryo per 3 mL. Larvae were fed the red flagellated algae *Rhodamonas lens* starting at 2 days post-fertilization (dpf) and received water changes 3-4 times a week through gentle reverse filtration. Larval health was checked visually throughout development (more frequently during embryonic stages, and on a daily basis during larval development). Cultures with >10% of larvae displaying signs of stress or poor health (i.e., asymmetry, exposed skeletal rods, prolapse of the gut), were discarded. Healthy larvae were observed and imaged as described below. Metamorphosis was induced by a 60-minute exposure to 50 mM excess KCl in

FSW, followed by 6 washes with FSW. Competent larvae were left to recover from the KCl exposure in culture vessels at 20°C with no agitation overnight. Metamorphosed juveniles were carefully transferred using a trimmed transfer pipette to petri dishes with natural biofilm growth and the diatom *Nitzschia alba*. Water changes occurred daily for juveniles, and they were observed daily for changes in morphology and growth.

Observation and Live Imaging of Development

Embryonic sea urchin development was observed, and successive cell divisions were timed under temperature control at 20°C. Embryos were imaged from fertilization through the early pluteus stage on a Zeiss LSM 700 confocal microscope (Jena, Germany) with a 20x objective using differential interference contrast (DIC). Images were captured using the Zen software suite, and micrograph measurements were added using ImageJ (National Institutes of Health, Bethesda, MD, USA). Composite DIC images were rendered from z-stacks of animals at the 8-cell stage, at late gastrulation, and at the prism and pluteus stages using Helicon Focus Pro Unlimited (v6.8.0, Helicon Soft Ltd.). Upon reaching the pluteus stage, larvae were imaged daily and scored for the number of arms present, and the development of the coelomic structures. There is reduction in synchrony of development at the onset of feeding. Therefore, we defined a developmental milestone as a time range averaged across multiple batches of larvae, where >85% of individuals had progressed to a developmental stage defined by morphological features.

Images of the larvae were captured using a 10x objective on a Zeiss Stemi 2000-C microscope with an AxioCam ERc 5s. Z-stacks of all larval stages were focus stacked using Helicon Focus Pro Unlimited (v6.8.0, Helicon Soft Ltd.). Larval Stages IV-VI were tiled, as well as focus-stacked. Imaging of the progression of internal larval structures was taken on a Zeiss LSM 700 microscope using 20x 0.8 NA plan-apo objective with DIC optics. Juveniles were

imaged live using a Leica M165F high magnification stereomicroscope with a Canon EOS 60D camera. A standard scale with 1 mm increments was used to measure post-metamorphic animals at each magnification imaged. The adult animals were imaged with a Canon EOS 60D camera. We focused our observations on cell populations of particular interest for developmental biologists including the small micromeres which later give rise to primordial germ cells[32,33,78,79], primary mesenchyme cells which contribute to skeletogenesis[35,36,80], and secondary mesenchyme cells[81] which later differentiate into immune cell populations as part of the larval and adult innate response[82,83].

2.7 ACKNOWLEDGEMENTS

Chapter 2, in full, is a reprint of the material as it appears in Developmental Dynamics 2021. Nesbit KT and Hamdoun A. The dissertation author is the primary investigator and author of this paper.

2.8 REFERENCES

1. Seaver EC, Thamm K, Hill SD. Growth patterns during segmentation in the two polychaete annelids, Capitella sp. I and Hydroides elegans: comparisons at distinct life history stages. *Evolution & development*. 2005;7(4):312-326.

2. King N, Carroll SB. A receptor tyrosine kinase from choanoflagellates: molecular insights into early animal evolution. *Proceedings of the National Academy of Sciences*. 2001;98(26):15032-15037.

3. Martindale MQ, Pang K, Finnerty JR. Investigating the origins of triploblasty:mesodermal'gene expression in a diploblastic animal, the sea anemone Nematostella vectensis (phylum, Cnidaria; class, Anthozoa). *Development*. 2004;131(10):2463-2474.

4. Rawson PD, Burton RS. Functional coadaptation between cytochrome c and cytochrome c oxidase within allopatric populations of a marine copepod. *Proceedings of the National Academy of Sciences*. 2002;99(20):12955-12958.

5. Armbrust EV, Berges JA, Bowler C, Green BR, Martinez D, Putnam NH, Zhou S, Allen AE, Apt KE, Bechner M, Brzezinski MA. The genome of the diatom Thalassiosira pseudonana: ecology, evolution, and metabolism. *Science*. 2004;306(5693):79-86.

6. Foltz K, Hamdoun A. *Echinoderms*. Academic Press; 2019.

7. Hedgecock D, Lin J-Z, DeCola S, Haudenschild CD, Meyer E, Manahan DT, Bowen B. Transcriptomic analysis of growth heterosis in larval Pacific oysters (Crassostrea gigas). *Proceedings of the National Academy of Sciences*. 2007;104(7):2313-2318.

8. Nichols SA, Dirks W, Pearse JS, King N. Early evolution of animal cell signaling and adhesion genes. *Proceedings of the National Academy of Sciences*. 2006;103(33):12451-12456.

9. Lemaire P. Evolutionary crossroads in developmental biology: the tunicates. *Development*. 2011;138(11):2143-2152.

10. Hodgkin AL, Huxley AF. Action potentials recorded from inside a nerve fibre. *Nature*. 1939;144(3651):710.

11. Skou JC. The influence of some cations on an adenosine triphosphatase from peripheral nerves. *Biochimica et biophysica acta*. 1957;23:394-401.

12. Chalfie M, Tu Y, Euskirchen G, Ward WW, Prasher DC. Green fluorescent protein as a marker for gene expression. *Science*. 1994;263(5148):802-805.

13. Heim R, Prasher DC, Tsien RY. Wavelength mutations and posttranslational autoxidation of green fluorescent protein. *Proceedings of the National Academy of Sciences*. 1994;91(26):12501-12504.

14. Metchnikoff E. *Untersuchungen über die intracelluläre Verdauung bei wirbellosen Thieren*. A. Hölder; 1883.

15. Evans T, Rosenthal ET, Youngblom J, Distel D, Hunt T. Cyclin: a protein specified by maternal mRNA in sea urchin eggs that is destroyed at each cleavage division. *Cell*. Jun 1983;33(2):389-96.

16. Hawkins RD, Abrams TW, Carew TJ, Kandel ER. A cellular mechanism of classical conditioning in Aplysia: activity-dependent amplification of presynaptic facilitation. *Science*. 1983;219(4583):400-405.

17. Shimomura O, Johnson FH, Saiga Y. Extraction, purification and properties of aequorin, a bioluminescent protein from the luminous hydromedusan, Aequorea. *Journal of cellular and comparative physiology*. 1962;59(3):223-239.

18. Sodergren E, Weinstock GM, Davidson EH, Cameron RA, Gibbs RA, Angerer RC, Angerer LM, Arnone MI, Burgess DR, Burke RD, Coffman JA. The genome of the sea urchin Strongylocentrotus purpuratus. *Science*. 2006;314(5801):941-952.

19. Cary GA, Hinman VF. Echinoderm development and evolution in the post-genomic era. *Developmental biology*. 2017;427(2):203-211.

20. Leahy PS. Laboratory culture of Strongylocentrotus purpuratus adults, embryos, and larvae. *Methods in cell biology*. Vol 27. Elsevier; 1986:1-13.

21. Leahy PS, Cameron RA, Knox MA, Britten RJ, Davidson EH. Development of sibling inbred sea urchins: normal embryogenesis, but frequent postembryonic malformation, arrest and lethality. *Mechanisms of development*. 1994;45(3):255-268.

22. Hinegardner RT. Growth and development of the laboratory cultured sea urchin. *The Biological Bulletin*. 1969;137(3):465-475.

23. Hinegardner RT. Morphology and genetics of sea-urchin development. *American Zoologist*. 1975:679-689.

24. Zigler KS, Lessios HA. Speciation on the coasts of the new world: phylogeography and the evolution of bindin in the sea urchin genus Lytechinus. *Evolution*. 2004;58(6):1225-1241.

25. Wray GA. The evolution of larval morphology during the post-Paleozoic radiation of echinoids. *Paleobiology*. 1992;18(3):258-287.

26. Gonzalez P, Lessios HA. Evolution of sea urchin retroviral-like (SURL) elements: evidence from 40 echinoid species. *Molecular biology and evolution*. 1999;16(7):938-952.

27. Wray GA, Lowe CJ. Developmental regulatory genes and echinoderm evolution. *Systematic biology*. 2000;49(1):28-51.

28. Lawrence JM. *Edible sea urchins: biology and ecology*. Elsevier; 2006.

29. Cameron RA. Two species of Lytechinus (Toxopneustidae: Echinoidea: Echinodermata) are completely cross-fertile. *Bulletin of the Southern California Academy of Sciences*. 1984;83(3):154-157.

30. Schuel H. Secretory functions of egg cortical granules in fertilization and development: A critical review. *Gamete Research*. 1978;1(3□4):299-382.

31. Steinhardt RA, Epel D. Activation of sea-urchin eggs by a calcium ionophore. *Proc Natl Acad Sci U S A*. May 1974;71(5):1915-9. https://doi.org10.1073/pnas.71.5.1915.

32. Juliano CE, Voronina E, Stack C, Aldrich M, Cameron AR, Wessel GM. Germ line determinants are not localized early in sea urchin development, but do accumulate in the small micromere lineage. *Developmental biology*. 2006;300(1):406-415.

33. Campanale JP, Hamdoun A. Programmed reduction of ABC transporter activity in sea urchin germline progenitors. *Development*. 2012;139(4):783-792.

34. Itza EM, Mozingo NM. Septate junctions mediate the barrier to paracellular permeability in sea urchin embryos. *Zygote*. 2005;13(3):255-264.

35. Piacentino ML, Ramachandran J, Bradham CA. Late Alk4/5/7 signaling is required for anterior skeletal patterning in sea urchin embryos. *Development*. 2015;142(5):943-952.

36. Schatzberg D, Lawton M, Hadyniak SE, Ross EJ, Carney T, Beane WS, Levin M, Bradham CA. H+/K+ ATPase activity is required for biomineralization in sea urchin embryos. *Developmental biology*. 2015;406(2):259-270.

37. Kimberly EL, Hardin J. Bottle cells are required for the initiation of primary invagination in the sea urchin embryo. *Developmental biology*. 1998;204(1):235-250.

38. Nakajima Y, Burke RD. The initial phase of gastrulation in sea urchins is accompanied by the formation of bottle cells. *Developmental biology*. 1996;179(2):436-446.

39. Ishizuka Y, Minokawa T, Amemiya S. Micromere descendants at the blastula stage are involved in normal archenteron formation in sea urchin embryos. *Development Genes & Evolution*. 2001;211(2).

40. Miller J, Fraser SE, McClay D. Dynamics of thin filopodia during sea urchin gastrulation. *Development*. 1995;121(8):2501-2511.

41. Annunziata R, Perillo M, Andrikou C, Cole AG, Martinez P, Arnone MI. Pattern and process during sea urchin gut morphogenesis: the regulatory landscape. *Genesis*. 2014;52(3):251-268.

42. Smith MM, Cruz Smith L, Cameron RA, Urry LA. The larval stages of the sea urchin, Strongylocentrotus purpuratus. *Journal of Morphology*. 2008;269(6):713-733.

43. Heyland A, Hodin J. A detailed staging scheme for late larval development in Strongylocentrotus purpuratus focused on readily-visible juvenile structures within the rudiment. *BMC developmental biology*. 2014;14(1):22.

44. Cameron RA, Hinegardner RT. Initiation of metamorphosis in laboratory cultured sea urchins. *The Biological Bulletin*. 1974;146(3):335-342.

45. Cameron RA, Hinegardner RT. Early events in sea urchin metamorphosis, description and analysis. *J Morphol*. Jul 1978;157(1):21-31. https://doi.org10.1002/jmor.1051570103.

46. Nieuwkoop PD. Normal table of Xenopus laevis (Daudin). *Normal table of Xenopus laevis (Daudin)*. 1956:162-203.

47. Nieuwkoop P, Faber J. Normal Table of Xenopus laevis (Daudin) Garland Publishing. *New York*. 1994;252.

48. Kakebeen A, Wills A. Advancing genetic and genomic technologies deepen the pool for discovery in Xenopus tropicalis. *Developmental Dynamics*. 2019;248(8):620-625.

49. Kimmel CB, Ballard WW, Kimmel SR, Ullmann B, Schilling TF. Stages of embryonic development of the zebrafish. *Developmental dynamics*. 1995;203(3):253-310.

50. Hamburger V, Hamilton HL. A series of normal stages in the development of the chick embryo. *Journal of morphology*. 1951;88(1):49-92.

51. Harvey EB. The growth and metamorphosis of the Arbacia punctulata pluteus, and late development of the white halves of centrifuged eggs. *The Biological Bulletin*. 1949;97(3):287-299.

52. MacBride EW. VI. The development of Echinus esculentus, together some points the development of E. miliaris and E. acutus. *Philosophical Transactions of the Royal Society of London Series B, Containing Papers of a Biological Character*. 1903;195(207-213):285-327.

53. Burke RD. The structure of the nervous system of the pluteus larva of Strongylocentrotus purpuratus. *Cell and tissue research*. 1978;191(2):233-247.

54. Burke RD. Development of pedicellariae in the pluteus larva of Lytechinus pictus (Echinodermata: Echinoidea). *Canadian Journal of Zoology*. 1980;58(9):1674-1682.

55. Burke RD. Morphogenesis of the digestive tract of the pluteus larva of Strongylocentrotus purpuratus: shaping and bending. *International Journal of Invertebrate Reproduction*. 1980;2(1):13-21.

56. Adams NL, Heyland A, Rice LL, Foltz KR. Procuring animals and culturing of eggs and embryos. *Methods in cell biology*. Vol 150. Elsevier; 2019:3-46.

57. Pawson DL, Miller J. Studies of genetically controlled phenotypic characters in laboratory-reared Lytechinus variegatus (Lamarck)(Echinodermata: Echinoidea) from Bermuda and Florida. Proceedings of the International Echinoderm Conference, Tampa Bay. AA Balkema, Rotterdam1982. p. 165-171.

58. Yaguchi S. Temnopleurus as an emerging echinoderm model. *Methods in cell biology*. Vol 150. Elsevier; 2019:71-79.

59. Croce J. *P. lividus* Stage Ontology. In: Nesbit KT, Hamdoun A, editors. Email thread of echinoderm staging and *P. lividus* development ed2019.

60. Steinhardt R. Intracellular free calcium and the first cell cycle of the sea-urchin embryo (Lytechinus pictus). *Journal of reproduction and fertility Supplement*. 1990;42:191.

61. Terasaki M, Jaffe LA. Organization of the sea urchin egg endoplasmic reticulum and its reorganization at fertilization. *J Cell Biol*. Sep 1991;114(5):929-40. https://doi.org10.1083/jcb.114.5.929.

62. Cserjesi P, Fairley P, Brandhorst BP. Functional analysis of the promoter of a sea urchin metallothionein gene. *Biochem Cell Biol*. Oct-Nov 1992;70(10-11):1142-50.

63. Cserjesi P, Fang H, Brandhorst BP. Metallothionein gene expression in embryos of the sea urchin Lytechinus pictus. *Molecular Reproduction and Development: Incorporating Gamete Research*. 1997;47(1):39-46.

64. Brandhorst BP. Two-dimensional gel patterns of protein synthesis before and after fertilization of sea urchin eggs. *Dev Biol*. Sep 1976;52(2):310-7.

65. Wu RS, Wilt FH. Poly A metabolism in sea urchin embryos. *Biochemical and biophysical research communications*. 1973;54(2):704-714.

66. Lee JJ, Calzone FJ, Britten RJ, Angerer RC, Davidson EH. Activation of sea urchin actin genes during embryogenesis: Measurement of transcript accumulation from five different genes in Strongylocentrotus purpuratus. *Journal of molecular biology*. 1986;188(2):173-183.

67. Nemer M, Infante AA. Messenger RNA in early sea-urchin embryos: size classes. *Science*. 1965;150(3693):217-221.

68. Poenie M, Alderton J, Tsien RY, Steinhardt RA. Changes of free calcium levels with stages of the cell division cycle. *Nature*. 1985;315(6015):147.

69. Lin C-Y, Su Y-H. Genome editing in sea urchin embryos by using a CRISPR/Cas9 system. *Developmental biology*. 2016;409(2):420-428.

70. Shevidi S, Uchida A, Schudrowitz N, Wessel GM, Yajima M. Single nucleotide editing without DNA cleavage using CRISPR/Cas9□deaminase in the sea urchin embryo. *Developmental Dynamics*. 2017;246(12):1036-1046.

71. Wessel GM, Kiyomoto M, Shen T-L, Yajima M. Genetic manipulation of the pigment pathway in a sea urchin reveals distinct lineage commitment prior to metamorphosis in the bilateral to radial body plan transition. *Scientific reports*. 2020;10(1):1-10.

72. Pickett C, Zeller RW. Efficient genome editing using CRISPR□Cas□mediated homology directed repair in the ascidian Ciona robusta. *genesis*. 2018;56(11-12):e23260.

73. Nakanishi N, Martindale MQ. CRISPR knockouts reveal an endogenous role for ancient neuropeptides in regulating developmental timing in a sea anemone. *Elife*. 2018;7:e39742.

74. Doudna JA, Charpentier E. The new frontier of genome engineering with CRISPR-Cas9. *Science*. 2014;346(6213):1258096.

75. Peng Y, Clark KJ, Campbell JM, Panetta MR, Guo Y, Ekker SC. Making designer mutants in model organisms. *Development*. 2014;141(21):4042-4054.

76. Hsu PD, Lander ES, Zhang F. Development and applications of CRISPR-Cas9 for genome engineering. *Cell*. 2014;157(6):1262-1278.

77. Nesbit KT, Fleming T, Batzel G, Pouv A, Rosenblatt HD, Pace DA, Hamdoun A, Lyons DC. The painted sea urchin, Lytechinus pictus, as a genetically-enabled developmental model. *Methods Cell Biol*. 2019;150:105-123. https://doi.org10.1016/bs.mcb.2018.11.010.

78. Pehrson JR, Cohen LH. The fate of the small micromeres in sea urchin development. *Developmental biology*. 1986;113(2):522-526.

79. Juliano CE, Swartz SZ, Wessel GM. A conserved germline multipotency program. *Development*. 2010;137(24):4113-4126.

80. Ettensohn CA. Cell interactions and mesodermal cell fates in the sea urchin embryo. *Development*. 1992;116(Supplement):43-51.

81. Tamboline CR, Burke RD. Secondary mesenchyme of the sea urchin embryo: ontogeny of blastocoelar cells. *Journal of Experimental Zoology*. 1992;262(1):51-60.

82. Smith LC, Rast JP, Brockton V, Terwilliger DP, Nair SV, Buckley KM, Majeske AJ . The sea urchin immune system. *Invertebrate Survival Journal*. 2006;3(1):25-39.

83. Ho EC, Buckley KM, Schrankel CS, Schuh NW, Hibino T, Solek CM, Bae K, Wang G, Rast JP. Perturbation of gut bacteria induces a coordinated cellular immune response in the purple sea urchin larva. *Immunology and cell biology*. 2016;94(9):861-874.

Glossary

Coelomic pouches
Mesodermal left and right structures that roll off the tip of the archenteron during late gastrulation. The primordial germ cells migrate to the pouches. The left pouch gives rise to the rudiment that becomes the juvenile urchin after metamorphosis.

Gonopore
A genital pore located on the aboral surface of the animals, through which egg or sperm are released during spawning.

Madreporite
A plate on the aboral surface of the sea urchin that serves as an entry point for sea water into the water vascular system.

Micromeres
Four small cells formed by unequal division at the fourth cleavage, located at the vegetal pole of the embryo at the 16 cell stage.

Oral hood
A ciliated extension of tissue that overhangs the opening to the larval mouth which helps direct a current to sort and collect food particles.

Pedicellariae
Three ectodermal claw-like appendages located on the larval body and the juvenile body which are used for grasping and defense.

Pigment cell
A subset of secondary mesenchyme cells containing the purple/red napthoquinone pigment echinochrome A. These cells are migratory and are an important component in innate immune responses of the larva.

Primary mesenchyme cell (PMC)
A population of skeletogenic cells that are first to invade the blastocoel at the initiation of gastrulation. They fuse together as syncytia and secrete the skeletal rods.

Rudiment
A disc-shaped structure that forms adjacent to the gut during larval development in the sea urchin. This structure is everted from the larval body to form the juvenile urchin at metamorphosis.

Secondary mesenchyme cell (SMC)
A population of cells that are second to invade the blastocoel during gastrulation. These cells differentiate into the various immune cell types found in the sea urchin larva

Small micromeres
A group of four small cells formed through unequal division of the micromeres at the 28-32 cell stage. These cells are located at the vegetal pole and differentiate into PGCs during development.

Spicule
Mineralized structures that support the larval body and are composed of calcite crystal and amorphous calcium carbonate, and are deposited by PMCs.

Vestibule
A small cavity formed on the left side of the larva from the invagination of the ectoderm during development. The vestibule gives rise to presumptive adult ectodermal structures.

Axis Orientation

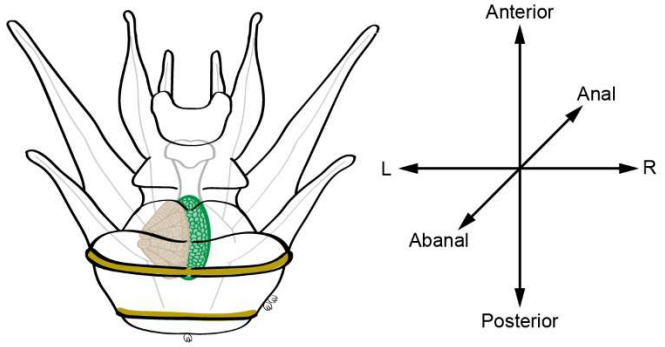

Figure 2.0. Glossary. Sea urchin terminology. List of important terms used in discussion of sea urchin development and morphology. Illustration depicts a Stage VI larva with some of the major morphological features labelled. This panel also depicts the larval axes, and how larvae are oriented in subsequent figures.

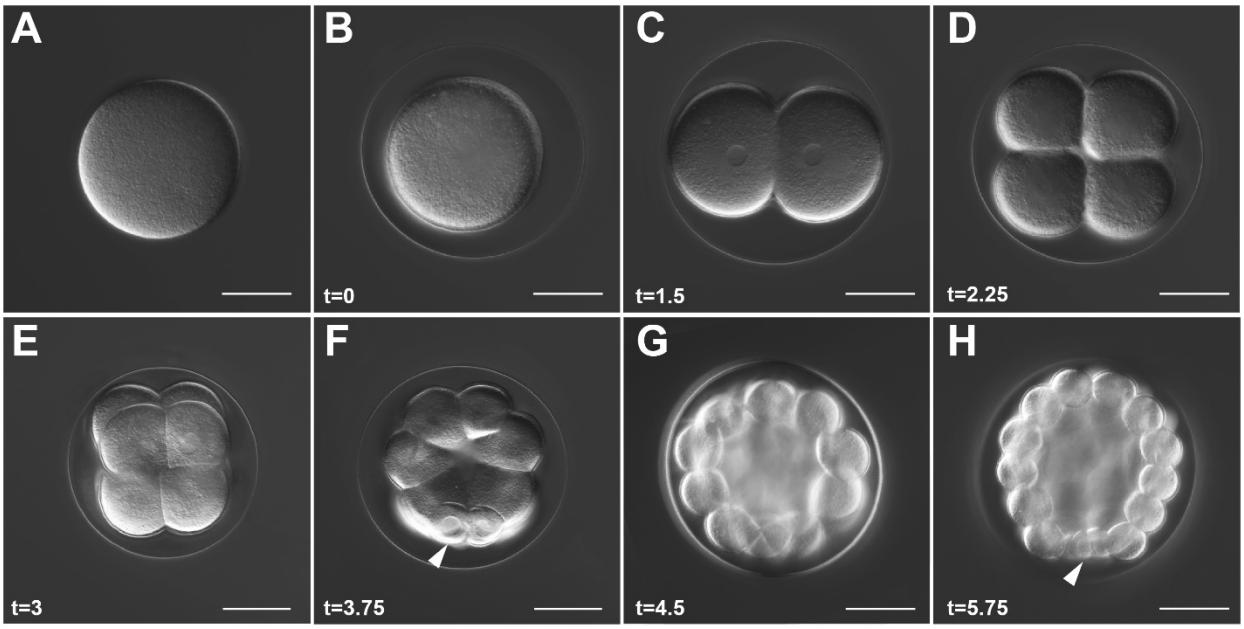

Figure 2.1. Early cleavages, A-V axis determination, and formation of the micromeres. A) Unfertilized egg. **B)** Zygote. **C)** 2-cell embryo. **D)** 4-cell embryo. **E)** 8-cell embryo. **F)** 16-cell embryo, white arrow points to the micromeres. **G)** 28-cell embryo. **H)** 60-cell embryo, white arrow points to the small micromeres. For all panels, scale = 50 μm. Time points listed in hours post-fertilization (hpf). All are oriented with the vegetal pole, where discernable (from the 16-60 cell stage), pointing down.

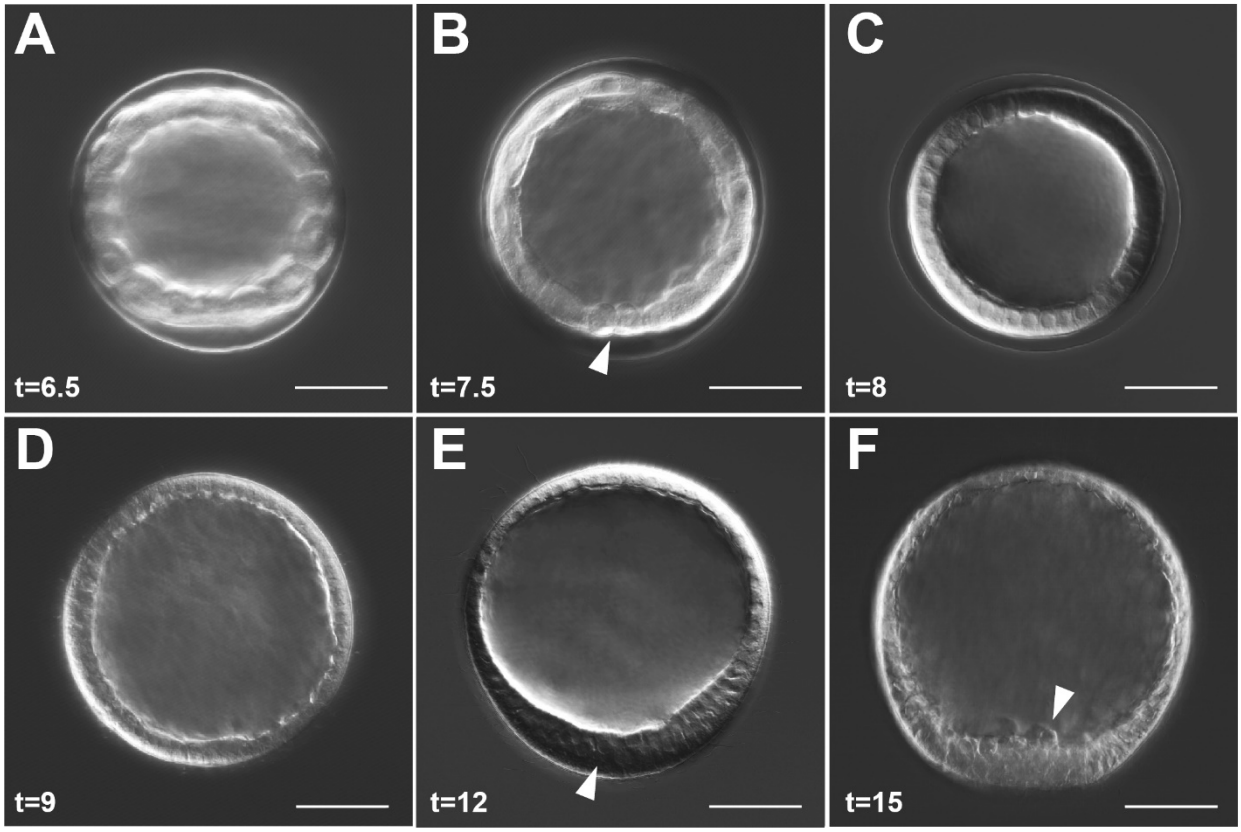

Figure 2.2. Blastula stages, hatching, and early ingression of PMCs in *L. pictus*. A) Early blastula stage. **B)** Embryos begin to demonstrate cell shape changes, and the small micromeres (white arrow) are visible at the vegetal pole. **C)** Blastula pre-hatching. **D)** Hatched blastula. **E)** White arrow points at the thickening at the vegetal plate. **F)** White arrow points at PMCs ingressing into the blastocoel, which are visible at the vegetal pole. For all panels, scale = 50 μm. Times listed in hours post-fertilization (hpf).

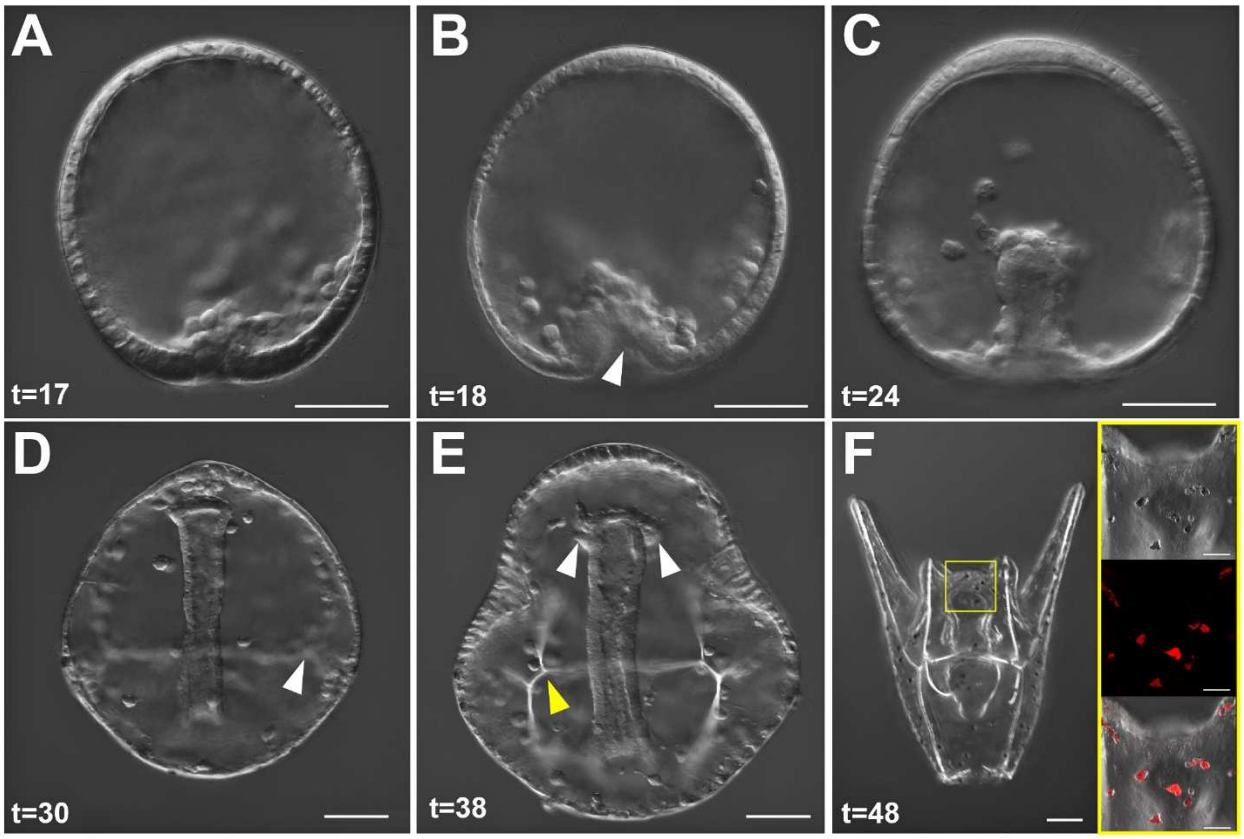

Figure 2.3. Gastrulation, SMC differentiation, and skeletal rod formation in *L. pictus*. A) First signs of invagination of the vegetal pole are apparent after ingression of PMCs. **B)** Primary gastrulation completes and the vegetal pole is turned inward as indicated by the white arrow. A population of SMCs ingress into the blastocoel and the PMCs begin to arrange around the developing archenteron. **C)** During mid-gastrulation the archenteron moves through the blastocoel and pigment cell precursors will migrate through the blastocoel to embed into the ectoderm during mid-late gastrulation. **D)** Late gastrulae have clear arrangement of PMCs and triradiate spicules which will further develop into the larval skeleton (white arrow). The archenteron has nearly reached the oral side of the animal. **E)** Evidence of the forming coelomic pouches (white arrows) on either side of the archenteron preclude the fusion of the mouth with the oral ectoderm during the prism larval stage, and the arms begin to bud out from the larval body as the skeletal supports (yellow arrow) are further elaborated. **F)** Composite stack of early pluteus larva in abanal view. The gut has differentiated into three parts. A yellow box surrounds the region of the larva shown in the inset. Inset shows DIC, fluorescence, and overlay of pigment cells which contain the autofluorescent pigment echinochrome A and are embedded into the ectoderm of the larva. For all panels, scale = 50 µm. Inset panels scale = 20 µm. Times listed in hours post-fertilization (hpf).

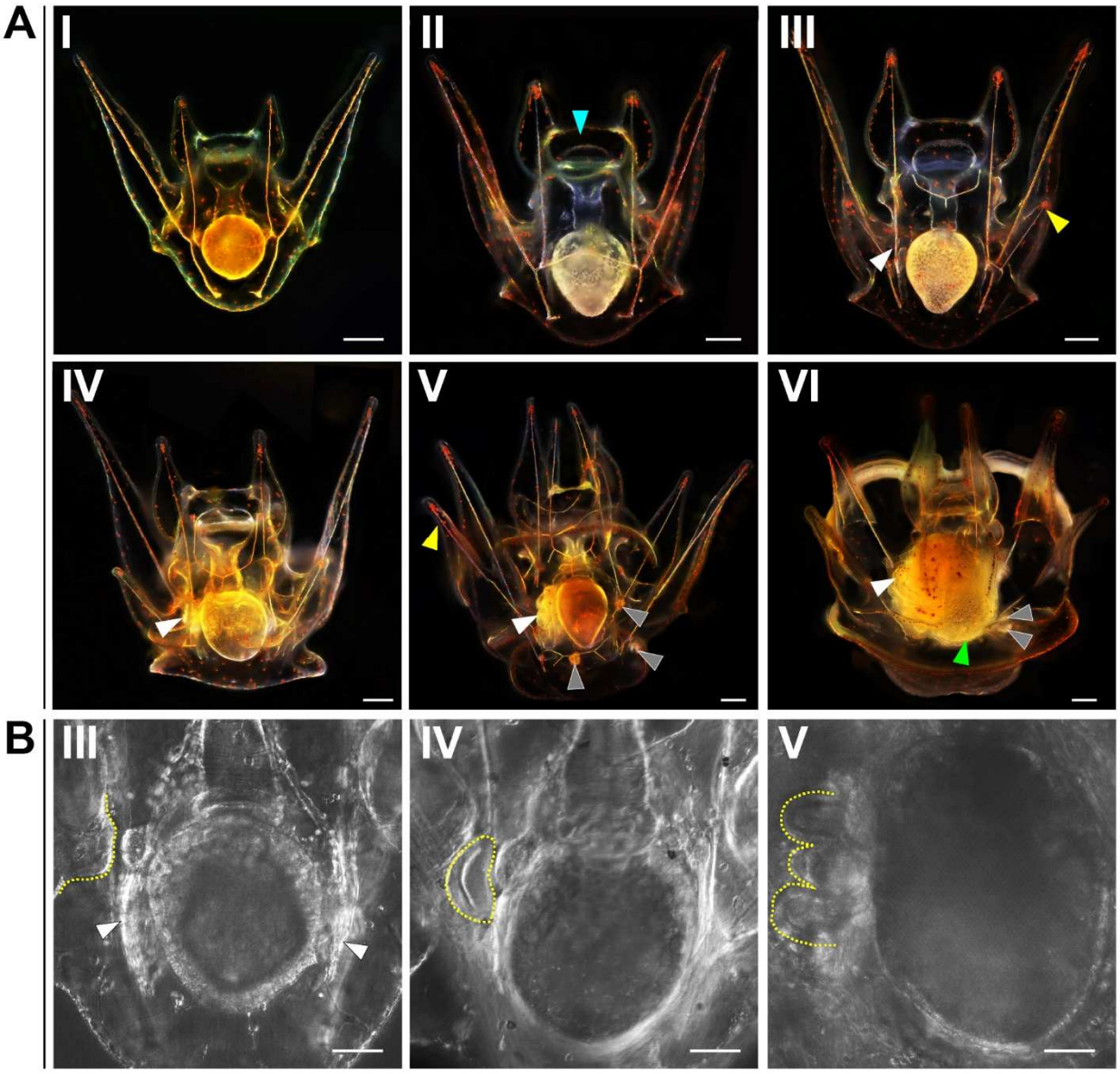

Figure 2.4. Larval staging of *Lytechinus pictus*. A) Scale = 250 microns. Stages I-VI of *L. pictus*. Blue arrow in 4A-II points to the oral hood tissue. White arrow in 4A-III marks the vestibular invagination. Yellow arrow in 4A-III marks the right posterodorsal arm. White arrow in 4A-IV marks the rudiment initiation adjacent to the gut. White arrow in 4A-V marks the pentagonal disc, while grey arrows denote the three pedicellariae, and the yellow arrow marks the fully formed left posterodorsal arm. White arrow in 4A-VI marks the fully formed rudiment, the green arrow marks the gut which now has a more textured appearance, and the grey arrows mark the two pedicellariae that are in view out of three. **B)** Scale = 50 microns. High magnification DIC imaging of the progression of development of coelomic structures during larval Stage III, IV, and V (from left to right). The dashed yellow lines highlight the vestibular invagination (left panel), the crescent-shaped initiation of the rudiment (middle), and the more elaborated organization of the rudiment tissues into the pentagonal disc (right panel).

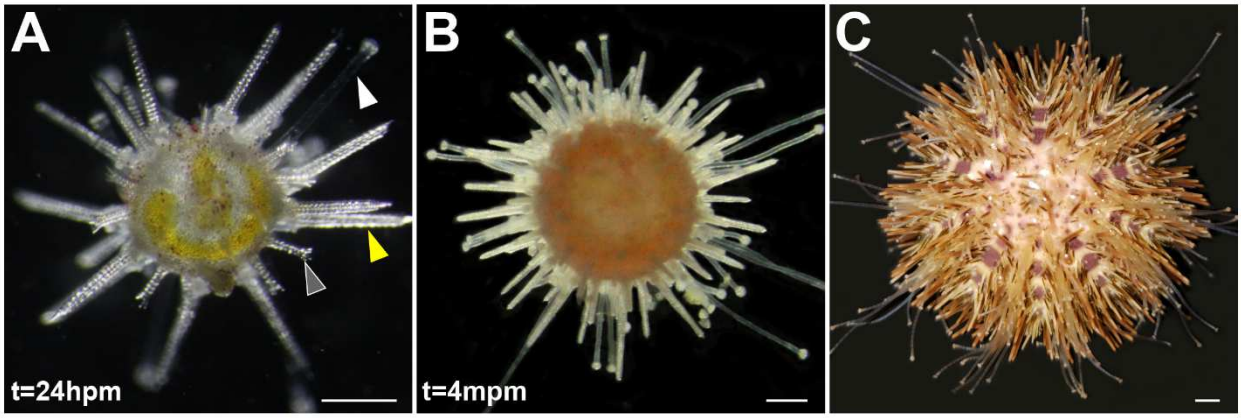

Figure 2.5. Post-metamorphic maturation of *L. pictus*. A) Juvenile at 24 hours post-metamorphosis (hpm). There are five tube feet (white arrow) as well as 20 walking spines (yellow arrow) and 10 juvenile spines (grey arrow). **B)** 4 months post-metamorphosis (mpm); **C)** Sexually mature adult. For all panels, scale = 0.5 mm.

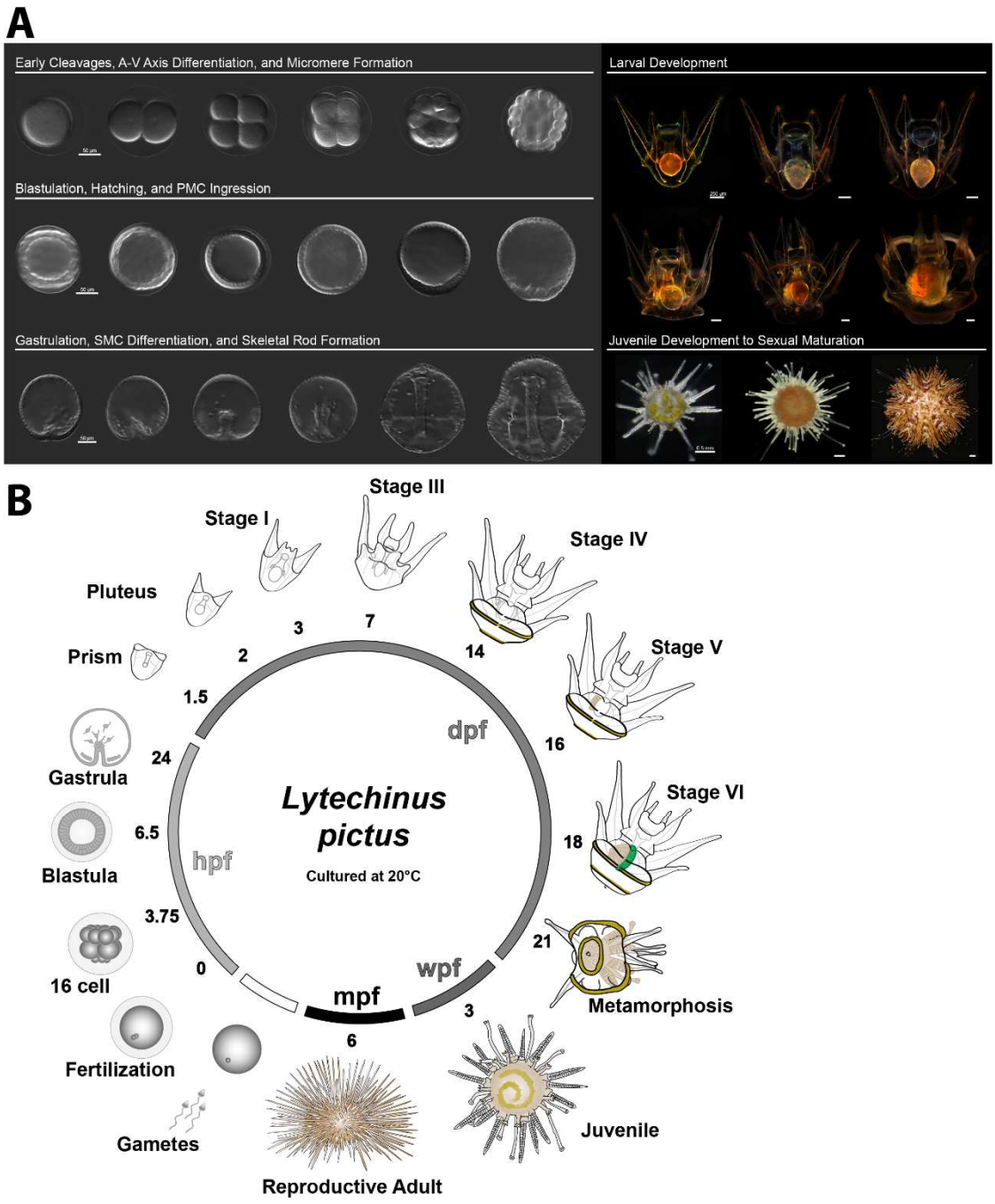

Figure 2.6. Summary of *L. pictus* development. Schematic of the *L. pictus* life cycle, illustrations are not to scale and time points are listed as the average time for >85% of individuals in a batch to reach a particular developmental stage.

CHAPTER 3

Small molecule transporters in *Lytechinus pictus* as potential targets of environmental and developmental chemical exposures

3.1 ABSTRACT

ATP-binding cassette transporter (ABCs) and solute carrier transporter (SLCs) gene families encode major proteins involved in small molecule transport (SMT). These proteins handle diverse signaling molecules important for cellular communication as well as have well-recognized roles in drug disposition and handling of toxic molecules. It is presumed that most of these transporters evolved from microbial proteins adapted for transport of lipids and toxic xenobiotics, and later became more specialized/selective in ligands with developmental functions. Thus, these proteins are situated at the interface of protective and developmental roles and are essential for diverse physiological processes. Members of the SMT system belong to gene families including the SLC22, SLCO, SLC47, and ABC transporter groups. They include well known proteins such as P-glycoprotein (P-gp/ABCB1) which is best known for its role in drug resistance of cancers, as well as ABCC4/5 which translocates well-known signal molecule ligands such as cyclic nucleotides and prostaglandins. Here we present the SMT system of *L. pictus* which includes a number of disease-relevant genes. We identified candidates spanning all of the major subfamilies involved in SMT. These data serve, in part, as validation of the automated annotation pipeline for the genome and as a launching point for functional study. We expect that these results will shed light on the selective pressures driving evolution of the SMT, and point to the physiological roles of these proteins.

3.2 INTRODUCTION

The movement of small molecules is important for a variety of different biological processes, especially within development, environmental sensing, and disease states. For example, the slime mold *Dictyostelium* relies on movement of cAMP to direct stalk formation[1]. The movement of neurotransmitters such as GABA help to regulate transmission of action

potentials along nerve cells[2]. Glucose is fed into aerobic glycolysis through upregulation of the facilitative glucose transporter in almost all cancers[3]. The ways in which small molecules can be moved by the cell is a matter of great importance because this directed movement of ligands is tightly regulated in space and time and accomplishes diverse physiological tasks. The machinery responsible for the movement of these important ligands are membrane transporters.

Membrane transporters can be grouped into three major categories: channels, carriers, and pumps[4]. The primary focus of this chapter will be on subsets of genes from the carrier and pump families – namely, the solute carrier transporters (SLCs) and ATP-binding cassette transporters (ABCs).

There are over 400 SLCs which have been discovered, and these genes can be grouped into 55 different subfamilies[5]. Overall, the proteins major mode of action can be described in one of three ways – as a cotransporter, an exchanger, or as facilitated transport. Here I explore the SLCs from the SLC22 (OAT/OCT)[6,7], SLCO (OATP)[5], and SLC47 (MATE)[8] subfamilies which are responsible for moving organic anions/cations and also have demonstrated roles in the movement of xenobiotic substances including drugs and toxic molecules.

ABC transporters are another larger superfamily of genes that can be grouped into subfamilies ABCA-H[9]. These proteins occur in all organisms and are best appreciated for their roles in drug resistance of cancers. Generally, the ABC- B, C, and G subfamilies, which contain multidrug resistance (MDR), multidrug resistance associated (MRP), and breast-cancer resistance (BCRP) proteins, play a major role in the handling of xenobiotics[10]. Other subfamilies play critical roles in lipid and cholesterol transport (ex. ABCA members)[11], antigen presentation (ABCB members TAP1/2)[12-14], ion movement (ABCC7/CFTR)[15], movement of acyl-CoA (ABCD members)[16,17], and development[18-22].

Collectively the ABC and SLC families for a system of regulated transport that handle a diverse and often overlapping array of signaling ligands, nutrients, metabolites, toxins and xenobiotics, which ultimately facilitate communication at all levels of biological organization (i.e. cells, tissues, organs, organ systems, and organisms)[23]. This remote-sensing and signaling system helps to maintain homeostasis and mediate interactions with the environment. The signaling networks can be disrupted by exposure to toxicants that accumulate and damage cells or inhibit mechanisms of cellular transport. For example, flame retardants like PBDE-100 can bind to and inhibit the function of ABCB1/P-gp[24]. Similarly, organophosphorus pesticides have been shown to inhibit the function of SLC47A1 (MATE1) and other SLCs from the OAT family[25]. Thus, these transporters are potential targets of exposure to natural and manufactured chemicals and other toxic molecules in the environment.

Given the importance of the small molecule transport system, I sought to characterize the ABC, and a subset of SLC, transporters in *L. pictus*. This was part of an effort to make molecular resources available to the research community and enable more widespread use of this echinoderm model species. These annotations are also an important contribution for assessing the completeness and quality of the newly generated, publicly available 998.9 Mb genome[26] of *L. pictus* and are part of a key resource for further investigations into developmental biology, evolution of SMT, and ecotoxicology.

3.3 RESULTS

As part of the effort to assess the completeness and quality of the *L. pictus* genome, we manually examined the annotations of the ATP-Binding Cassette (ABC) transporter superfamily. This group of genes has a number of features which make it attractive for assembly assessment: The ABC transporters are a large multigene family[9], they include large genes which can span

several hundred kilobases[27], and they are well characterized in a related echinoderm, *S. purpuratus*. The proteins are essential for ion regulation[28], developmental signaling[20], cell migration[19], antigen presentation[29], and in humans, mutations in many of these genes are associated with disease[30-34] (Table 3.1).

There are 54 *L. pictus* ABC gene candidates in our assembly (Table 3.2), spanning all subfamilies of ABCs found in sea urchins (A-H)[35,36]. These include putative orthologs of disease-relevant genes such as ABCA1, ABCB1, ABCC1, ABCC9, ABCD1 and ABCG5 (Table 3.1). To assess the quality of individual annotations we focused on the ABCC subfamily (Fig. 3.1). A feature of ABC families in the sea urchins is the relative expansion of the ABCC family as compared to humans[37]. Consistent with this, *L. pictus* have 20 putative C-subfamily candidates compared to the 12 ABCC members in human (Table 3.3). Of these C-subfamily members in urchins, the *S. purpuratus* ABCC1 contains 29 exons and spans approximately 45.5 kb. We identified a *L. pictus* ABCC1 candidate of 31 exons and 59.9 kb, encoding a 1,471 aa open reading frame. Similarly, the *S. purpuratus* ABCC4a gene, encoding another major plasma membrane transporter, has 27 exons spanning approximately 43.8 kb in length. A corresponding annotation for this isoform of ABCC4 in *L. pictus* is 24 exons and approximately 31.7 kb long, encoding a 1,334 aa open reading frame.

Another group of particular interest among the ABC transporter annotations were the ABCB1 and ABCB4 genes which are full-length transporters with high homology to each other. For example, in humans, ABCB1 and ABCB4 share 75.8% identity, with even greater conservation in the nucleotide binding domains (NBD) (86.8% identical at NBD1, and 88.5% identical at NBD2). ABCB1a and ABCB1b paralogs in mouse are 83.9% identical to each other, and 73.6% and 69.8% identical to murine ABCB4 respectively. The sea urchin *S. purpuratus* has

multiple P-gp like ABC transporters: ABCB1a, ABCB1b, and ABCB4a[36,38,39]. We have identified an ABCB1a and paralogs in *L. pictus* as well. Of three candidate B1-like transporters, phylogenetic analysis (Fig. 3.2) and alignment of the peptide sequences allowed us to distinguish between these highly similar proteins. The *Lytechinus* ABCB1a (henceforth referred to as LpB1a) is 28 exons long and spans 150 kb in the genome, encoding a 1321 aa long peptide[40]. As anticipated, LpB1a clusters with the *S. purpuratus* ABCB1a and other vertebrate P-gp proteins. Other B1 and B4 like genes cluster with protostome and other invertebrate proteins. This further indicates that the sea urchin B1a may serve functional roles more similar to mammalian P-gp.

Among the SLC transporters that were included in this study, we were able to identify 31 transporters from the SLC22, SLC47 and SLCO subfamilies (Table 3.4). For the SLC22 (OAT/OCT) subfamily, we identified 20 candidate sequences. More of these candidate sequences are predicted cation transporters, supporting previous work that suggests a relative expansion of this family in sea urchin and limited presence of anion transporters[35,41]. Key among the SLC22 candidates identified are SLC22A1 and SLC22A5 which are important organic cation transporters. The *L. pictus* homolog of SLC22A1 (LPI_026177) is 10 exons long and spans ~19.5 Kb in the genome to encode a 518 aa protein. The human SLC22A1 in contrast is 38.7 Kb in length, spanning 11 exons and encoding a 554 aa protein[42]. The homolog of SLC22A5 in *L. pictus* (LPI_024901) is 8 exons long and covers ~8.6 Kb of the genome, encoding a 392aa long protein. In humans, SLC22A5 is 10 exons long[43], spanning a ~25.9 Kb region of the genome to yield a 557 aa protein[44].

From the SLC47 subfamily, which is involved in multidrug and toxicant efflux (MATE), we identified a single member (LPI_010431). This gene is 15 exons long, covering ~17.6 kb of the genome and encodes a peptide that is 658 aa long. In contrast to the singular MATE

candidate in *L. pictus*, humans have two SLC47 proteins, SLC47A1 (MATE1) and SLC47A2 (MATE2). Human MATE1 is 17 exons long and spans ~45.1 kb on chromosome 17 encoding a 570 aa peptide. Human MATE2 has 22 exons, spanning ~38.2 kb on chromosome 17 and encoding a 602 aa peptide. Other invertebrate MATE and MATE-like proteins are sister-taxa to sea urchin MATE proteins, and are distinct from the vertebrate MATE groupings (Fig. 3.3). Given the divergence between vertebrate and invertebrate MATE proteins, and even between teleost and other vertebrate MATEs[45], it is difficult to say which MATE the *L. pictus* candidate is most similar to. Thus, additional work characterizing the synteny, subcellular localization, expression territories, and substrate specificity may help to clarify whether the urchin MATE is more similar to MATE1 or MATE2 or whether its structural and functional role is distinct indicative of more ancient evolutionary origins.

There are 10 candidates annotated from the *L. pictus* genome that encode putative SLCO (OATP) transporters (Table 3.4), close in number to the 11 SLCO genes identified in humans. In *L. pictus*, the SLCO2A1 gene (LPI_014926) is a 10 exon gene that is ~18.9 Kb and encodes a 556 aa long protein. The human SLCO2A1 gene is 16 exons spanning ~119.4 KB of the genome and produces a protein that is 643 aa long. The *L. pictus* homolog of SLCO5A1 (LPI_013851) is composed of 12 exons and spans ~30.5 Kb of the genome encoding a 748 aa protein. In comparison, the human SLCO5A1 is 13 exons long and spans ~168 Kb yielding a protein that is 848 aa long.

3.4 DISCUSSION

Assessment of the Lytechinus pictus genome assembly

Collectively these results are in agreement with the outputs of the automated pipeline annotations for the *L. pictus* genome, and the significant hits of *L. pictus* gene models against

RefSeq and *S. purpuratus* protein databases, supporting the 'completeness' of this assembly and annotation. The chromosomal-level resolution of this genome assembly[26] will be a valuable resource for further functional and comparative study, especially in consideration of the high contiguity assemblies of related species such as *L. variegatus*[46] and *S. purpuratus*[47]. The evolutionary placement of *L. pictus* and practical advantages of working with this species in the lab set this model up as a key experimental system for the scientific community – in particular for the generation of transgenic lines of animal[40] as this model is well-suited to laboratory culture through multiple generations[48-50]. Collectively these molecular resources represent an important contribution for the field of sea urchin cellular, molecular, and developmental biology.

The Lytechinus pictus small molecule transport system

Small molecule transporters compose an important signaling network that is responsible for a diverse array of physiological tasks. The subsets of genes from the ABC and SLC transporters presented here are important for the disposition of a diverse array of endo- and exogenous molecules including steroids, lipid signals, cyclic nucleotides, dietary toxins and metabolites, as well as anthropogenic chemicals and drugs. In addition to the importance of this data for informing on what ligands are potentially able to be moved by the cell and by what players, these data also give us better insight into the evolution of SMT across large phylogenetic distances. Sea urchins are poised at a major evolutionary branching point as a basal deuterostome. Thus, aspects of SMT in urchins shares some SMT features with more derived organisms (such as the grouping of urchin ABCB1/P-gp with mammalian ABAB1) and are highly divergent with respect to other components of their SMT systems (such as the expansion of ABCC transporters or the clustering of sea urchin MATE with other invertebrates). These differences may reflect changes coinciding with important branching points in developmental

mode, signaling strategies, or other major evolutionary transitions. Further examination of these evolutionary relationships across broad phylogenetic distances may also inform on the selective pressures driving evolution of SMT systems and point to functional roles of these proteins in development and protection of the cell and embryo.

SMTs as targets of exposure

The interactions of SMTs with man-made chemicals and therapeutics is a continually growing area of interest. Anthropogenic chemicals and drugs are widely used in our everyday lives in manufacturing, personal care products, agriculture and more, and are essential for the effective treatment of diseases. Despite the number of ways in which chemicals have improved our lives, many of these compounds are highly toxic and have major negative consequences on human health. Exposures to chemicals from anthropogenic sources are continuous, pervasive, and by definition unintentional and thus have the potential to influence the function of SMT networks in varied, and sometimes even conflicting, ways.

Determining the role of specific genes or the influence of specific individual chemicals on SMT under realistic exposure conditions is a challenging undertaking. However, the availability of genetic tools, such as CRISPR-Cas gene editing technologies and transgenic SMT knockout animal lines in *L. pictus*, coupled with the ease of functional assay in this model help us get closer to understanding the complex SMT-mediated interactions between the cell or embryo and the environment. In many cases it is helpful to think of these interactions as a balancing act; a cell or embryo must protect itself against a seemingly endless barrage of dynamic environmental insults while simultaneously coordinating complex developmental and homeostatic signals. The contributions of individual SMTs can at times be geared more towards protective roles, and at others be more developmentally relevant. Similarly, individual chemical

interactions can have developmental or cytotoxic impacts, and these effects are not necessarily mutually exclusive. With a now-defined suite of players composing an SMT network in a genetically tractable model, the individual roles of specific SMTs and the impacts of specific chemical constituents of environmentally relevant exposures conditions can be better targeted for investigation.

3.5 CONCLUSIONS

Significance of SMT in L. pictus

The newly available genome of *L. pictus* is a valuable resource for the echinoderm community and enables studies at the intersection of cellular and developmental biology, toxicology, immunology, and more. Molecular resources such as these enable the scientific community to ask more targeted questions about the role of individual gene in diverse physiological process. Moreover, high quality data sets such as this enable deeper comparative perspectives across short and long phylogenetic distances. Echinoderms are also basal deuterostomes, occupying an important position in evolutionary history, and can provide valuable insight into how the movement of small molecules has changed at major transition points in developmental mode (e.g., the protostome-deuterostome divergence). The data presented here on SMTs support the quality and accuracy of the automated assembly. Communication networks like SMTs are critical for understanding cell interactions within the embryo and with the environment. As such, these data also lay the groundwork for more specific perturbations of SMTs in a whole-embryo model to better understand their functional contributions to protection and development *in vivo*. This is especially important because environmental exposures are widespread and pervasive. Therefore, animals and humans need to balance protective strategies with the requirements for development and homoeostasis.

Determining the specific influences of individual chemicals on individual gene targets is a multifaceted challenge, and may not always be reflective of the real-life exposure scenarios that humans and animals encounter in the environment. However, these data which define a SMT system in a whole-embryo model can be leveraged for environmentally-relevant exposures and targeted gene perturbations using CRISPR gene-editing technologies. This better enables us to understand how SMT networks influence diverse biological processes, and to further understand the role of these proteins as targets of drug and chemical exposure.

3.6 METHODS

Genome mining

To identify putative homologs of known xenobiotic transporters from the ABC and SLC gene families, known sequences from human, mouse, and purple sea urchin (*S. purpuratus*) were curated into query lists. Sequences from the query list were used as input for pBLAST searches of the second assembly of the *Lytechinus pictus* genome gene models. We also used the list of queries to mine through the *L. pictus* transcriptome's translated peptides, and mapped transcriptome results to the gene models. Results from the BLAST searches were curated into a hit table, and redundant sequences and low-quality hits were eliminated. Hits were ultimately deemed positive via sequence homology to known ABC or SLC transporters and through structural analysis. The length of the protein encoded by each transcript or gene model is also included in these tables as well as the genomic coordinates of the gene models for all identified *L. pictus* ABC and SLC candidates.

Analysis of protein conservation and structure

To help confirm the identity of the putative *L. pictus* ABC and SLC candidates identified from the genome and transcriptome mining, we analyzed the amino acid sequences of the

deduced protein encoded by our candidate hits. We used protocols that have been previously employed for the characterization of protein structural motifs, such as identification of transmembrane domains (TMHMM and TOPCONS), and other motifs (SMART). Default parameters for all of these programs were selected when performing our analysis.

Sequence similarity

To determine the protein most similar to our candidates identified from the *L. pictus* genome, we performed reciprocal pBLAST searches with each of our candidate sequences as the query against annotated proteins in NCBI and SwisProt databases. We excluded hypothetical and uncharacterized proteins. Reciprocal pBLAST searches through Echinobase against annotated peptides in *S. purpuratus* were also performed using each *L. pictus* candidate ABC and SLC transporter sequence as the query. Alignment of candidate sequences to each other, and to reference sequences of known ABC and SLC transporters was performed using ClustalW. Homology matrices of pairwise comparisons of all sequences within an alignment were also constructed using ClustalW. Candidate sequences with >97% identity to another candidate sequence were manually checked, and the shorter sequence of the pair was eliminated to minimize redundancy.

Phylogenetic analysis and tree-building

Annotated sequences curated from NCBI and Echinobase of known ABC and SLC transporters from multiple organisms (Supplementary File 3.1) were used as reference sequences for each gene family in order to construct phylogenetic trees. These reference sequences and the candidate ABC and SLC transporters identified in *L. pictus* were included in subsequent phylogenetic analysis. Peptide sequences from candidate transporters were aligned in Geneious (v11.1.5) using the ClustalW alignment method with default parameters. The resultant alignment

was run through ProtTest (v.3.4.2) to predict the best fit model for tree construction. A maximum likelihood tree (RaxML-HPC2 on XSEDE) with 1000 bootstraps was then produced running the selected best-fit model, with a selected outgroup (*S. cerevisiae* for the ABCB and -C transporter trees, *E. coli* for SLC transporter trees), through the CIPRES Science Gateway (v.3.3)[51]. Remaining parameters were used with default settings. The resulting tree was exported and visualized and annotated in FigTree (v1.4.4).

3.7 ACKNOWLEDGEMENTS

Chapter 3, in part, is a reprint of material as it appears in Genome Biology and Evolution (2021). Warner JF, Lord J, Schreiter SA, Nesbit KT, Hamdoun A, and Lyons DC. The dissertation author is a co-author of this paper. Additional portions of Chapter 3 have been submitted for publication in PLOS Biology (2021). Espinoza JA, Vyas H, Schrankel CS, Mitchell K, Nesbit KT, Jackson E, and Hamdoun A. The dissertation author is a coauthor of this paper.

3.8 REFERENCES

1. Miranda ER, Nam EA, Kuspa A, Shaulsky G. The ABC transporter, AbcB3, mediates cAMP export in D. discoideum development. *Developmental biology*. 2015;397(2):203-211.

2. Jewett BE, Sharma S. Physiology, GABA. 2018.

3. Amann T, Hellerbrand C. GLUT1 as a therapeutic target in hepatocellular carcinoma. *Expert opinion on therapeutic targets*. 2009;13(12):1411-1427.

4. Almén MS, Nordström KJ, Fredriksson R, Schiöth HB. Mapping the human membrane proteome: a majority of the human membrane proteins can be classified according to function and evolutionary origin. *BMC biology*. 2009;7(1):1-14.

5. He L, Vasiliou K, Nebert DW. Analysis and update of the human solute carrier (SLC) gene superfamily. *Human genomics*. 2009;3(2):1-12.

6. Nigam SK. The SLC22 transporter family: a paradigm for the impact of drug transporters on metabolic pathways, signaling, and disease. *Annual review of pharmacology and toxicology*. 2018;58:663-687.

7. Sweet DH. Organic anion transporter (Slc22a) family members as mediators of toxicity. *Toxicology and applied pharmacology*. 2005;204(3):198-215.

8. Motohashi H, Inui K-i. Multidrug and toxin extrusion family SLC47: physiological, pharmacokinetic and toxicokinetic importance of MATE1 and MATE2-K. *Molecular aspects of medicine*. 2013;34(2-3):661-668.

9. Dean M, Annilo T. Evolution of the ATP-binding cassette (ABC) transporter superfamily in vertebrates. *Annu Rev Genomics Hum Genet*. 2005;6:123-142.

10. Fletcher JI, Williams RT, Henderson MJ, Norris MD, Haber M. ABC transporters as mediators of drug resistance and contributors to cancer cell biology. *Drug Resistance Updates*. 2016;26:1-9.

11. Albrecht C, Viturro E. The ABCA subfamily—gene and protein structures, functions and associated hereditary diseases. *Pflügers Archiv-European Journal of Physiology*. 2007;453(5):581-589.

12. Gaudet R, Wiley DC. Structure of the ABC ATPase domain of human TAP1, the transporter associated with antigen processing. *The EMBO Journal*. 2001;20(17):4964-4972.

13. Androlewicz MJ, Anderson KS, Cresswell P. Evidence that transporters associated with antigen processing translocate a major histocompatibility complex class I-binding peptide into the endoplasmic reticulum in an ATP-dependent manner. *Proceedings of the National Academy of Sciences*. 1993;90(19):9130-9134.

14. Abele R, Tampë R. Function of the transport complex TAP in cellular immune recognition. *Biochimica et Biophysica Acta (BBA)-Biomembranes*. 1999;1461(2):405-419.

15. Mehta A. CFTR: more than just a chloride channel. *Pediatric pulmonology*. 2005;39(4):292-298.

16. Morita M, Imanaka T. Peroxisomal ABC transporters: structure, function and role in disease. *Biochimica et Biophysica Acta (BBA)-Molecular Basis of Disease*. 2012;1822(9):1387-1396.

17. van Roermund CW, Visser WF, IJlst L, van Cruchten A, Boek M, Kulik W, Waterham HR, Wanders RJ. The human peroxisomal ABC half transporter ALDP functions as a homodimer and accepts acyl–CoA esters. *The FASEB Journal*. 2008;22(12):4201-4208.

18. Jin D, Ni TT, Sun J, Wan H, Amack JD, Yu G, Fleming J, Chiang C, Li W, Papierniak A, Cheepala S. Prostaglandin signalling regulates ciliogenesis by modulating intraflagellar transport. *Nature cell biology*. 2014;16(9):841-851.

19. Kassmer SH, Rodriguez D, Langenbacher AD, Bui C, De Tomaso AW. Migration of germline progenitor cells is directed by sphingosine-1-phosphate signalling in a basal chordate. *Nature communications*. 2015;6(1):1-10.

20. Petrášek J, Friml J. Auxin transport routes in plant development. *Development*. 2009;136(16):2675-2688.

21. Yabe T, Suzuki N, Furukawa T, Ishihara T, Katsura I. Multidrug resistance-associated protein MRP-1 regulates dauer diapause by its export activity in Caenorhabditis elegans. *Development*. 2005;132(14):3197-3207.

22. Ricardo S, Lehmann R. An ABC transporter controls export of a Drosophila germ cell attractant. *Science*. 2009;323(5916):943-946.

23. Wu W, Dnyanmote AV, Nigam SK. Remote communication through solute carriers and ATP binding cassette drug transporter pathways: an update on the remote sensing and signaling hypothesis. *Molecular Pharmacology*. 2011;79(5):795-805.

24. Nicklisch SC, Rees SD, McGrath AP, Gökirmak T, Bonito LT, Vermeer LM, Cregger C, Loewen G, Sandin S, Chang G, Hamdoun A. Global marine pollutants inhibit P-glycoprotein: Environmental levels, inhibitory effects, and cocrystal structure. *Science advances*. 2016;2(4):e1600001.

25. Chedik L, Bruyere A, Fardel O. Interactions of organophosphorus pesticides with solute carrier (SLC) drug transporters. *Xenobiotica*. 2019;49(3):363-374.

26. Warner JF, Lord JW, Schreiter SA, Nesbit KT, Hamdoun A, Lyons DC. Chromosomal-level genome assembly of the painted sea urchin Lytechinus pictus, a genetically enabled model system for cell biology and embryonic development. *Genome Biology and Evolution*. 2021.

27. Luciani MF, Denizot F, Savary S, Mattei MG, Chimini G. Cloning of two novel ABC transporters mapping on human chromosome 9. *Genomics*. 1994;21(1):150-159.

28. Bryan J, Muñoz A, Zhang X, Düfer M, Drews G, Krippeit-Drews P, Aguilar-Bryan L . ABCC8 and ABCC9: ABC transporters that regulate K+ channels. *Pflügers Archiv-European Journal of Physiology*. 2007;453(5):703-718.

29. Schumacher T, Kantesaria DV, Heemels MT, Ashton-Rickardt PG, Shepherd JC, Fruh K, Yang Y, Peterson PA, Tonegawa S, Ploegh HL. Peptide length and sequence specificity of the mouse TAP1/TAP2 translocator. *The Journal of experimental medicine*. 1994;179(2):533-540.

30. Borst P, Elferink RO. Mammalian ABC transporters in health and disease. *Annual review of biochemistry*. 2002;71(1):537-592.

31. Dean M. The human ATP-binding cassette (ABC) transporter superfamily. 2002.

32. Gottesman MM, Ambudkar SV. Overview: ABC transporters and human disease. *Journal of bioenergetics and biomembranes*. 2001;33(6):453-458.

33. Silverton L, Dean M, Moitra K. Variation and evolution of the ABC transporter genes ABCB1, ABCC1, ABCG2, ABCG5 and ABCG8: implication for pharmacogenetics and disease. *Drug metabolism and drug interactions*. 2011;26(4):169.

34. Tarling EJ, de Aguiar Vallim TQ, Edwards PA. Role of ABC transporters in lipid transport and human disease. *Trends in Endocrinology & Metabolism*. 2013;24(7):342-350.

35. Goldstone J, Hamdoun A, Cole B, Howard-Ashby M, Nebert DW, Scally M, Dean M, Epel D, Hahn ME, Stegeman JJ. The chemical defensome: environmental sensing and response genes in the Strongylocentrotus purpuratus genome. *Developmental biology*. 2006;300(1):366-384.

36. Shipp LE, Hamdoun A. ATP□binding cassette (ABC) transporter expression and localization in sea urchin development. *Developmental Dynamics*. 2012;241(6):1111-1124.

37. Gökirmak T, Campanale JP, Reitzel AM, Shipp LE, Moy GW, Hamdoun A. Functional diversification of sea urchin ABCC1 (MRP1) by alternative splicing. *American Journal of Physiology-Cell Physiology*. 2016;310(11):C911-C920.

38. Gökirmak T, Campanale JP, Shipp LE, Moy GW, Tao H, Hamdoun A. Localization and substrate selectivity of sea urchin multidrug (MDR) efflux transporters. *Journal of Biological Chemistry*. 2012;287(52):43876-43883.

39. Gökirmak T, Shipp LE, Campanale JP, Nicklisch SC, Hamdoun A. Transport in technicolor: Mapping ATP□binding cassette transporters in sea urchin embryos. *Molecular reproduction and development*. 2014;81(9):778-793.

40. Espinoza J, Vyas H, Schrankel C, Mitchell K, Nesbit KT, Jackson E, Chang N, Hamdoun A. Propagation of ABCB1 CRISPR mutants in the sea urchin, *Lytechinus pictus*. *PLOS Biology*. 2021; (*In preparation.*).

41. Engelhart DC, Azad P, Ali S, Granados JC, Haddad GG, Nigam SK. Drosophila SLC22 orthologs related to OATs, OCTs, and OCTNs regulate development and responsiveness to oxidative stress. *International journal of molecular sciences*. 2020;21(6):2002.

42. Arimany-Nardi C, Koepsell H, Pastor-Anglada M. Role of SLC22A1 polymorphic variants in drug disposition, therapeutic responses, and drug–drug interactions. *The pharmacogenomics journal*. 2015;15(6):473-487.

43. Wang Y, Ye J, Ganapathy V, Longo N. Mutations in the organic cation/carnitine transporter OCTN2 in primary carnitine deficiency. *Proceedings of the National Academy of Sciences*. 1999;96(5):2356-2360.

44. SLC22A5 Gene (Protein Coding) - Solute Carrier Family 22 Member 5. Gene Cards: The Human Gene Database: Weizmann Institute of Science.

45. Lončar J, Popović M, Krznar P, Zaja R, Smital T. The first characterization of multidrug and toxin extrusion (MATE/SLC47) proteins in zebrafish (Danio rerio). *Scientific reports*. 2016;6(1):1-15.

46. Davidson PL, Guo H, Wang L, Berrio A, Zhang H, Chang Y, Soborowski AL, McClay DR, Fan G, Wray GA. Chromosomal-level genome assembly of the sea urchin Lytechinus variegatus substantially improves functional genomic analyses. *Genome biology and evolution*. 2020;12(7):1080-1086.

47. Sodergren E, Weinstock GM, Davidson EH, Cameron RA, Gibbs RA, Angerer RC, Angerer LM, Arnone MI, Burgess DR, Burke RD, Coffman JA. The genome of the sea urchin Strongylocentrotus purpuratus. *Science*. 2006;314(5801):941-952.

48. Hamdoun A, Schrankel CS, Nesbit KT, Espinoza JA. Sea Urchins as Lab Animals for Reproductive and Developmental Biology. 2018.

49. Nesbit KT, Fleming T, Batzel G, Pouv A, Rosenblatt HD, Pace DA, Hamdoun A, Lyons DC. The painted sea urchin, Lytechinus pictus, as a genetically-enabled developmental model. *Methods Cell Biol*. 2019;150:105-123. https://doi.org10.1016/bs.mcb.2018.11.010.

50. Nesbit KT, Hamdoun A. Embryo, larval, and juvenile staging of L*ytechinus pictus* from fertilization through sexual maturation. Developmental Dynamics; 2020.

51. Miller MA, Pfeiffer W, Schwartz T. Creating the CIPRES Science Gateway for inference of large phylogenetic trees. *Proceedings of the Gateway Computing Environments Workshop (GCE)*. 2010:1-8.

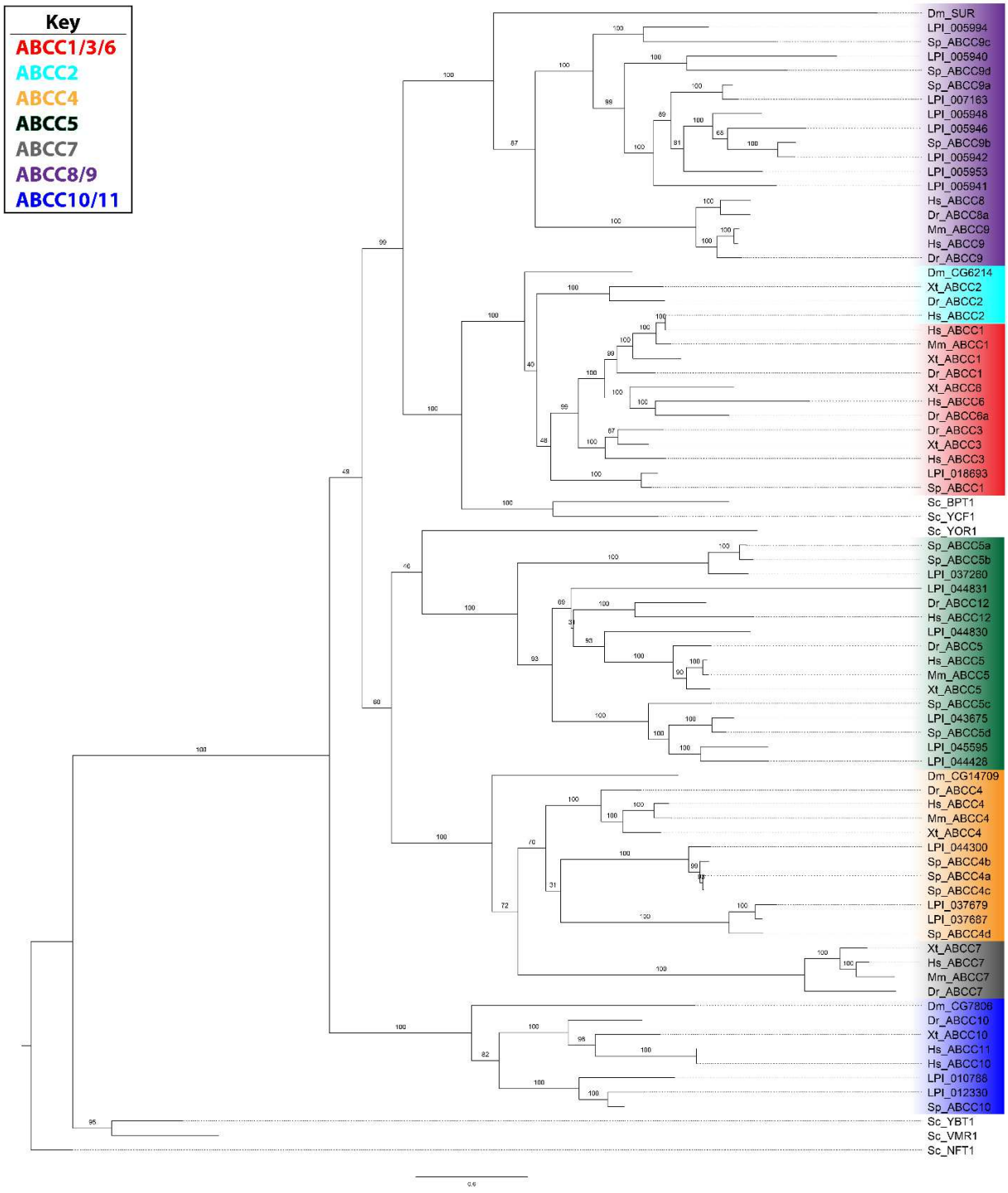

Figure 3.1. Phylogenetic analysis of ABCC-subfamily transporters reveal expansions in *L. pictus* Evolutionary context enables distinction between paralogs of the expanded C-subfamily of transporters. Genes are listed as a two-letter abbreviation for the species, followed by the gene name or gene model ID (e.g., Hs_ABCC1 for human ABCC1). Organisms represented include: Dr (*Danio rerio*), Dm (*Drosophila melanogaster*), Hs, (*Homo sapiens*), Mm (*Mus musculus*), Sc (*Saccharomyces cerevisiae*), Sp (*Strongylocentrotus purpuratus*), Lp (*Lytechinus pictus*), and Xt (*Xenopus tropicalis*). Groupings of major paralogs are color coded: ABCC1/3/6 in red, ABCC2 in cyan, ABCC4 in orange, ABCC5 in green, ABCC7 in grey, ABCC8/9 in purple, and ABCC10/11 in blue. Yeast (*Saccharomyces cerevisiae*) serves as the outgroup for the tree. Bootstraps (1000) are shown for each branch.

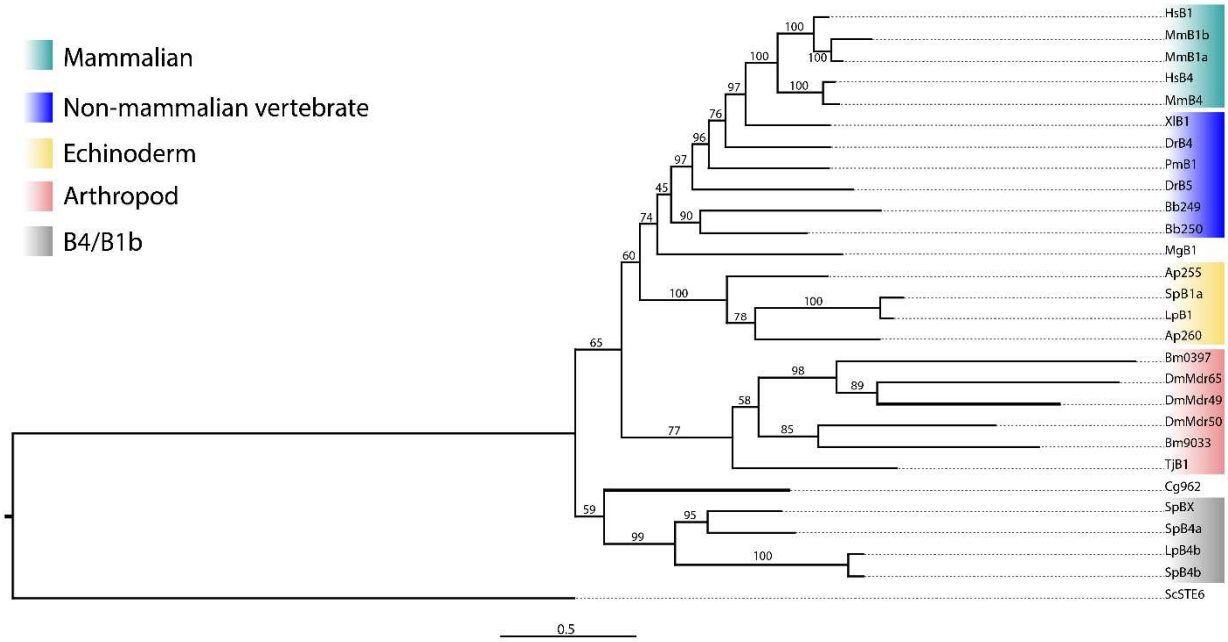

Figure 3.2. The *L. pictus* ABCB1 paralog is similar to mammalian P-gp. Genes are listed as a two-letter abbreviation for the species, followed by the gene name or gene model ID (e.g., HsB1 for human ABCB1). Organisms represented include: Ap (*Acanthaster planci*), Bb (*Branchiostoma belcheri*), Bm (*Bombyx mori*), Cg *(Crassostrea gigas*), Dm (*Drosophila melanogaster*), Dr (*Danio rerio*), Hs (*Homo sapiens*), Lp (*Lytechinus pictus*), Mg (*Mytilus galloprovincialis*), Mm (*Mus musculus*), Pm (*Petromyzon marinus*), Sc (*Saccharomyces cerevisiae*), Sp (*Strongylocentrotus purpuratus*), Tj (*Tigriopus japonica*), Xl (*Xenopus laevis*). Groupings of major clades are color coded: mammalian B1 (green), other vertebrate B1 and zebrafish B4 (blue), echinoderm B1 (yellow), arthropods (red), and echinoderm B4 paralogs (grey). Yeast (*Saccharomyces cerevisiae*) serves as the outgroup for the tree. Bootstraps (1000) are shown for each branch.

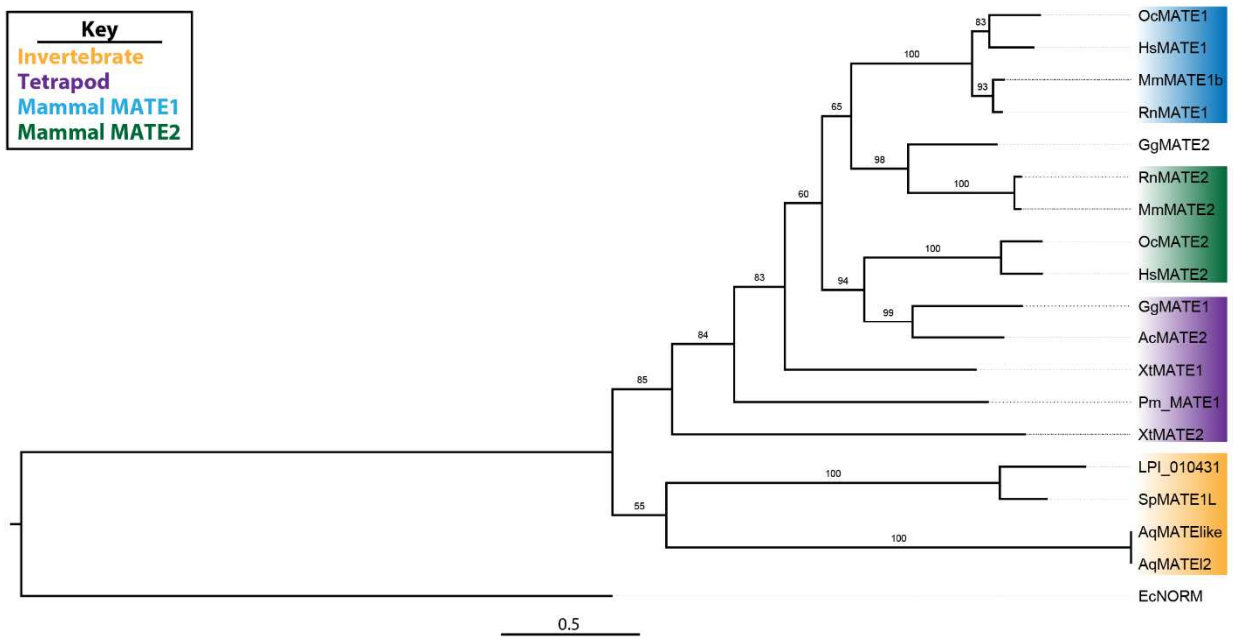

Figure 3.3. MATE proteins in *L. pictus* are unlike vertebrates. Genes are listed as a two-letter abbreviation for the species, followed by the gene name or gene model ID (e.g., HsMATE1 for human SLC41A1/MATE1). Organisms represented include: *Anolis carolinensis* (Ac), *Amphimedon queenslandica* (Aq), *Escherichia coli* (Ec), *Gallus Eco* (Gg), *Homo sapiens* (Hs), *Lytechinus pictus* (LPI_XXXXXX), *Mus musculus* (Mm), *Oryctolagus cuniculus* (Oc), *Petromyzon marinus* (Pm), *Rattus norvegicus* (Rn), *Strongylocentrotus purpuratus* (Sp), and *Xenopus tropicalis* (Xt). Groupings of major clades are color coded: invertebrates (yellow), non-mammalian tetrapods (purple), mammalian MATE1 (blue), and mammalian MATE2 (green). *E. coli* serves as the outgroup for the tree. Bootstraps (1000) are shown for each branch.

Table 3.1. Disease-associated small molecular transporters (SMTs) from the ABC and SLC superfamilies. Homologs of disease-associated SMTs that are present in the *L. pictus* genome assembly are marked with a (+) and are accompanied by the associated gene model ID. Those that are absent from the *L. pictus* assembly are marked with a (-).

Mammalian Transporter	Disease Associations	*L. pictus* Homolog	LPI_ID
ABCA1	Tangier disease	+	LPI_035401
ABCA2	Alzheimers	+	LPI_037644
ABCB1	IBS	+	LPI_040201
ABCB4	PFIC	+	LPI_038761
ABCC1	Cancers (drug resistance)	+	LPI_018693
ABCC2	Dubin-Johnson syndrome	-	N/A
ABCC6	Pseudoxanthoma elasticum	-	N/A
ABCC7	Cystic fibrosis	-	N/A
ABCC9	Cantu syndrome	+	LPI_005953
ABCD1	Adrenoleukodystrophy	+	LPI_004627
ABCG2	Cancers (drug resistance)	+	LPI_048338
ABCG5	Sitosterolemia	-	N/A
SLC22A1	Metabolic disease, leukemia	+	LPI_026177
SLC22A5	Metabolic disease, Crohn's disease	+	LPI_024901
SLC22A18	Cancers, Beckwith-Wiedemann syndrome	+	LPI_015842
SLC47 1&2	Metabolic disease, Smith-Magenis syndrome	+	LPI_010431
SLCO1B1	Gilbery syndrome, Rotor syndrome	-	N/A
SLCO2A1	Chronic enteropathy	+	LPI_014926
SLCO2B1	Ileum and prostate cancers, Bronchiectasis	+	LPI_035323
SLCO5A1	Mesomelia, mesomelia-synostoses	+	LPI_013851

Table 3.2. ABC transporters identified in the *L. pictus* genome. Genes are identified down to the subfamily level of resolution. Genomic coordinated for the gene model are listed and used to calculate the gene length. Orientation of the identified gene models follows the coordinates, where (F) represents location on the plus strand and (R) indicates genes on the minus strand.

Subfamily	LPI_ID	Length (AA)	Genomic Coordinates
A	LPI_023418	784	ScPm3Vo_328_HRSCAF_1282: 18,495,015-18,588,069 (F)
	LPI_035401	981	ScPm3Vo_531_HRSCAF_2080:17,924,275-17,981,400 (R)
	LPI_037644	1760	ScPm3Vo_215_HRSCAF_529:20,465,067-20,653,668 (F)
	LPI_009483	810	ScPm3Vo_478_HRSCAF_1922:37,496,452-37,797,136 (F)
	LPI_019163	1029	ScPm3Vo_221_HRSCAF_562:38,543,825-38,570,151 (R)
	LPI_018846	684	ScPm3Vo_221_HRSCAF_562:30,630,755-30,660,401 (R)
	LPI_018849	1453	ScPm3Vo_221_HRSCAF_562:30,713,541-30,771,293 (F)
B	LPI_039763	279	ScPm3Vo_356_HRSCAF_1397:19,785,110-19,802,033 (R)
	LPI_041125	256	ScPm3Vo_296_HRSCAF_1117:3,607,714-3,619,489 (F)
	LPI_041142	427	ScPm3Vo_296_HRSCAF_1117:3,754,102-3,783,026 (F)
	LPI_041144	305	ScPm3Vo_296_HRSCAF_1117:3,784,474-3,791,250 (F)
	LPI_040201	1206	ScPm3Vo_356_HRSCAF_1397:27,337,659-27,402,132 (R)
	LPI_038761	1134	ScPm3Vo_356_HRSCAF_1397:3,221,753-3,287,581 (R)
	LPI_039764	804	ScPm3Vo_356_HRSCAF_1397:19,801,895-19,829,840 (F)
	LPI_042449	724	ScPm3Vo_296_HRSCAF_1117:26,482,321-26,512,600 (R)
	LPI_042976	500	ScPm3Vo_296_HRSCAF_1117:30,449,293-30,491,085 (F)
	LPI_026707	273	ScPm3Vo_247_HRSCAF_834:36,073,005-36,114,167 (F)
	LPI_027655	270	ScPm3Vo_1245_HRSCAF_4185:8,528,437-8,541,856 (R)
	LPI_011806	702	ScPm3Vo_478_HRSCAF_1922:84,071,549-84,103,907 (R)
	LPI_012330	860	ScPm3Vo_1088_HRSCAF_3292:6,555,169-6,582,642 (R)
	LPI_012758	473	ScPm3Vo_1088_HRSCAF_3292:15,188,466-15,199,817 (R)
C	LPI_018693	1471	ScPm3Vo_221_HRSCAF_562:27,452,310-27,512,257 (R)
	LPI_044300	1334	ScPm3Vo_1237_HRSCAF_4130:13,840,624-13,872,304 (F)
	LPI_037679	1125	ScPm3Vo_215_HRSCAF_529:21,156,816-21,208,410 (F)
	LPI_037687	1135	ScPm3Vo_215_HRSCAF_529:21,258,518-21,318,499 (R)
	LPI_037260	1324	ScPm3Vo_215_HRSCAF_529:13,153,043-13,175,568 (R)
	LPI_044428	1139	ScPm3Vo_1237_HRSCAF_4130:15,930,847-15,959,079 (R)
	LPI_045595	488	ScPm3Vo_1237_HRSCAF_4130:33,474,129-33,489,820 (F)
	LPI_043675	689	ScPm3Vo_1237_HRSCAF_4130:1,592,303-1,605,566 (F)
	LPI_044830	432	ScPm3Vo_1237_HRSCAF_4130:21,760,464-21,764,853 (F)
	LPI_044831	613	ScPm3Vo_1237_HRSCAF_4130:21,767,169-21,792,238 (F)
	LPI_005940	955	ScPm3Vo_1193_HRSCAF_3749:51,541,716-51,555,741 (F)
	LPI_005953	1529	ScPm3Vo_1193_HRSCAF_3749:51,703,079-51,744,577 (F)
	LPI_007163	1541	ScPm3Vo_1193_HRSCAF_3749:78,821,647-78,861,157 (F)
	LPI_005942	1386	ScPm3Vo_1193_HRSCAF_3749:51,573,418-51,603,568 (R)
	LPI_005948	428	ScPm3Vo_1193_HRSCAF_3749:51,642,956-51,651,252 (R)
	LPI_005941	436	ScPm3Vo_1193_HRSCAF_3749:51,561,920-51,570,183 (F)
	LPI_005994	672	ScPm3Vo_1193_HRSCAF_3749:52,562,363-52,580,645 (F)
	LPI_005946	1488	ScPm3Vo_1193_HRSCAF_3749:51,615,425-51,640,328 (F)
	LPI_010788	1556	ScPm3Vo_478_HRSCAF_1922:63,335,696-63,352,910 (R)
	LPI_012330	860	ScPm3Vo_1088_HRSCAF_3292:6,555,169-6,582,642 (R)
D	LPI_004620	240	ScPm3Vo_1193_HRSCAF_3749:15,295,750-15,324,607 (R)
	LPI_004627	476	ScPm3Vo_1193_HRSCAF_3749:15,404,158-15,409,477 (R)
	LPI_022655	592	ScPm3Vo_328_HRSCAF_1282:7,557,030-7,605,742 (R)
	LPI_016849	332	ScPm3Vo_473_HRSCAF_1904:48,382,242-48,392,414 (R)
	LPI_016850	232	ScPm3Vo_473_HRSCAF_1904:48,399,120-48,402,111 (R)
E	LPI_000360	563	ScPm3Vo_285_HRSCAF_1033:7,673,757-7,697,195 (F)
F	LPI_038291	492	ScPm3Vo_215_HRSCAF_529:33,767,772-33,798,978 (R)
	LPI_043295	564	ScPm3Vo_296_HRSCAF_1117:36,281,299-36,305,948 (F)
	LPI_038637	326	ScPm3Vo_356_HRSCAF_1397:415,346-435,866 (R)
G	LPI_048338	538	ScPm3Vo_305_HRSCAF_1169:8,480,262-8,511,705 (F)
	LPI_017065	588	ScPm3Vo_473_HRSCAF_1904:52,384,978-52,405,963 (F)
	LPI_017071	591	ScPm3Vo_473_HRSCAF_1904:52,468,957-52,495,127 (R)
H	LPI_022034	249	ScPm3Vo_193_HRSCAF_276:42,676,694-42,691,951 (F)

Table 3.3. Cross-species comparison of ABC transporter members. Comparison between *L. pictus*, the purple sea urchin *Strongylocentrotus purpuratus*, and humans (*H. sapiens*). Sea urchins have a relative expansion of the C-subfamily, with more individual members. Other subfamilies have comparable numbers of individual genes.

Transporter Subfamily	*L. pictus*	*S. purpuratus*	*H. sapiens*
A	7	12	12
B	14	13	11
C	20	36	12
D	5	3	4
E	1	1	1
F	3	4	3
G	3	9	5
H	1	1	0
Total	54	79	48

Table 3.4. SLC transporters from the SLC22, SLC47, and SLCO subfamilies identified in the *L. pictus* genome. Genes are identified down to the subfamily level of resolution. Genomic coordinated for the gene model are listed and used to calculate the gene length. Orientation of the identified gene models follows the coordinates, where (F) represents location on the plus strand and (R) indicates genes on the minus strand.

Subfamily	LPI_ID	Length (AA)	Genomic Coordinates
SLC22	LPI_000749	592	ScPm3Vo_285_HRSCAF_1033:16,105,081-16,117,877 (R)
	LPI_015813	149	ScPm3Vo_473_HRSCAF_1904:28,278,029-28,280,323 (F)
	LPI_015814	92	ScPm3Vo_473_HRSCAF_1904:28,282,583-28,284,384 (F)
	LPI_015842	476	ScPm3Vo_473_HRSCAF_1904:28,988,886-28,999,019 (R)
	LPI_020946	371	ScPm3Vo_193_HRSCAF_276:23,542,919-23,575,690 (F)
	LPI_024901	392	ScPm3Vo_247_HRSCAF_834:2,857,422-2,866,061 (R)
	LPI_025715	230	ScPm3Vo_247_HRSCAF_834:19,841,362-19,849,421 (F)
	LPI_025716	256	ScPm3Vo_247_HRSCAF_834:19,891,882-19,897,567 (F)
	LPI_025729	252	ScPm3Vo_247_HRSCAF_834:20,066,784-20,087,842 (R)
	LPI_025734	420	ScPm3Vo_247_HRSCAF_834:20,156,299-20,168,840 (F)
	LPI_025832	372	ScPm3Vo_247_HRSCAF_834:21,868,580-21,887,463 (F)
	LPI_026111	579	ScPm3Vo_247_HRSCAF_834:25,983,271-25,996,770 (F)
	LPI_026134	437	ScPm3Vo_247_HRSCAF_834:26,327,583-26,346,453 (R)
	LPI_026174	483	ScPm3Vo_247_HRSCAF_834:26,974,549-26,986,210 (R)
	LPI_026177	518	ScPm3Vo_247_HRSCAF_834:27,004,534-27,024,122 (R)
	LPI_026180	496	ScPm3Vo_247_HRSCAF_834:27,039,973-27,053,356 (F)
	LPI_026181	577	ScPm3Vo_247_HRSCAF_834:27,061,877-27,073,715 (R)
	LPI_026185	573	ScPm3Vo_247_HRSCAF_834:27,108,132-27,123,845 (F)
	LPI_025775	507	ScPm3Vo_247_HRSCAF_834:20,940,122-20,970,190 (F)
	LPI_026472	523	ScPm3Vo_478_HRSCAF_1922:56,368,400-56,433,920 (R)
SLC47	LPI_010431	658	ScPm3Vo_1088_HRSCAF_3292:41,533,449-41,551,049 (F)
SLCO	LPI_013851	748	ScPm3Vo_473_HRSCAF_1904:7,778,317-7,808,877 (F)
	LPI_014905	716	ScPm3Vo_473_HRSCAF_1904:7,933,830-7,977,181 (R)
	LPI_014920	748	ScPm3Vo_473_HRSCAF_1904:7,978,031-7,991,412 (R)
	LPI_014922	698	ScPm3Vo_473_HRSCAF_1904:8,000,891-8,011,258 (F)
	LPI_014925	715	ScPm3Vo_473_HRSCAF_1904:8,000,891-8,011,258 (F)
	LPI_014926	556	ScPm3Vo_473_HRSCAF_1904:8,024,382-8,043,294 (F)
	LPI_016135	642	ScPm3Vo_473_HRSCAF_1904:35,691,477-35,713,658 (R)
	LPI_017031	426	ScPm3Vo_473_HRSCAF_1904:51,443,036-51,501,955 (F)
	LPI_035323	215	ScPm3Vo_531_HRSCAF_2080:16,403,311-16,407,068 (R)
	LPI_015003	780	ScPm3Vo_473_HRSCAF_1904:9,587,214-9,609,543 (R)

CHAPTER 4

Exposure to cyclosporin A impairs larval pigment cell responses to infection in the sea urchin *Lytechinus pictus*

4.1 ABSTRACT

Echinoderms are a whole-animal system to study innate immune function. As a basal deuterostome with an innate, complement-like immune system, urchins share components of, and are likely evolutionary precursors to, more complex immune systems such as adaptive immunity found in mammals. Innate immune systems are a first line of defense and interact with diverse and potentially harmful environmental agents including pathogenic microbes and xenobiotic molecules. Xenobiotics can impair the immune system by disrupting the functions of immune cells (e.g., migration, signaling, or cytokine release) or by impacting differentiation of immune cell types in development. To test these consequences of exposure, we exposed sea urchin larvae to chemicals and challenged them with bacteria. Normally the pigment cells (immunocytes) of the larva migrate from the ectoderm to the gut to aid in pathogen clearance when infected with *Vibrio diazotrophicus*. We treated larvae with the immunosuppressant drug Cyclosporin A to determine the effects on pigment cell (PC) migration. Larvae treated with Cyclosporin A at high doses (10μM) had reduced PC migration throughout a 24-hour infection (hpi). Larvae treated with Cyclosporin A at low doses (0.5μM) were not significantly different from unexposed larvae early on, but by 24 hpi have significantly reduced PC migration. These data provide the first description of an immunocompromised echinoderm model. This model will help us understand the influence of chemical exposures on innate immune function. This model enables us to quantify the impact of individual chemical components and to expand our scope to combinatorial impacts of chemical mixtures. This model is also a powerful tool for studying the cross-talk of development and environmental sensing.

4.2 INTRODUCTION:

The immune system is a dynamic network composed of a heterogenous population of cells that detect and respond to health threats in the environment. Immunity can be divided into two major categories: first is innate immunity which is a preprogrammed response to a broad spectrum of common pathogens and serves as the first line of defense; second is adaptive, where highly specific immune memory is generated through the production of antibodies. Adaptive immunity is a more derived feature, which first appeared in the ancestor to the vertebrate lineage[1]. In contrast, innate immunity is shared across all metazoans[2], meaning the vast majority of the animal kingdom is operating with a more universal system of protection.

The purple sea urchin larva has an innate, complement-like immune system that is composed of a well-defined immune cell population[3,4]. This system can be challenged through an immune response assay[5] that provides an ideal model for studying the coordinate cellular responses to infection. Each purple urchin embryo forms 50-80[5] immunocytes that begin to differentiate at approximately 24 hours post-fertilization (hpf), called pigment cells (PCs). PCs are migratory and express unique genes[6,7], including ones involved in immune recognition[4,8]. Upon infection, PCs dissociate from the ectoderm and migrate much like mammalian immune cells such as neutrophils, macrophages, and dendritic cells. In the larva, the PCs travel to the gut in a dose-dependent and reversible manner[5]. The gut epithelium constricts and thickens as a barrier against microbial invasion. Dynamic changes at the molecular level also accompany this phenotypic response. Upregulation of immune genes such as the scavenger receptor (*srcr142*) and a complement-like protein (*tecp2*) occur, as well as increased expression of the echinoderm immune marker *158/333* and the pro-inflammatory cytokine interleukin-17 (*IL-17*). A globular cell gene (*macpfA2*) and a macrophage inhibitory factor (*mif7*) are downregulated. The

magnitude of changes in expression of these immune indicator genes corresponds to the magnitude of the invoked immune response.

The immune system of an organism such as the sea urchin larva can be harmed by damaging agents in the environment, such as chemical exposures. In particular, developmental exposures are linked to dysfunction of the developing immune system. Harmful consequences[9-13] of exposures on immune system function in both adults and embryonic/developing stages include decreased differentiation of immune cell types[14-16], diminished cell proliferation[17], reduced antigen production[15], suppressed cellular responses[18], and increased markers of infection severity[19]. Precise mechanisms underlying the immunotoxic effects of exposure to many man-made chemicals have largely focused on adaptive components, but it is unlikely that chemical exposures have no impact on the components of innate immunity. The diversity of chemicals which affect innate immunity, and the mechanisms through which that is accomplished remains largely underexplored.

Given that exposures can impair immune health, a better understanding of the pathways protecting developing innate immune systems is essential for predicting and mitigating the effects of immunotoxic exposures. Exposures can impair the nascent immune system through two major "routes": 1) by disrupting the differentiation of populations of immune cells, effectively decreasing the number of cells participating in an immune response; or 2) by impairing the cellular machinery of a fully differentiated immunocyte, rendering it ineffective at performing its role *in vivo*, for example migration or cytokine/signaling molecule release. Both the differentiation and functional tasks of immune cells require precise coordination among heterogenous populations of cells to either generate a sufficient cell population to protect the animal or mount an appropriate and effective immune response. The timing, concentration,

duration, and composition of an exposure dictate which "route" is taken to transition from a healthy functioning immune system to an immunocompromised state.

Thus, the overarching goal of this chapter is to generate an echinoderm model of immunosuppression using the painted white urchin, *Lytechinus pictus*. Having such a model will enable us to more rapidly assess the impacts of exposures to toxicants that have the potential to impair immune cell migration, effectively increasing the vulnerability of the organism by suppressing the immune response.

4.3 RESULTS:

The most conspicuous cell type involved in the larval sea urchin immune response are the pigment cells (PCs). The pigment cells begin to differentiate during gastrulation at approximately 16 hours post-fertilization (hpf)[20] from a subpopulation of mesenchymal cells on the oral side of the embryo. The larvae of *Lytechinus pictus* reach the 2 arm pluteus stage by 2 days post-fertilization[20] and the pigment cells are embedded into the ectoderm. The larvae of *L. pictus* have between 80-120 pigment cells (Fig. 4.1), which is greater than the number of pigment cells in individual larvae of *S. purpuratus*.

To assess whether the PCs of *L. pictus* responded phenotypically to infection in a manner similar to the response in *S. purpuratus*, we infected larvae with the marine nitrogen-fixing bacteria *Vibrio diazotrophicus* which was first isolated from the gut of the sea urchin[21]. Infection responses varied across mate pairs with distinct genetic backgrounds (Fig. 4.2). Despite the level of individual mate pair variability, infected larvae consistently had a greater number of active, migratory PCs over the course of the 24-hour infection period compared to wild-type, uninfected animals when pooled across mate pairs (Fig. 4.3A). Phenotypically, this PC migration response

is accompanied by gut epithelial inflammation and an overall reduction in size of the stomach (Fig. 4.3B).

Knowing that the infection response could be successfully recapitulated in *L. pictus*, we then sought to suppress the immune system of the larvae through chemical exposure to the immunosuppressant drug cyclosporin A[22]. Cyclosporin A is commonly administered to transplant patients to reduce the likelihood of rejection of organs or other transplanted tissues[23]. This drug works primarily through disrupting T cell proliferation via binding of cyclophilin which blocks the activity of calcineurin, inhibiting expression of interleukin-2 (IL-2) which is necessary for T-cell activation[24]. Though this primary mechanism of action exerts influence over an adaptive immune cell type, it is unlikely that innate immune components are unaltered by chemical exposures. It has been shown in other marine organisms, such as sponges[25], ascidians[26], and oyster[27], that cyclosporin exposure disrupts immune functions such as allorecognition and pathogen clearance. The larvae of *L. pictus* possesses molecular machinery, such as calcineurin, involved in the pathway that cyclosporin A acts upon as well as other molecular targets relevant to immunity or protection[28] that could be influenced by chemical exposures (Table 4.1).

These molecular targets relevant to immunity and drug exposure with homologs in *L. pictus* include genes from diverse families such as enzymes, transcription factors, cytokines and effector molecules, signal mediators, and components involved in pattern recognition (Table 4.1). The homology of these components ranges from highly conserved (e.g., transcription factors) to highly divergent molecules (e.g., the echinoderm specific effector molecules) including many that are dynamically up- or down-regulated throughout the course of infection[5,8]. Given the combination of a phenotypic data and the detection of homologous protective

machinery in *L. pictus*, we hypothesized that cyclosporin A exposure would impair the cell migratory response of the larval PCs.

Infected larvae exposed to cyclosporin A did have a reduction in migratory pigment cells compared to larvae that were not exposed to the drug (Fig. 4.4A). It appears as though the overall magnitude of the PC migration is not dampened, but rather delayed. The number of active PC moving through the larvae to sites of infection catches up (for example at 12 hpi) to numbers comparable to the unexposed larvae groups at earlier times (at 6 hpi). By 24 hpi though, infected larvae from both the low and high dose treated groups have significantly reduced numbers of active migrating pigment cells compared to infected larvae that were not exposed to cyclosporin A. This impact is only observed when larvae are challenged with infection and chemical exposure, as chemical exposure alone does not significantly impact the number of migratory PCs in the larvae at low doses or at earlier time points (Fig. 4.4B). Only at later time points and at high doses are any significant differences in pigment cell migration observed in comparison to wild type, unexposed larvae.

4.4 DISCUSSION:

Since the Nobel-prize winning discovery of phagocytosis in the sea star larvae by Elie Metchnikoff, echinoderms have been an important whole-animal system for understanding the origins and function of innate immunity. The data here represents the first description of an immunosuppression model in an echinoderm.

With an array of key molecular components annotated, the next steps to strengthen our understanding of the innate immune response during chemical exposure include quantifying the dynamic regulation of protective machinery in immunity and drug disposition. Such data would inform on the magnitude of immune responses and the delay in immune activation observed

when exposures and infections are paired in this system. With quantification of those components, and a phenotypic assay that is dose-dependent at hand, it would then be possible to test the influence of other environmental chemicals on immunity in this whole-animal system. This includes man-made toxicants like persistent organic pollutants which are resistant to degradation in the environment and hydrophobic, lending to their tendency to bioaccumulate in organisms as a consequence of these chemical properties. Examples of persistent organic pollutants include polybrominated diphenyl ethers (PBDEs), hydrocarbons such as phenanthrene from crude oil, pesticides like DDT, and other industrial chemicals like perfluorochemicals (PFCs). The negative impacts of exposure to these types of chemicals include immunotoxicity[11,14,15,17], but the extent to which these impacts have been tested in heterogenous cell populations, observed in real time *in vivo*, or in combination with relevant immune challenges is still limited. Furthermore, much attention on the immunotoxicity of environmental chemicals is centered around systems which contain adaptive immune system. This added layer of complexity may overshadow other more fundamental impacts exerted on innate immune cell types which also interact with damaging agents in the environment. Thus, *L. pictus* offers the ideal system in which to begin filling in this gap in our knowledge.

4.5 CONCLUSIONS:

Studies that expand our comprehension of immunotoxicity of diverse environmental chemicals will remain relevant, as legacy pollutants and other contaminants continue to persist in the environment. Moreover, the foundation established by this work will enable us to compare the activity of man-made chemicals and structurally-related naturally produced molecules – for example, brominated molecules manufactured as flame retardants and naturally synthesized by sponges[29]. The system developed here for generating animals in immunocompromised states also

enables us to better understand the mechanisms or action of these pollutants and how abiotic factors such as concentration, timing, duration, and composition of exposures may be influencing health outcomes throughout the life cycle of the animal and across generations.

4.6 METHODS:

Animal husbandry and larval culturing

Adult *Lytechinus pictus* were collected off the coast of Southern California and maintained in flow-through sea water tanks help at 20°C. Adults are fed fresh kelp (*Macrocystis*) *ad libidum* and tanks are cleaned twice weekly. To collect gametes, adults were spawned by intracoelomic injection (1ml syringe with a 27g needle) of 100-200µl of 0.5M KCl. Animals are gently shaken after injection and observed for gamete release. Females are kept submerged during spawning to minimize desiccation stress on the animal. Males are placed in a shallow dish of sea water and sperm is collected concentrated with a glass pipette off the aboral surface of the animal and stored in an Eppendorf tube. Eggs are washed 6-10x with filtered sea water (FSW) to remove the jelly coating. Eggs are observed for quality, and estimates of density are calculated. Test fertilizations are performed to ensure high (>98%) success fertilization. Eggs are then fertilized and set up in culture at a density no greater than 1 embryo/ml and grown with gentle agitation at 23°C. Larvae were sampled 2-4 days post-fertilization to ensure that no developmental abnormalities were observed and no immune activation occurred preceding infection assay. Larvae were fed the red flagellated alga *Rhodamonas* at 2 days post-fertilization (dpf) at a concentration of 3,000 cells/ml. Larvae were starved for 24 hours pre-infection.

Bacteria preparation

The marine nitrogen-fixing bacterium *Vibrio diazotrophicus* was cultured from frozen stock in fresh marine broth media (MB2216) and grown overnight at 15°C. To prepare bacteria

for infection assay, cultures were spun down (5000 x g) three times and washed with FSW. Bacteria were resuspended in FSW and diluted for counting on a Petroff-Hausser chamber to determine cell density.

Larval infection and chemical exposures

Larvae were infected with *Vibrio diazotrophicus* (Vd) at a density of 10^7 cells/ml, as described in Ho *et al*. 2016. Briefly, prepped bacteria were added to cultures of larvae for a simple sea water exposure and left in culture for up to 24 hours post-infection (hpi).

In addition to treatment groups that were infected with Vd only, some larvae were treated with varying doses of anthropogenic chemicals (Cyclosporin A, PBDE-100, 4'4'-DDT). Chemical stocks of Cyclosporin A were prepared in fresh DMSO and stored at -20°C. Working concentrations were diluted out in FSW and vortexed to ensure no particles precipitated out of solution. The concentration of DMSO was never >1:1000 in order to avoid adverse effects of the vehicle.

Larvae were sampled at 0, 6, 12, and 24 hpi and imaged live on a Zeiss LSM 700 confocal microscope (Jena, Germany) with a 20x objective using differential interference contrast (DIC). The number of migratory pigment cells in each individual larvae was counted by eye during live imaging. Images for gut morphometric analysis were captured using the Zen software suite, and micrograph measurements of the largest cross-section of the stomach (mid-gut) were performed using ImageJ (National Institutes of Health, Bethesda, MD, USA).

Data analysis

Data were analyzed and visualized using the GraphPad Prism 9 (v.9.2.0.332) software program. Each individual experiment was performed with a single mate pair (sibling larvae) and treatment significance was determined using minimum n=3 batches (mate pairs) of sibling

larvae. Treatment significance was determined using ANOVA. Data were plotted using the GraphPad suite and exported as high quality (300dpi) image files labelled in Adobe Illustrator.

4.7 ACKNOWLEDGEMENTS

Chapter 4 is currently being prepared for submission for publication. Nesbit KT and Hamdoun A. The dissertation author is the primary investigator and author of this material

4.8 REFERENCES

1. Flajnik MF, Kasahara M. Origin and evolution of the adaptive immune system: genetic events and selective pressures. *Nature Reviews Genetics*. 2010;11(1):47-59.

2. Buchmann K. Evolution of innate immunity: clues from invertebrates via fish to mammals. *Frontiers in immunology*. 2014;5:459.

3. Hirano M. Echinoderm immunity: is the larval immune system immature? *Immunology and Cell Biology*. 2016;94(9):809.

4. Smith LC, Rast JP, Brockton V, Terwilliger DP, Nair SV, Buckley KM, Majeske AJ. The sea urchin immune system. *Invertebrate Survival Journal*. 2006;3(1):25-39.

5. Ho EC, Buckley KM, Schrankel CS, Schuh NW, Hibino T, Solek CM, Bae K, Wang G, Rast JP. Perturbation of gut bacteria induces a coordinated cellular immune response in the purple sea urchin larva. *Immunology and cell biology*. 2016;94(9):861-874.

6. Shipp LE, Hill RZ, Moy GW, Gökırmak T, Hamdoun A. ABCC5 is required for cAMP-mediated hindgut invagination in sea urchin embryos. *Development*. 2015;142(20):3537-3548.

7. Calestani C, Rast JP, Davidson EH. Isolation of pigment cell specific genes in the sea urchin embryo by differential macroarray screening. 2003.

8. Buckley KM, Ho ECH, Hibino T, Schrankel CS, Schuh NW, Wang G, Rast JP. IL17 factors are early regulators in the gut epithelium during inflammatory response to Vibrio in the sea urchin larva. *Elife*. 2017;6:e23481.

9. Roze E, Meijer L, Bakker A, Van Braeckel KN, Sauer PJ, Bos AF. Prenatal exposure to organohalogens, including brominated flame retardants, influences motor, cognitive, and behavioral performance at school age. *Environmental health perspectives*. 2009;117(12):1953-1958.

10. Darnerud PO. Toxic effects of brominated flame retardants in man and in wildlife. *Environment international*. 2003;29(6):841-853.

11. Estrada I, Calderon-Aranda ES. DDT inhibits the functional activation of murine macrophages and decreases resistance to infection by Mycobacterium microti. *Toxicology*. 2002;174(3):201-210.

12. Luebke B. Pesticide-induced immunotoxicity: are humans at risk? *Human and Ecological Risk Assessment: An International Journal*. 2002;8(2):293-303.

13. Forawi HA, Tchounwou PB, McMurray RW. Xenoestrogen modulation of the immune system: effects of dichlorodiphenyltrichloroethane (DDT) and 2, 3, 7, 8-tetrachlorodibenzo-p-dioxin (TCDD). *Reviews on environmental health*. 2004;19(1):1-14.

14. Leijs MM, Koppe JG, Olie K, Aalderen WMv, Voogt Pd, Tusscher GWt. Effects of dioxins, PCBs, and PBDEs on immunology and hematology in adolescents. *Environmental science & technology*. 2009;43(20):7946-7951.

15. Thuvander A, Darnerud PO. Effects of polybrominated diphenyl ether (PBDE) and polychlorinated biphenyl (PCB) on some immunological parameters after oral exposure in rats and mice. *Toxicological & Environmental Chemistry*. 1999;70(1-2):229-242.

16. Liu X, Zhan H, Zeng X, Zhang C, Chen D. The PBDE-209 exposure during pregnancy and lactation impairs immune function in rats. *Mediators of inflammation*. 2012;2012.

17. Pullen S, Tiegs G. Immunotoxic effects of polybrominated flame retardants. NAUNYN-SCHMIEDEBERGS ARCHIVES OF PHARMACOLOGY: SPRINGER-VERLAG 175 FIFTH AVE, NEW YORK, NY 10010 USA; 2001. p. R141-R141.

18. Fowles JR, Fairbrother A, Baecher-Steppan L, Kerkvliet NI. Immunologic and endocrine effects of the flame-retardant pentabromodiphenyl ether (DE-71) in C57BL/6J mice. *Toxicology*. 1994;86(1-2):49-61.

19. Watanabe W, Shimizu T, Hino A, Kurokawa M. Effects of decabrominated diphenyl ether (DBDE) on developmental immunotoxicity in offspring mice. *Environmental Toxicology and Pharmacology*. 2008;26(3):315-319.

20. Nesbit KT, Hamdoun A. Embryo, larval, and juvenile staging of L*ytechinus pictus* from fertilization through sexual maturation. Developmental Dynamics; 2020.

21. Guerinot M, West P, Lee J, Colwell R. Vibrio diazotrophicus sp. nov., a marine nitrogen-fixing bacterium. *International Journal of Systematic and Evolutionary Microbiology*. 1982;32(3):350-357.

22. Borel JF, Feurer C, Gubler H, Stähelin H. Biological effects of cyclosporin A: a new antilymphocytic agent. *Agents and actions*. 1994;43(3):179-186.

23. Dunn CJ, Wagstaff AJ, Perry CM, Plosker GL, Goa KL. Cyclosporin. *Drugs*. 2001;61(13):1957-2016.

24. Stepkowski SM. Molecular targets for existing and novel immunosuppressive drugs. *Expert reviews in molecular medicine*. 2000;2(4):1-23.

25. Sabella C, Faszewski E, Himic L, Colpitts KM, Kaltenbach J, Burger MM, Fernàndez-Busquets X. Cyclosporin A suspends transplantation reactions in the marine sponge Microciona prolifera. *The Journal of Immunology*. 2007;179(9):5927-5935.

26. Oren M, Paz G, Douek J, Rosner A, Amar KO, Rinkevich B. Marine invertebrates cross phyla comparisons reveal highly conserved immune machinery. *Immunobiology*. 2013;218(4):484-495.

27. Li C, Liang J, Ma Z, Hu Y, Yan Z, Li Q, Fang Z, Wang H, Zhang G, Xie L, Zhang R. Calcineurin mediates the immune response of hemocytes through NF-κB signaling pathway in pearl oyster (Pinctada fucata). *Fish & shellfish immunology*. 2010;28(2):253-260.

28. Warner JF, Lord JW, Schreiter SA, Nesbit KT, Hamdoun A, Lyons DC. Chromosomal-level genome assembly of the painted sea urchin Lytechinus pictus, a genetically enabled model system for cell biology and embryonic development. *Genome Biology and Evolution*. 2021.

29. Agarwal V, Blanton JM, Podell S, Taton A, Schorn MA, Busch J, Lin Z, Schmidt EW, Jensen PR, Paul VJ, Biggs JS. Metagenomic discovery of polybrominated diphenyl ether biosynthesis by marine sponges. *Nature chemical biology*. 2017;13(5):537-543.

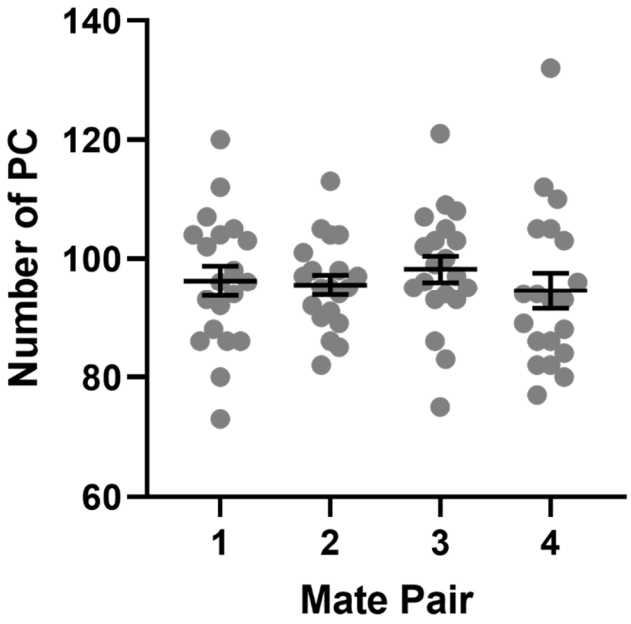

Figure 4.1. Pigment cell numbers in *L. pictus* larvae. Pigment cell numbers counted in 3 day old larvae. N=20 larvae from 4 genetically distinct mate pairs.

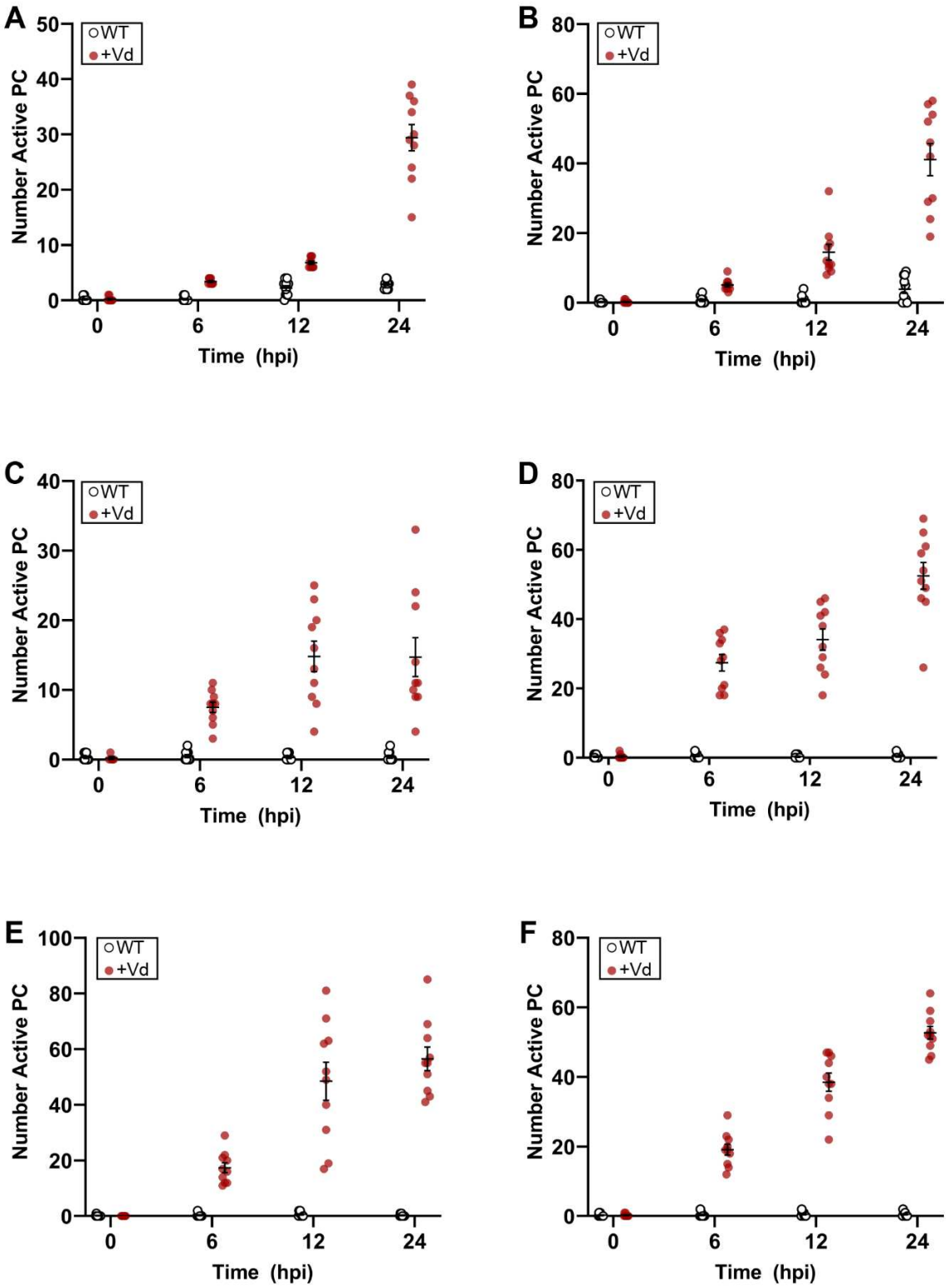

Figure 4.2. Pigment cell migration in response to infection varies by mate pair. Immune responses vary among siblings within a single mate pair, and across mate pairs over the course of a 24 hour infection period (hpi). Wild type, uninfected animals are white circles. Larvae infected with 10^7 cells/ml of *Vibrio diazotrophicus* are red circles. Mean with SEM shown. Panels A-F correspond to mate pairs 1-6 respectively.

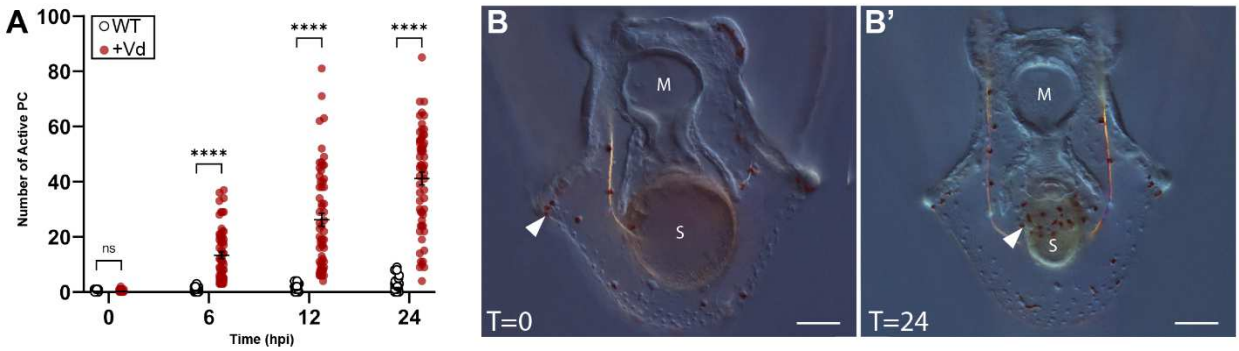

Figure 4.3. Infection with *Vibrio* causes significant differences in pigment cell migration. A) Quantification of migratory pigment cell responses pooled from genetically distinct mate pairs. N=6 mate pairs. Statistical labelling: ns – not significant ($P > 0.05$); "****" means $P > 0.0001$. **B)** Phenotypic response of larvae to infection. Scale = 50 µm. Panel B depicts a 3dpf larvae at T=0, the start of infection. Pigment cells (white arrow) are embedded in the ectoderm, the stomach (S) is large and round. M labels the mouth. In B', at 24 hours post-infection, the stomach (S) is dramatically reduced in size, and pigment cells (white arrow) are clustered around the stomach. The epithelia of the stomach is thickened due to inflammation.

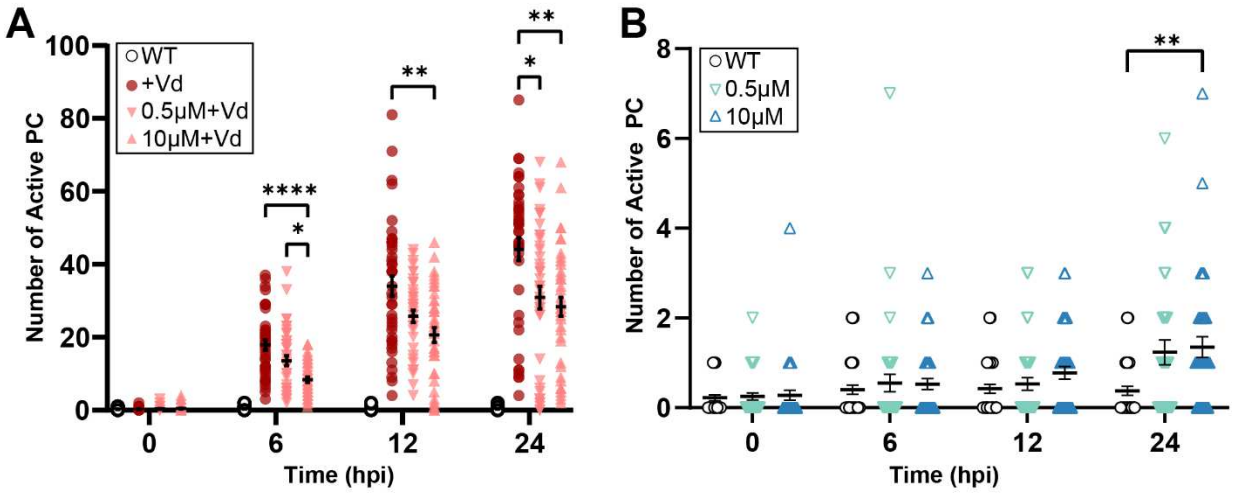

Figure 4.4. Cyclosporin A exposure impairs pigment cell migration during larval infection. N=4 mate pairs. Statistical labelling: insignificant relationships (P > 0.05) are not labelled; "*" means 0.05 > P > 0.0332; "**" means 0.0332 > P > 0.0021; "****" means P < 0.0001. **A)** At low concentration (0.5µM), there is no significant difference between infected (+Vd, red circles) and low does exposed and infected (0.5µM+Vd, pink inverted triangles) larvae until 24 hours post-infection (hpi). In contrast, infected larvae treated with higher doses (10µM+Vd, pink triangles) of drug had significantly reduced PC migration throughout the course of infection. All infected larvae (red and pink shapes) had significantly different PC migration compared to uninfected wild-type larvae (WT, white circles). **B)** Drug exposure alone did not significantly affect PC migration at low doses (0.5µM) or at earlier time points. Exposure at high doses (10µM) for longer periods of time (24hpi) did result in a significant increase in PC migration compared to wild type untreated larvae.

Table 4.1. Molecular targets of toxicant exposure involved in immunity and pigment cell function. Dashed lines indicate no hits for a particular column.

Category	Gene Family	LPI ID	Length (AA)	NCBI Top Hit	E-value	Identity	Echinobase Top Hit	E-value	Identity	SMART Motif Prediction
Cytokines	IL17	LPI_035120.1	186	---	---	---	XP_041483820.1	4.00E-118	94	---
	IL17	LPI_035120.2	169	---	---	---	XP_041483821.1	3.00E-118	94	---
	IL17	LPI_036360	155	---	---	---	XP_041484085.1	7.00E-98	89	---
	MIF	LPI_006139	140	---	---	---	XP_041460209.1	7.00E-101	98	---
Effectors	185/333 candidate	LPI_016013	315	---	---	---	XP_041454462.1	3.00E-107	92	---
	185/333 candidate	LPI_016016.1	128	---	---	---	XP_041454462.1	7.00E-18	97	---
	185/333 candidate	LPI_016016.2	118	---	---	---	XP_041454462.1	5.00E-11	98	---
	MacpfA2	LPI_044171	497	---	---	---	XP_001200514.2	0.00E+00	66	---
	MacpfA2	LPI_045230	513	---	---	---	XP_041483343.1	0.00E+00	89	MACPF
	MacpfA2	LPI_045240	490	---	---	---	XP_041483343.1	0.00E+00	87	MACPF
	MacpfA2	LPI_047049	519	---	---	---	XP_041452753.1	1.00E-162	52	---
	MacpfA2	LPI_003970	512	---	---	---	XP_041465790.1	0	81	---
Enzymes	MAPK	LPI_003909	349	Q61532	3.33E-122	55.3	XP_041465658.1	0	99	S_TKc
	MAPK	LPI_004995	342	Q90336	1.94E-173	67.5	XP_041458487.1	0	94	S_TKc
	MAPK	LPI_011813	271	P27361	1.94E-160	69.4	XP_041457074.1	0.00E+00	83	S_TKc
	NOS	LPI_011621.1	1153	B1B557	0.00E+00	47.8	XP_041456933.1	0.00E+00	93	---
	NOS	LPI_011621.2	113	O19132	1.76E-36	55.8	XP_041456933.1	6.00E-72	100	PDZ
	NOS	LPI_011664	458	Q9ZQJ4	1.73E-131	46.3	XP_041456958.1	0.00E+00	98	---
	PKS	LPI_000046	1109	C8VJR7	3.28E-171	32.2	XP_041457046.1	0	99	PKS_AT
	PKS	LPI_037472.1	525	G4N296	2.77E-112	42.1	XP_041481149.1	0.00E+00	98	---
	SULT	LPI_005443.1	304	Q9BR01	1.47E-54	34.4	XP_041461041.1	0	96	---
	SULT	LPI_005443.2	284	Q9WUW9	4.68E-52	35.7	XP_041461041.1	0	96	---
	SULT	LPI_023848.1	281	Q8JG30	1.47E-60	39.9	XP_041475933.1	0.00E+00	95	---
	SULT	LPI_023848.2	274	Q8JG30	1.58E-60	39.9	XP_041475933.1	0.00E+00	95	---
	SULT	LPI_037238	238	O75897	4.09E-42	35.4	XP_041480796.1	2.00E-163	82	---
	SULT	LPI_041227.1	255	Q9WUW9	2.26E-65	40.4	XP_041478771.1	4.00E-173	84	---
	SULT	LPI_041227.2	264	Q9WUW9	3.26E-65	40.4	XP_041478771.1	2.00E-178	84	---
	SULT	LPI_041240	185	P0DMM9	5.35E-41	45.8	XP_041479107.1	1.00E-132	93	---
	SULT	LPI_041252	163	Q9D939	3.44E-36	39.4	XP_041479021.1	1.00E-111	89	---
	SULT	LPI_046907	249	Q6IMI6	4.43E-47	34.9	XP_041453028.1	2.00E-179	89	---
Mediators	Calcineurin	LPI_013278	168	P63098	1..13e-95	82.1	XP_041468705.1	2.00E-109	93	Efh (x4)
	Calcineurin	LPI_013279	156	P63098	1.63E-95	87.8	XP_041468705.1	8.00E-110	100	Efh (x4)
	Calcineurin	LPI_013646	165	P61022	1.33E-63	60.6	XP_041469049.1	2.00E-119	99	Efh (x2)
	Calmodulin	LPI_012879	146	P21251	4.58E-102	99.3	XP_041468344.1	7.00E-103	100	Efh (x4)
	Cyclophilins	LPI_048300	160	P91791	1.59E-95	80.6	XP_041485310.1	2.00E-83	90	---
	Cyclophilins	LPI_003957	223	P24369	1.56E-98	64.7	XP_041465837.1	2.00E-120	90	TMD
	Cyclophilins	LPI_006206	169	A2AR02	6.73E-81	66.9	XP_041460172.1	2.00E-94	99	---
	Cyclophilins	LPI_006216	169	A2AR02	6.73E-81	66.9	XP_041460172.1	2.00E-94	99	---
	Tecp (α macroglobulin)	LPI_003357	745	P28665	8.06E-33	24.4	XP_041464162.1	0	61	Thiol-ester_cl
	Tecp (α macroglobulin)	LPI_003136	978	P20740	5.23E-136	32.1	XP_041465276.1	0	88	A2M, Thiol-ester_cl, A2M_recep
	Tecp (α macroglobulin)	LPI_003446	847	Q8IZJ3	1.18E-66	26.5	XP_041464161.1	0	85	A2M_N_2, A2M
	Tecp (α macroglobulin)	LPI_003447	476	P01023	1.31E-44	28.1	XP_041464161.1	0	92	---
	Tecp (α macroglobulin)	LPI_014634	694	P20742	1.07E-108	32.8	XP_041482013.1	0.00E+00	88	A2M, Thiol-ester_cl
	Traf	LPI_010689	371	Q61382	1.30E-141	49.2	XP_041455445.1	0.00E+00	98	RING
	Traf	LPI_018830	154	A7XUJ6	1.20E-26	42.3	XP_041474300.1	7.00E-107	97	RING
Pattern Recognition	srcr	LPI_010148.1	811	Q9UGM3	0.00E+00	42.1	XP_030831078.1	0.00E+00	54	SR (x8)
	srcr	LPI_010148.2	814	Q9UGM3	0.00E+00	42.1	XP_030831078.1	0.00E+00	54	SR (x8)
	srcr	LPI_010154.1	918	F7J220	0.00E+00	38.2	XP_041453692.1	0.00E+00	80	SR (x9)
	srcr	LPI_010154.2	926	F7J220	0.00E+00	38.2	XP_041453692.1	0.00E+00	80	SR (x9)
	srcr	LPI_010154.3	918	F7J220	0.00E+00	38.2	XP_041453692.1	0.00E+00	80	SR (x9)
Transciption Factors	Ahr	LPI_000687	362	Q9BE97	2.11E-177	65.6	XP_041464012.1	0	91	HLH, PAS, PAC
	bmp	LPI_014108	356	P21274	2.18E-120	51.1	XP_041469447.1	0.00E+00	99	TGFB
	bmp	LPI_048555	170	Q7T2X7	7.54E-38	42.7	XP_041486073.1	1.00E-108	100	coiled coil, TGFB
	bmp	LPI_048556	170	Q7T2X7	7.54E-38	42.7	XP_041486073.1	1.00E-108	100	coiled coil, TGFB
	GCM	LPI_036453	703	Q27403	2.46E-33	54.4	XP_041483779.1	0.00E+00	97	---
	HIF	LPI_013032	128	Q99814	2.57E-36	53.9	XP_041468476.1	8.00E-66	96	HLH
	Hnf1a	LPI_010951	177	P15257	2.40E-61	52.8	XP_041456344.1	3.00E-121	81	HOX
	Hnf4	LPI_008792	359	P79926	2.11E-167	68.2	XP_041454631.1	0.00E+00	97	ZnF_C4, HOLI
	NF-Atc	LPI_009108	268	D3ZGB1	3.12E-78	53.7	XP_041454816.1	0.00E+00	99	IPT
	NF-ATF	LPI_005300	398	Q8R0S1	1.86E-64	37.4	XP_041459199.1	0	96	ZnF_C2H2, BRLZ
	NFkB	LPI_011978.1	226	O54910	1.04E-40	41.2	XP_041467783.1	6.00E-160	96	ANK (x6)
	NFkB	LPI_011978.2	228	O54910	1.30E-41	41.3	XP_041467783.1	1.00E-161	96	ANK (x6)
	NFkB	LPI_048802	201	---	---	---	XP_041485049.1	1.00E-100	70	ANK (x2)
	RXR	LPI_036774	268	Q90415	3.07E-131	59.8	XP_030853251.1	2.00E-154	75	HOLI
	six	LPI_013603	174	Q9UIU6	4.37E-89	69	XP_781616.2	8.00E-132	99	HOX
	six	LPI_013608	332	Q6NZ04	2.50E-135	84.7	XP_041469016.1	8.00E-177	95	HOX
	six	LPI_013611	188	O95475	2.66E-121	90.4	XP_781696.1	3.00E-140	100	HOX
	TGF-b related	LPI_014107	364	P48970	0.00E+00	83.1	XP_041469445.1	0.00E+00	99	TGFB

CHAPTER 5

Epilogue: Unpublished results from this dissertation research

5.1 ABSTRACT

There are many experiments attempted throughout the course of one's dissertation research. With certainty, a number of these endeavors prove unsuccessful, yielding negative results or lacking motivating pieces of data that justify further pursuit. This chapter summarizes the results of several preliminary experiments that did not yield data that has contributed to formal publications, but may prove useful for the next generation of students in the lab as they consider what to do or not do, or may spark ideas for future investigation and tool development. The information presented here are subdivided into mini-projects that highlight experimental efforts focused on cAMP-mediated signaling in urchin gastrulation, imaging tools in *L. pictus*, development of bacterial strains for experiments, and identifying regulatory machinery in *L. pictus*. Each mini project is organized into relevant background information, results, discussion and conclusions, and methods.

5.2 MINI-PROJECT 1: Identification of an ADORA receptor in *Strongylocentrotus purpuratus*

5.2.1 INTRODUCTION:

It was recently discovered that one mechanism of transport for cAMP in the sea urchin is via the ABC transporter ABCC5a. Interestingly, ABCC5a was recently demonstrated to play a role in gastrulation - a critical and highly conserved developmental process - by secreting sAC-derived cAMP into the blastocoel from pigment cells embedded in the ectoderm[1]. When the ABCC5a transporter was knocked down using morpholino, the embryos developed a prolapsed gut during secondary invagination, but were rescued by exposure to membrane permeable cAMP[1]. This nucleotide signal is proposed to reach a population of cells in the hindgut, and

assist in coordination of invagination of the larval gut. However, a specific characterization of a receptor of cAMP in the sea urchin embryo is unknown.

The primary mechanism for reception of cyclic nucleotides in other organisms is through G-protein coupled receptors (GPCRs). GPCRs are one of the largest classes of membrane proteins. In humans, for example, there are 791 different GPCRs[2]. Within the sea urchin genome, GPCRs account for a significant portion of annotated genes and the largest subgroup is the Rhodopsin-like GPCR subgroup [3,4]. Importantly this means the sea urchin is likely to have at least one GPCR sensitive to cAMP.

The major GPCRs for cAMP are likely homologs of the ADORA (adenosine receptor) group. Initially discovered in the early 1970's in mammalian models (i.e. guinea pig [5], mouse [6], rat [7]) following a history of clinical observations of the cardiac and other physiological effects of adenosine compounds [8], the ADORA receptors are now divided into four main types – A1, A2a, A2b, and A3 [9]. The A1 and A2a type receptors are the most widespread, and play roles in the cardiovascular system and CNS in mammals including. A2b type receptors are less commonly expressed, but are found in most cell types at very low expression levels - however there is evidence of increased expression of A2b receptors in the intestine and bladder in humans. The A3 type receptors are often minimally expressed, and in patterns that are highly species dependent [9]. Of these four groups, only the A2a and A2b type adenosine receptors have been identified in the genome of the sea urchin [10].

The A2a receptor is specifically receptive to adenosine signals which are produced by ectonucleotides that hydrolyze cAMP to adenosine outside of the cell [11]. The A2a receptor is unique in that it is pre-coupled to a G_s protein, which by definition sets up a restricted collision coupling system, meaning that the receptor is unable to access all G_s units and activate all the

adenylyl cyclase units subsequently [12]. The A2a-G_s complex is tightly bound and resistant to dissociation by guanine nucleotides, and is also unique in that is has a large intracellular C-terminus which is thought to be capable of binding to other intracellular accessory proteins besides just G_s type proteins [13]. It is also possible that A2a may be able to receive cyclic nucleotide signals independent of ectonucleotidase activity like A1 -type receptors, however this has yet to be validated further [14].

Key to understanding signaling pathways is knowledge of 1) the identity of the signal, 2) how signals are generated, compartmentalized, and transported, and 3) how signals are received and generate downstream cascades in the embryo (Fig. 5.1). The goal of this study was to identify and localize adenosine receptors in the sea urchin, to better understand the role of cAMP in gastrulation. I hypothesize that an adenosine receptor is expressed on the surface of the hindgut in the urchin embryo during gastrulation. Furthermore, that perturbation of this receptor will alter patterning of the gut during gastrulation and result in phenotypic responses akin to those induced by morpholino knockdown of ABCC5a

5.2.2 RESULTS

In silico *techniques for identification of putative adenosine signal receptors in the sea urchin:*

Reciprocal BLAST of the human ADORA2a gene against the sea urchin peptide database (Echinobase) yielded the top hit as the most likely candidate for a putative adenosine receptor. The subsequent hits were manually annotated for two other types of GPCRs and their isoforms which are sensitive to dopamine and histamine. The identified A2a receptor candidate encodes a 400-amino acid long polypeptide, which is a likely full-length peptide (Table 5.1). The gene consists of a single exon that is 4925 bp long, with the coding sequence only spanning 1203 bp (Fig. 5.2A).

The identified sea urchin A2a candidate also has high peptide sequence homology to known A2a receptors, with 58.15% identity and 73.53% similarity to the human form of this receptor, which is greater than the homology to the human A2b type receptors (at 45.18% identity and 71.98% similarity), strongly suggesting that SPU_008789 is a true A2a-like receptor (Fig. 5.2B). The identified candidate also has seven transmembrane domains (TMDs), characteristic of GPCRs, which closely align with the TMDs of known adenosine receptors. There is also higher identity and similarity in these structural motifs, than the overall peptide sequence homology indicating that these functional domains are highly conserved across groups, and strengthen the support that the identified peptide sequence in sea urchin is a true A2a-like receptor (Fig. 5.2B).

Expression data curated from the developmental transcriptome in Echinobase reveals that the expression of the candidate A2a receptor (SPU_008789) increases starting at approximately 36 hours post fertilization. This tracks behind the noted increase in expression of ABCC5a, which begins at gastrulation approximately 30 hours post fertilization (Table 5.2). Collectively, the *in silico* analyses suggest the identified candidate A2a receptor in the sea urchin is a true, full length, A2a-like receptor.

Cloning of a putative sea urchin ADORA2a:

The partial sequence cloned from the primers against SPU_008789 yielded successful insertion of an approximately 900bp insert into the vector. Quality check on the insert shows that the clone has 25.35% identity and 42.72% similarity to the full candidate receptor nucleotide sequence, which is to be expected given that the clone is a partial sequence. In the region of overlap, the clone shares 36.00% identity and 60.68% similarity to the receptor nucleotide sequence. The translated peptide sequence for the clone against this candidate receptor has

70.5% coverage and 100% identity to the endogenously generated receptor, indicative that the levels of identity and similarity of the cloned sequence are sufficient to generate a probe targeting the endogenous transcript encoding the A2a receptor (Fig. 5.2A).

Fluorescent in situ *hybridization of a putative sea urchin ADORA2a*

Fluorescent *in situ* hybridization has revealed some preliminary patterning in the embryo at the early stages of gastrulation. Localization of the sea urchin A2a transcript at 36 and 48 hours post fertilization (hpf) does occur within areas of the hindgut, but appears to also be expressed in other cell types (Fig. 5.3). These preliminary experiments would suggest that A2a is not restricted to the hindgut. To get the protocol working, a control probe – *gcm* – which labels mesenchymal cells that aggregate in the hindgut and ultimately migrate off the tip of the archenteron [15], was used (Fig. 5.3). It is evident that further validation of these observations is necessary to confirm our hypothesized expression patterning. Additional relevant controls, such as a sense probe and additional developmental stages are needed. Moreover, other markers of the hindgut, non-skeletogenic mesoderm, and other cell-specific markers will be utilized as relevant controls when verifying A2a patterning observations.

5.2.3 DISCUSSION AND CONCLUSIONS

Sea urchins are a highly polymorphic organism, and as such it is expected that the partial clone generated from the A2a candidate identified from the genome would likely not be a perfect match to the endogenous transcript in other individuals. However, the levels of identity and similarity of the sequence are sufficient to specifically target an A2a type transcript in the embryo as opposed to other non-target transcripts.

Preliminary localization data is inconclusive as to whether the sea urchin ADORA2a is present in the hindgut during gastrulation, as hypothesized. The evidence demonstrated by Shipp

et al. 2015 alludes to the importance of a cAMP receptor in the hindgut. Embryos accumulate ABCC5a substrates in this region, and membrane permeable cAMP rescued the prolapsed gut phenotype embryos with impaired ABCC5a function and induced hyper-invagination of the gut in wild type embryos [1]. It is anticipated that this receptor will be located on the surface of those hindgut cells. It is thus far unclear how exactly a surface adenosine receptor may contribute to gastrulation in the sea urchin.

The well-studied slime mold *Dictyostelium,* relies upon extracellular cAMP to induce expression of several classes of developmentally regulated genes [16]. It is also well recognized that cAMP levels can alter accessibility of histones [17], alter ionic conditions which influence chromosome structure [18], or even overcome transcriptional polarity [19] effectively changing gene expression. *Dictyostelium* also displays motile behaviors and migrates towards cAMP [20] , indicating that in addition to altering gene expression, more immediate cellular responses can be elicited from exposure to extracellular cAMP. We propose that these sorts of mechanics – i.e., altered gene expression or elicited cellular behavioral responses - may be operating within the urchin embryo to assist in coordination of gastrulation, and require further investigation of the function of sea urchin A2a to validate this hypothesis.

These preliminary localization data could be interpreted as showing expression of the sea urchin ADORA in other cell types within the embryo. These cell types may also be receptive to adenosine signals. For example, the secondary mesenchyme cells contained small amounts of A2a expression and thus may rely upon adenosine signals to coordinate the embedding behavior of pigment cells or other migratory/orientation cues. It may also be the case that the widespread use of cAMP signals requires expression of these receptors on varied cell types and that a

different type of receptor – such as A2b – may be more developmentally relevant for gastrulation.

Future investigation into this receptor subtype for its role in gastrulation include functional perturbation via pharmacological methods. For example, A2a type receptor activity is well known to be inhibited by caffeine – however, due to the widespread effects of caffeine on multiple systems, the more specific and well-known analogs of caffeine, istradefylline and ATL-444, can be used to block signal reception. Once signal is blocked, the phenotypic responses in the developing embryos can be observed with special attention to the potential for prolapses of the gut to arise.

Other perturbations of sea urchin A2a include the use of the CRISPR/Cas9 gene editing technology to interrupt the function of this receptor at the genetic level, and screening for subsequent phenotypic responses. More specifically, the double stranded breaks in the DNA encoding this gene caused by the Cas9 enzyme can yield mistakes when the DNA repairs itself, and consequently hinder production of a functional transcript and receptor protein. The hypothesis is that perturbation of this gene will yield phenotypes like that of the ABCC5a knockdown – a prolapsed gut.

It should be noted that these results and predictions were originally compiled based off of an earlier assembly of the sea urchin genome (v.3.1) and associated resources. Since my initial inquiries into this topic, the identified adenosine receptor candidate (SPU_008789) has received updated annotation as an A2b-type receptor, not an A2a receptor.

5.2.4 METHODS

Identification of putative signal molecule receptors in the sea urchin:

Genome mining for putative receptors of cyclic nucleotides: A sequence of the well-known adenosine receptor, ADORA2a (A2a), from human (NCBI) was used in reciprocal BLAST searches against the sea urchin genome in Echinobase. Candidate receptors were then translated in ExPASy Translate tool and aligned to the query sequence using MAAFT. Percent identity and similarity were then calculated by taking the number of identical amino acid residues and dividing by the total number of residues in the longest sequence and multiplying by 100, or taking the sum of identical, highly similar, and similar residues and dividing by the number of amino acid residues in the longest sequence and then multiplying by 100, respectively. Manual annotations for the candidate receptor genes within Echinobase were also taken into consideration to determine whether a reciprocal BLAST hit was a true ADORA2a homolog. Membrane topology for the identified candidate receptor was then determine and vetted using three different structural/topology prediction programs – SMART, TMHMM, and TOPCONS. Structural domains that were agreed upon between all three predictions were considered highly vetted predictions. The 3D structural prediction program Phyre was used to model the putative receptors, and the program model was visually compared to the crystal structure for known A2a receptors for any anomalous motifs. Experimentally determined binding residues or residues essential for protein function identified in the literature for the human and mouse A2a receptors were then identified, and the sea urchin putative receptor sequence was examined to see if such residues were conserved and could serve roles of similar importance in the urchin.

Expression data from a developmental transcriptome to screen for developmentally relevant receptors:

Expression levels of candidate receptors identified from genome mining were determined from the Echinobase developmental transcriptome for Strongylocentrotus purpuratus. The candidates that had a significant increase in expression around gastrulation were determined to be more likely candidates with roles in receiving signals relevant to this process. Those candidates which also increased in expression following the increase in expression of the ABC transporter ABCC5a were also considered relevant candidates.

Localization of candidate receptors via molecular cloning and fluorescent in situ hybridization (FISH):

Probe generation: The candidate receptor sequence identified from genome mining was then used to design primers and generate an *in situ* probe for localization within the urchin embryo. Using the following primer set, a portion of the A2a gene was amplified out from cDNA of the embryo 24 hours post fertilization via PCR (Primer set: Forward 5'- CAA TGA CTC AGA ACC GGA CTA-3' ; Reverse 5'- CTT ATG GAA CGT CCT CCT GAA-3'). The amplified fragment was isolated using column clean-up and the product was run on a 0.8% agarose gel for 30 minutes at 200V to confirm amplification of the approximately 900bp fragment. The fragment was isolated and extracted from the gel using standard gel-cleanup procedures and then cloned and transformed into NEB 10-β E. coli cells. Miniprep isolation of DNA from transformed cells was sent for sequencing to confirm insertion of the fragment encoding the *in situ* probe, and orientation of the fragment within the plasmid was determined via sequence analysis and alignment in Sequencher. Isolated plasmid was then linearized using SpeI or Not-HF for generation of the antisense and sense probes respectively. Linearized plasmid was then used for in vitro transcription to synthesize the RNA probe and validated for concentration and quality via Nanospec and gel electrophoresis.

FISH: Protocols for in situ hybridization of the probe specific to sea urchin A2a are modified from preexisting published protocols. Pre-hybridization washes, hybridization, and post-hybridization washes follow Shipp and Hamdoun 2012[21], and remaining steps are in accordance with Chen et al. 2011[22]. Control probes for *gcm* were used to mark aboral non-skeletogenic mesoderm cells and their derivatives - the pigment cells [23].

Imaging: For FISH, embryos were mounted in TBST (Tris-buffered saline + 01% Tween-20) and viewed on a Zeiss LSM 700 microscope using a 20x objective. Imaging for the DIC developmental time series of Lytechinus was also undertaken on the Zeiss LSM 700 using a 20x objective. Images were processed using Fiji, and the developmental time series was processed using Imaris 7.6.1 (Bitplane).

5.3 MINI-PROJECT 2: Imaging tools and techniques in *L. pictus*

5.3.1 INTRODUCTION

Microscopy has been a foundational tool for biological discovery dating back to the 17th century when Robert Hooke first published his famous work "Micrographia"[24] detailing the structure of numerous objects and organisms (notably plants and insects). Since then, the tools and techniques have significantly advanced, but the core components of imaging systems, and their importance for uncovering the structural and functional features of living things is unparalleled.

Imaging systems consist of four main elements: 1) an illumination source; 2) an object to observe; 3) a lens; and 4) a detector. These elements are shared across diverse imaging approaches including basic light microscopy, scanning and transmission electron microscopy, and fluorescence microscopy to view both live and fixed specimens. The ability to utilize a

variety of imaging approaches is a great advantage for uncovering the complex biology of the sea urchin embryo.

The urchin embryo has a number of key advantages that make it ideal for microscopy – namely the optical clarity of the embryo and relatively large size make visualization with cellular resolution possible. Live-imaging in particular allows for the observation of the dynamic interactions within and among cells, and with the environment. A number of excellent techniques and tools have been developed for working with sea urchin embryos for live and fixed imaging including: *in situ* hybridization, immunolabelling, overexpression of mRNA, and small molecule accumulation among others. The majority of these techniques have been optimized for use in the purple sea urchin, *Strongylocentrotus purpuratus*. However, the painted white urchin, *Lytechinus pictus*, offers some distinct advantages for imaging over purple urchins.

The enhanced transparency of the egg and embryo, as well as larger size and rapid pace of development mean that fine-tuning of some of the live-cell visualization approaches is needed to achieve optimal results. For example, RNA toxicity is a major concern when overexpressing constructs in the embryo. Too little construct, or if poor quality mRNA is used, and the labelling can be difficult to resolve; too much, or again if poor quality reagent is used, and the embryos can get sick and display developmental defects including delay or arrest of development, abnormal cell division, blebbing, and apoptosis of cells. With small molecule labelling, dialing in concentrations is key to capturing the dynamic range accumulated by the cell. Here I present data on the adaptation of live-imaging approaches for utilization in *L. pictus* – specifically, on modifications relevant for overexpression of mRNAs and small molecules labeling.

5.3.2 RESULTS

Optimization of mRNA Overexpression in L. pictus

The eggs of *L. pictus* are more transparent, and larger than those of *S. purpuratus* (Fig. 5.4A). As such, when smaller amounts of mRNA for overexpression were delivered to the embryo via zygotic microinjection, similar detailed imaging of the subcellular localization of these constructs *in vivo* was achieved. The concentrations used in *L. pictus* compared to *S. purpuratus* are summarized in Table 5.3. Moreover, these constructs have the same localization patterns (Fig. 5.4B-E) to that in *S. purpuratus* which means these well-established imaging tools can be repurposed in an additional model species and confidently relied on as markers of particular cells or structures. For example, the mCherry-TJP construct which labels tight junctions in the embryo and is visible at approximately the 60-cell stage in *S. purpuratus* also labels cellular junctions in *L. pictus* and comes up at the comparable developmental timepoint (Fig. 5.4C). The pleckstrin homology domain from human phospholipase c-delta (PH Domain) labelled with Citrine is localized to the plasma membrane, and is enriched in the primordial germ cells (PGCs) at the tip of the archenteron during gastrulation in *S. purpuratus*. When overexpressed in *L. pictus*, this construct also localizes to the membrane and is enriched in the PGCs at the tip of the archenteron during gastrulation (Fig. 5.4D). Other labels for the membrane and nuclear proteins, such as histone (H2b) and a lymphocyte tyrosine kinase membrane anchoring domain (LCK) localize as expected in *L. pictus* as they do in *S. purpuratus* (Fig. 5.4B, C, and E).

Small molecule labelling of live embryos

Labelling of embryonic cells with small molecules is a useful tool for tracking dynamic populations of cells over time. The methods for exposing live embryos to the small molecules calcein-AM for labelling of PGCs are identical between *L. pictus* and *S. purpuratus*. Increased uptake of CAM in the micromeres (Fig. 5.4F) can be observed as early as the 16-28-cell stages,

when asymmetric cell divisions take place, forming this group of cells at the vegetal pole. Another method investigated in *L. pictus* for cell labeling is through the use of lipophilic carbocyanine dyes, such as DiI. Use of these dyes results in the random labelling of individual cells. These dyes can be used individually or in combination to generate multi-spectral labelled animals (Fig. 5.4G). Overall, it appears that the established small molecule labelling techniques in sea urchin are easily-translated across species, and require little to no modification of protocols for the specific approaches presented here.

5.3.3 DISCUSSION AND CONCLUSIONS

Though some minor modifications are required for live-cell imaging in *L.* pictus, overall, it is helpful that the bulk of tools and techniques for imaging in other sea urchin species can be translated with relative ease to this model. The modifications for overexpression, for example, leverage the enhanced optical clarity of the embryo and require small amounts of reagent to generate bright fluorescent expression. Applications for the overexpression approaches can

For small molecule labelling, it is useful to be able to observe changes in cell populations through space and time *in vivo*. These approaches take advantage of simple protocols and yield labelling patterns that are spectrally akin to the genetically controlled multispectral labelled systems in mouse[25], fruit fly[26], and zebrafish[27]. With small molecule tools, patches or clones of cells can be monitored, and when used in combination, individual cells with varying spectral properties can be distinguished from one another at different developmental stages. One disadvantage of the lipophilic carbocyanine dye approach is that cells are labelled randomly. The lack of genetic control over cell-type-specific expression of fluorophores limits the utility of this approach. However, the generation of new molecular tools for *L. pictus* such as a genome with chromosomal resolution[28] in combination with rapid advances in genetic tools like CRISPR-Cas

genome editing technologies[29], mean that it is possible a transgenic line of sea urchin with genetically controlled fluorescent-labeling of cells is on the horizon.

5.3.4 METHODS

Generation of mRNA markers for overexpression

Fluorescently labelled markers for different cellular structures were generated using standard approaches in the lab. Briefly, plasmid backbones containing the labelled construct were linearized through restriction enzyme digest. Linear constructs were purified using the NucleoSpin® Gel and PCR Clean-up protocol (Macherey-Nagel) and quality and concentration of the purification was assessed on a Nanodrop ND-1000 Spectrophotometer. Capped mRNA constructs for injection were then synthesized using the T7/SP6 mMessage Machine kit (Thermo Fisher). A slight modification to the mMessage Machine protocol was utilized, where at T=2 hours, the reaction was spiked with 2 µl of additional enzyme and 2 µl of GTP and held at 37°C for an additional 2 hours. Finally, 1 µl of TurboDNAse was added to the reaction for an addition 15 minute incubation at 37°C. The mRNA was precipitated from solution by adding LiCl to the reaction and storing at -20°C overnight. The next day the precipitated mRNA was spun down at 4°C for 15 minutes at 12,000 rpm in a Microfuge® 22R centrifuge (Beckman Coulter™). Supernatant was removed at the mRNA was washed with 70% molecular grade ethanol and spun again for 15 minutes. Finally, the supernatant was removed and the pellet was allowed to air dry before elution in nuclease-free water. Concentration and quality of a 1:10 dilution of the mRNA was assessed using the Nanodrop and running an aliquot of the mRNA on a 1% agarose gel (200V for 35 minutes). The gel was imaged on a Gel Doc™ XR+ with Image Lab™ Software. The concentrated mRNA was diluted to a stock concentration of 2 µg/µl and aliquoted for longer-term storage at -80°C until ready for use for microinjections.

Zygotic microinjection of Lytechinus pictus

Gametes were collected from adult animals maintained at 20°C in flow-through sea water aquaria by injection with 0.5M KCl through the peristomal membrane. Sperm were collected concentrated and stored in an Eppendorf tube at 15°C until ready for dilution. Eggs were collected in a beaker and washed 6-10x with filtered sea water (FSW) to remove the jelly layer from the egg and eliminate debris. Eggs were rowed using a mouth-pipette onto a petri dish coated with 0.25% protamine sulfate. Fresh sperm dilution (2 µl of concentrated sperm into 25 ml of FSW) was prepared and a few drops were added to each plate preceding injection. Fine needles for microinjection were pulled from glass capillaries on a Flaming/Brown Micropipette Puller (Model P-1000, Sutter Instruments). Needles were loaded with injection solution (containing the overexpression construct diluted in water) and attached to a Picosprintzer®III microinjector (Parker Automation) and InjectMan NI2 micromanipulator (Eppendorf). Embryos were injected once the fertilization envelope was raised, and let to grow to the desired developmental stage in dishes at 20°C.

Labelling of primordial germ cells using calcein-AM

The methods for cell labelling using calcein-AM (CAM) are well described in Campanale and Hamdoun 2012[30]. Briefly, embryos were exposed to 250 nM CAM at 2 hours post-fertilization (hpf). For embryos treated with inhibitor, embryos were exposed to 1 µM PSC833 at 1 hour and 50 minutes post-fertilization, ten minutes before exposure to CAM. Embryos were cultured at 22°C until the 16-cell stage or 28-cell stage and then mounted for imaging.

Multispectral labelling in L. pictus using lipophilic carbocyanine dyes

Labeling of embryos using lipophilic carbocyanine dyes was performed as described in Volnoukhin and Brandhorst 2015[31]. Briefly, the Vybrant® Multicolor Cell-labeling Kit was

purchased from Life Technologies and included DiI, DiD, and DiO. Standard DiI and DiO were also purchased from Life Technologies (Waltham, MA). Embryo cultures were generated using standard procedures and the fertilization envelope was removed by gently passing zygotes through a 125 μm mesh to label embryos before hatching. The exposed embryos were then placed into solution with labelling agents. The final concentrations of dyes were 1 μM unless otherwise specified. Incubations in dyes ranged from 45 minutes to 1.5 hours, and were performed with gentle agitation on a rocker both sequentially and simultaneously. After exposure to the dye(s), embryos were washed with fresh FSW three times to remove any excess labeling agents and mounted for imaging.

Confocal imaging of fluorescent-labelled embryos

Embryos were mounted onto slides and imaged live. Images of the embryonic stages were captured using a 20x, 0.8 NA plan-apo objective with DIC optics on a Zeiss LSM 700 confocal microscope (Jena, Germany). Z-stacks of embryonic stages were used to create maximum intensity projections (MIP) using Fiji (Image J). Figures were compiled in Adobe Illustrator.

5.4 MINI-PROJECT 3: Generation of antibiotic resistant bacterial strains for experimental use

5.4.1 INTRODUCTION

Strains of bacteria with specific characteristics are an important tool in biological research. Bacteria can be cultivated for diverse applications in medicine, biotechnology, pharmaceutical development, and alternative energy or other green industries. Creating customized bacteria strains with antibiotic resistance is of particular interest as a method for counterselection and maintaining purity of axenic cultures of microbes. Here I present the

generation of antibiotic resistant strains of the marine nitrogen-fixing bacterium *Vibrio diazotrophicus* for use in immunological assay in the sea urchin. This bacterium was first isolated from the gut of an adult sea urchin[32], and continues to be a valuable tool for inducing immune responses in the urchin larva[33,34]. In addition, I present data on a strain of DNA-restriction-deficient *Vibrio* that I generated to facilitate future labelling efforts of bacteria through conjugation approaches.

5.4.2 RESULTS

Generating antibiotic resistant and DNA-restriction-deficient Vibrio

Strains of *V. diazotrophicus* that are resistant to rifampicin were generated through spontaneous mutation. Out of the colonies that grew on antibiotic-containing plates, six were selected for 16S PCR amplification. From the 6 colonies selected, only three had bands (Fig. 5.5A) indicating successful amplification of the 16S region. Identity of these bacteria was validated using 16S sequencing. The first colony was likely not the target microbe, as the BLAST results came back for a target in mouse (Fig. 5.5B). Colonies (4 and 6) selected for antibiotic resistance were 99.5% and 99% identical respectively to a reference 16S sequence for *Vibrio diazotrophicus* (Fig. 5.5C). Thus, we could confidently identify these microbes as rifampicin-resistant strains of *Vibrio diazotrophicus* generated through spontaneous mutation.

DNA-restriction-deficient *V. diazotrophicus* with rifampicin resistance and kanamycin sensitivity were successfully generated. Out of the 60 colonies screened after conjugations, only a single colony was kanamycin-sensitive and rifampicin resistant, indicating that it was a potential candidate colony for DNA restriction deficiency. Identity of this colony was confirmed with 16S amplification (Fig. 5.6A) and sequencing. The selected colony was sequenced and was 72% identical to a reference 16S sequence from *Vibrio diazotrophicus* (Fig. 5.6B).

5.4.3 DISCUSSION AND CONCLUSIONS

Generating strains of bacteria for future use in experimental settings is a valuable asset for researchers. These bacteria can be utilized in the Hamdoun Lab for larval infection assay of *L. pictus* and *S. purpuratus*. Furthermore, additional microbial labelling efforts can be undertaken using conjugation-based approaches to insert plasmids containing fluorescent proteins or other molecular tags. Expression of these tags can facilitate tracking of microbes *in vivo* and will allow for a more detailed understanding of host-microbe interactions during infection. Visualization of labelled bacteria throughout development can also inform on microbial selection in the gastrointestinal tract, microbe interactions during metamorphosis, and other host-microbe interactions in other systems beyond the urchin embryo. Ultimately, generation of these sorts of tools for experimental applications will advance our understandings of the complex and dynamic ways in which microbes interact with host organisms, in both pathological and symbiotic contexts.

5.4.4 METHODS

Development of antibiotic resistant strains of Vibrio diazotrophicus for infection assay

Wild-type bacteria were acquired as a gift from the Courtney Smith lab at George Washington University (Washington, D.C. USA). Frozen stocks were streaked onto fresh plates of marine broth (MB2216) and identity was validated using 16S sequencing. Once confirmed, cells were plated onto fresh MB2216 plates + 50 µg/ml Rifampicin and allowed to grow at 15°C. Spontaneous mutants were visible on the plates after 2 weeks. Isolated colonies were selected for growth in liquid culture (MB2216+Rif at 50µg/ml) and colony PCR. Colony identity of the antibiotic resistant cells was verified once more using 16S sequencing and frozen stocks were made from liquid cultures of individual colonies after growth at 15°C overnight with agitation.

Glycerol frozen stocks were made by combining 350 µl of overnight liquid culture cells with 150 µl of 50% glycerol in dH_2O, tapping to gently mix. Stocks are stored at -80°C.

Development of a DNA-restriction-deficient strain of Vibrio diazotrophicus

Generation of a DNA-restriction-deficient strain of *Vibrio* was performed using standard approaches. The transfer-positive strain of bacteria, *E. coli* MC1061 was a gift from the Bartlett Lab at Scripps Institution of Oceanography. The *E. coli* MC1061 contained three plasmids with a variety of antibiotic resistance genes (pKT231 for kanamycin and streptomycin resistance; pRK24 for ampicillin and tetracycline resistance; and pRL528 for chloramphenicol resistance). The rifampicin-resistant *Vibrio* (Vd-RIF) strain was tested for kanamycin sensitivity at 50, 100, and 200 µg/ml. Liquid cultures of *E. coli* and Vd-RIF were grown up to approximately equal densities. The *E. coli* was washed by centrifugation at 9,000 x g for 1 minute and resuspended in fresh, antibiotic-free marine broth (MB2216). Conjugations were set up on sterile polycarbonate filters in a fresh MB2216 plate. On one filter, cells were mixed 1:1 Vd-RIF: *E. coli*, on a second filter just Vd-RIF were added, and the third filter contained just *E. coli*. The plate was cultured in the dark at 15°C overnight. The next day, the filters were removed from the plate and placed into 15mL falcon tubes with 5 ml of fresh MB2216. The falcon tubes were vortexed to release the cells from the filter and resuspend them in the media. Cells were pelleted by centrifugation (5000 rpm, 5 minutes) and resuspended in 100 µl of MB2216. Cell suspensions were then plated onto fresh MB2215 plates containing kanamycin (100 µg/ml) and rifampicin (50 µg/ml) and grown at 15°C for 48 hours. Colonies growing on the MB2216+KAN/RIF plates successfully underwent conjugation and were selected for growth in MB2216 liquid media + rifampicin (50 µg/ml) to facilitate conjugated bacteria to eliminate the pKT231 plasmid. Then, 100 µl of these cultured cells were plated onto fresh MB2216 and colonies were selected to test for kanamycin

sensitivity. Colonies with successful growth on MB2216 and unsuccessful growth on MB2216+KAN (100 µg/ml) were selected grown in fresh MB2216 and used to generate frozen stocks. This method was ultimately applied to facilitate efforts to generate labelled bacteria and aid in ease of conjugation when inserting plasmids with fluorescent proteins.

5.5 MINI-PROJECT 4: Transcriptional regulators of ABC transporters in *L. pictus*

5.5.1 INTRODUCTION

Anthropogenically sourced environmental chemicals can mimic hormone activity *in vivo*[35-42]. One famous example of these effects comes from the widespread use of the pesticide atrazine which acts as an endocrine disrupting chemical (EDC) and induces feminization on frogs[43]. Anthropogenic chemicals including EDCs in the environment also have the potential to interact with and disrupt defensive machinery of the cell[44,45]. The "defensome" of the cell is a network of genes that aid in detoxification as well as environmental sensing[46]. This includes efflux pumps from the ATP-binding cassette (ABCs) and solute carrier transporter (SLCs) families, oxidizing enzymes such as cytochrome P450, conjugating enzymes like glutathione, and stress-activated receptors such as nuclear hormone receptors. One example of the interaction between environmental chemicals and protective machinery in the defensome is the halogenated flame retardant PBDE-100 which can directly bind to, and inhibit the function of, ABCB1 (P-gp)[44] which is an important protein involved in xenobiotic efflux and drug disposition.

Nuclear hormone receptors (NHRs) are a group of ligand-regulated transcription factors that influence the expression of diverse genes. NHR ligands include estrogen, progesterone, thyroid hormones, retinoic acid, and others[47,48]. As such, these transcription factors also have the potential to be impacted directly or indirectly by EDCs in the environment. The genes regulated by NHRs are involved in diverse processes from metabolism and reproduction, to development

and the defensome. The downstream targets of NHRs include other protective genes that can also interact with environmental chemicals including EDCs, such as the ATP-binding cassette transporters (ABCs)[49-52].

Given the potential for overlapping influences between environmental chemicals with multiple components of the defensome machinery – specifically NHRs and efflux transporters – we sought to identify potential homologs of NHRs in *L. pictus* as a compliment to the characterizations of ABC and SLC transporters in this species (described in Chapter 3).

5.5.2 RESULTS

Identification of L. pictus NHRs

Leveraging computational tools, 42 candidate genes for NHRs were identified and represent 24 different transcription factors families (Table 5.4). The candidate NHR sequences in *L. pictus* do not include any putative pregnane receptors (PXR), androgen receptors (AR), nor constitutive androstane receptors (CAR) which are well-recognized for their interactions with xenobiotics[53]. However, we were able to identify candidate sequences for other NHRs involved in xenobiotic sensing and responses including the well-studied aryl-hydrocarbon receptor (AhR), peroxisome proliferator-activated receptors (PPAR), and retinoid X receptors (RXR).

The most-likely candidate AhR in *Lytechinus pictus* is a seven exon-long gene (LPI_032614) spanning 1.6 KB of the genome and yields a 749 aa protein. This is shorter in comparison to the human AhR which is 11 exons long spanning ~47.5 KB on chromosome 7, and encodes an 848 aa long protein.

The *L. pictus* PPAR candidate (LPI_034236) is a 6 exon-long gene model that covers a ~5.9 KB region of the genome. The resultant protein is 330 aa long. Again, this is truncated in

comparison to the human PPARα which spans 9 exons over ~93.2 KB of chromosome 22, encoding a 468 aa protein.

The RXR candidate (LPI_036784) in the *L. pictus* genome is 4 exons long spanning a ~34.3 KB region of the genome and producing a 474 aa long protein. In humans, RXRα is 10 exons long and covers ~114 KB region on chromosome 9. The protein encoded is 462 aa long, making it slightly shorter than the urchin homolog we identified.

5.5.3 DISCUSSION AND CONCLUSIONS

Humans, mice, and rats have 48, 49, and 47 NHRs respectively[54], indicating that an expansion of these receptors types occurs in mammals compared to the sea urchin which possess 33 NHRs[55]. The putative annotations presented here represent a relatively permissive estimate of the number and types of nuclear receptors in the *L. pictus* genome. Despite this flexibility in opening up our annotations to include more candidates, the gene repertoire represented here is missing some key players that would normally be expected to play roles in xenobiotic interactions – specifically the PXR, AR, and CAR receptor types. However, the evolution of NHRs across the metazoa includes a number of losses and duplications, so this absence of key mammalian genes is not altogether unsurprising[56].

The lack of key xenobiotic-sensing components that are better studied in mammalian or other vertebrate counterparts opens the question on what the role of NHRs is for invertebrates. The fruit fly (*Drosophila melanogaster)* and the nematode (*Caenorhabditis elegans*) are among the better-studied invertebrate systems for these proteins, however NHRs have also been examined in several marine invertebrates including tunicates[57], molluscs[58,59], and cnidarians[60,61] and echinoderms[46,55]. From this work, NHRs have been implicated in developmental processes such as developmental transitions including metamorphosis, neurogenesis, and skeletogenesis[56].

Despite this emerging evidence, the overall functions of NHRs in marine invertebrates remains relatively understudied. This highlights an open question in the field: what the impacts of exposure to endocrine-disrupting chemicals on environmental sensing and signaling machinery in marine invertebrates and their endocrinology. In fact, there is debate as to whether some chemical exposures would impact these animals at all given their differences in gene repertoire[62]. Expansion of these types of data, coupled with investment in functional studies of NHRs, to remedy this gap in knowledge and resolve debate are essential. This information will help inform on the protection and preservation of marine organisms and their habitats, as well as improve our understanding the fundamental processes that govern environmental sensing and development of divergent species in dynamic environments.

5.5.4 METHODS

Genome mining

To identify putative homologs of known nuclear hormones receptors (NHRs), known sequences from human, and purple sea urchin (*S. purpuratus*) were curated into query lists. Sequences from the query list were used as input for pBLAST searches of the second assembly of the *Lytechinus pictus* genome gene models. We also used the list of queries to mine through the *L. pictus* transcriptome's translated peptides, and mapped transcriptome results to the gene models. Results from the BLAST searches were curated into a hit table, and redundant sequences and low-quality hits were eliminated. Hits were ultimately deemed positive via sequence homology to known NHRs and through structural analysis. The length of the protein encoded by each transcript or gene model as well as the genomic coordinates of the gene models is also included in these tables for all identified *L. pictus* NHR candidates.

Analysis of protein conservation and structure

To help confirm the identity of the putative *L. pictus* NHR candidates identified from the genome and transcriptome mining, we analyzed the amino acid sequences of the deduced protein encoded by our candidate hits. We used protocols that have been previously employed for the characterization of protein structural motifs, such as identification of transmembrane domains (TMHMM and TOPCONS), and other motifs (SMART). Default parameters for all of these programs were selected when performing our analysis.

Sequence similarity

To determine the protein most similar to our candidates identified from the *L. pictus* genome, we performed reciprocal pBLAST searches with each of our candidate sequences as the query against annotated proteins in NCBI and SwisProt databases. We excluded hypothetical and uncharacterized proteins. Reciprocal pBLAST searches through Echinobase against annotated peptides in *S. purpuratus* were also performed using each *L. pictus* candidate NHR transporter sequence as the query.

5.6 ACKNOWLEDGEMENTS

Chapter 5, is unpublished with coauthors. Chang N, Le KP, Nesbit KT and Hamdoun A. The dissertation author will be a co-author of this material.

5.7 REFERENCES

1. Shipp LE, Hill RZ, Moy GW, Gökırmak T, Hamdoun A. ABCC5 is required for cAMP-mediated hindgut invagination in sea urchin embryos. *Development*. 2015;142(20):3537-3548.

2. Bjarnadóttir TK, Gloriam DE, Hellstrand SH, Kristiansson H, Fredriksson R, Schiöth HB. Comprehensive repertoire and phylogenetic analysis of the G protein-coupled receptors in human and mouse. *Genomics*. 2006;88(3):263-273.

3. Materna SC, Berney K, Cameron RA. The S. purpuratus genome: a comparative perspective. *Developmental biology*. 2006;300(1):485-495.

4. Raible F, Tessmar-Raible K, Arboleda E, Kaller T, Bork P, Arendt D, Arnone MI. Opsins and clusters of sensory G-protein-coupled receptors in the sea urchin genome. *Developmental biology*. 2006;300(1):461-475.

5. Chasin M, Rivkin I, Mamrak F, Samaniego S, Hess S. α-and β-adrenergic receptors as mediators of accumulation of cyclic adenosine 3', 5'-monophosphate in specific areas of guinea pig brain. *Journal of Biological Chemistry*. 1971;246(9):3037-3041.

6. Bonnafous J-C, Dornand J, Mani J-C. Hormone-like action of adenosine in mouse thymocytes and splenocytes: Evidence for the existence of membrane adenosine receptors coupled to adenylate cyclase. *FEBS letters*. 1979;107(1):95-99.

7. Perkins JP, Moore MM. Characterization of the adrenergic receptors mediating a rise in cyclic 3', 5'-adenosine monophosphate in rat cerebral cortex. *Journal of Pharmacology and Experimental Therapeutics*. 1973;185(2):371-378.

8. Bennet D, Drury A. Further observations relating to the physiological activity of adenine compounds. *The Journal of physiology*. 1931;72(3):288.

9. Klotz K-N. Adenosine receptors and their ligands. *Naunyn-Schmiedeberg's archives of pharmacology*. 2000;362(4):382-391.

10. Burke R, Angerer L, Elphick M, Humphrey GW, Yaguchi S, Kiyama T, Liang S, Mu X, Agca C, Klein WH, Brandhorst BP. A genomic view of the sea urchin nervous system. *Developmental biology*. 2006;300(1):434-460.

11. Rittiner JE, Korboukh I, Hull-Ryde EA, Jin J, Janzen WP, Frye SV, Zylka MJ. AMP is an adenosine A1 receptor agonist. *Journal of Biological Chemistry*. 2012;287(8):5301-5309.

12. Lohse MJ, Klotz K-N, Schwabe U. Mechanism of A2 adenosine receptor activation. I. Blockade of A2 adenosine receptors by photoaffinity labeling. *Molecular pharmacology*. 1991;39(4):517-523.

13. Zezula J, Freissmuth M. The A2A□adenosine receptor: a GPCR with unique features? *British journal of pharmacology*. 2008;153(S1):S184-S190.

14. Calker Dv, Müller M, Hamprecht B. Adenosine regulates via two different types of receptors, the accumulation of cyclic AMP in cultured brain cells. *Journal of neurochemistry*. 1979;33(5):999-1005.

15. Ransick A, Rast JP, Minokawa T, Calestani C, Davidson EH. New early zygotic regulators expressed in endomesoderm of sea urchin embryos discovered by differential array hybridization. *Developmental biology*. 2002;246(1):132-147.

16. Soede R, Insall RH, Devreotes PN, Schaap P. Extracellular cAMP can restore development in Dictyostelium cells lacking one, but not two subtypes of early cAMP receptors (cARs). Evidence for involvement of cAR1 in aggregative gene expression. *Development*. 1994;120(7):1997-2002.

17. Fasy TM, Inoue A, Johnson EM, Allfrey VG. Phosphorylation of H1 and H5 histones by cyclic AMP-dependent protein kinase reduces DNA binding. *Biochimica et Biophysica Acta (BBA)-Nucleic Acids and Protein Synthesis*. 1979;564(2):322-334.

18. Whitlock J. The conformation of the chromatin core particle is ionic strength-dependent. *Journal of Biological Chemistry*. 1979;254(13):5684-5689.

19. Ullmann A, Joseph E, Danchin A. Cyclic AMP as a modulator of polarity in polycistronic transcriptional units. *Proceedings of the National Academy of Sciences*. 1979;76(7):3194-3197.

20. Chen M-Y, Insall RH, Devreotes PN. Signaling through chemoattractant receptors in Dictyostelium. *Trends in genetics*. 1996;12(2):52-57.

21. Shipp LE, Hamdoun A. ATP□binding cassette (ABC) transporter expression and localization in sea urchin development. *Developmental Dynamics*. 2012;241(6):1111-1124.

22. Chen JH, Luo YJ, Su YH. The dynamic gene expression patterns of transcription factors constituting the sea urchin aboral ectoderm gene regulatory network. *Developmental Dynamics*. 2011;240(1):250-260.

23. Materna SC, Ransick A, Li E, Davidson EH. Diversification of oral and aboral mesodermal regulatory states in pregastrular sea urchin embryos. *Developmental biology*. 2013;375(1):92-104.

24. Hooke R. *Micrographia: or some physiological descriptions of minute bodies made by magnifying glasses, with observations and inquiries thereupon*. Courier Corporation; 2003.

25. Livet J, Weissman TA, Kang H, Draft RW, Lu J, Bennis RA, Sanes JR, Lichtman JW. Transgenic strategies for combinatorial expression of fluorescent proteins in the nervous system. *Nature*. 2007;450(7166):56-62.

26. Hampel S, Chung P, McKellar CE, Hall D, Looger LL, Simpson JH. Drosophila Brainbow: a recombinase-based fluorescence labeling technique to subdivide neural expression patterns. *Nature methods*. 2011;8(3):253-259.

27. Pan YA, Freundlich T, Weissman TA, Schoppik D, Wang XC, Zimmerman S, Ciruna B, Sanes JR, Lichtman JW, Schier AF. Zebrabow: multispectral cell labeling for cell tracing and lineage analysis in zebrafish. *Development*. 2013;140(13):2835-2846.

28. Warner JF, Lord JW, Schreiter SA, Nesbit KT, Hamdoun A, Lyons DC. Chromosomal-level genome assembly of the painted sea urchin Lytechinus pictus, a genetically enabled model system for cell biology and embryonic development. *Genome Biology and Evolution*. 2021.

29. Jinek M, Chylinski K, Fonfara I, Hauer M, Doudna JA, Charpentier E. A programmable dual-RNA–guided DNA endonuclease in adaptive bacterial immunity. *science*. 2012;337(6096):816-821.

30. Campanale JP, Hamdoun A. Programmed reduction of ABC transporter activity in sea urchin germline progenitors. *Development*. 2012;139(4):783-792.

31. Volnoukhin M, Brandhorst BP. Multispectral labeling of embryonic cells with lipophilic carbocyanine dyes. *Molecular reproduction and development*. 2015;82(7-8):619-624.

32. Guerinot M, West P, Lee J, Colwell R. Vibrio diazotrophicus sp. nov., a marine nitrogen-fixing bacterium. *International Journal of Systematic and Evolutionary Microbiology*. 1982;32(3):350-357.

33. Ho EC, Buckley KM, Schrankel CS, Schuh NW, Hibino T, Solek CM, Bae K, Wang G, Rast JP. Perturbation of gut bacteria induces a coordinated cellular immune response in the purple sea urchin larva. *Immunology and cell biology*. 2016;94(9):861-874.

34. Buckley KM, Ho ECH, Hibino T, Schrankel CS, Schuh NW, Wang G, Rast JP. IL17 factors are early regulators in the gut epithelium during inflammatory response to Vibrio in the sea urchin larva. *Elife*. 2017;6:e23481.

35. Colborn T, Vom Saal FS, Soto AM. Developmental effects of endocrine-disrupting chemicals in wildlife and humans. *Environmental health perspectives*. 1993;101(5):378-384.

36. Fowles JR, Fairbrother A, Baecher-Steppan L, Kerkvliet NI. Immunologic and endocrine effects of the flame-retardant pentabromodiphenyl ether (DE-71) in C57BL/6J mice. *Toxicology*. 1994;86(1-2):49-61.

37. Roepke TA, Snyder MJ, Cherr GN. Estradiol and endocrine disrupting compounds adversely affect development of sea urchin embryos at environmentally relevant concentrations. *Aquatic Toxicology*. 2005;71(2):155-173.

38. Tabb MM, Blumberg B. New modes of action for endocrine-disrupting chemicals. *Molecular endocrinology*. 2006;20(3):475-482.

39. Schug TT, Janesick A, Blumberg B, Heindel JJ. Endocrine disrupting chemicals and disease susceptibility. *The Journal of steroid biochemistry and molecular biology*. 2011;127(3-5):204-215.

40. Sifakis S, Androutsopoulos VP, Tsatsakis AM, Spandidos DA. Human exposure to endocrine disrupting chemicals: effects on the male and female reproductive systems. *Environmental toxicology and pharmacology*. 2017;51:56-70.

41. Kahn LG, Philippat C, Nakayama SF, Slama R, Trasande L. Endocrine-disrupting chemicals: Implications for human health. *The Lancet Diabetes & Endocrinology*. 2020;8(8):703-718.

42. Yilmaz B, Terekeci H, Sandal S, Kelestimur F. Endocrine disrupting chemicals: exposure, effects on human health, mechanism of action, models for testing and strategies for prevention. *Reviews in endocrine and metabolic disorders*. 2020;21(1):127-147.

43. Hayes TB, Khoury V, Narayan A, Nazir M, Park A, Brown T, Adame L, Chan E, Buchholz D, Stueve T, Gallipeau S. Atrazine induces complete feminization and chemical castration in male African clawed frogs (Xenopus laevis). *Proceedings of the National Academy of Sciences*. 2010;107(10):4612-4617.

44. Nicklisch SC, Rees SD, McGrath AP, Gökirmak T, Bonito LT, Vermeer LM, Cregger C, Loewen G, Sandin S, Chang G, Hamdoun A. Global marine pollutants inhibit P-glycoprotein: Environmental levels, inhibitory effects, and cocrystal structure. *Science advances*. 2016;2(4):e1600001.

45. Nicklisch SC, Hamdoun A. Disruption of small molecule transporter systems by Transporter□Interfering Chemicals (TICs). *FEBS letters*. 2020;594(23):4158-4185.

46. Goldstone J, Hamdoun A, Cole B, Howard-Ashby M, Nebert DW, Scally M, Dean M, Epel D, Hahn ME, Stegeman JJ. The chemical defensome: environmental sensing and response genes in the Strongylocentrotus purpuratus genome. *Developmental biology*. 2006;300(1):366-384.

47. Sever R, Glass CK. Signaling by nuclear receptors. *Cold Spring Harbor perspectives in biology*. 2013;5(3):a016709.

48. Aranda A, Pascual A. Nuclear hormone receptors and gene expression. *Physiological reviews*. 2001;81(3):1269-1304.

49. Zollner G, Fickert P, Fuchsbichler A, Silbert D, Wagner M, Arbeiter S, Gonzalez FJ, Marschall HU, Zatloukal K, Denk H, Trauner M. Role of nuclear bile acid receptor, FXR, in adaptive ABC transporter regulation by cholic and ursodeoxycholic acid in mouse liver, kidney and intestine. *Journal of hepatology*. 2003;39(4):480-488.

50. Huuskonen J, Vishnu M, Pullinger CR, Fielding PE, Fielding CJ. Regulation of ATP-binding cassette transporter A1 transcription by thyroid hormone receptor. *Biochemistry*. 2004;43(6):1626-1632.

51. Chen T. Overcoming drug resistance by regulating nuclear receptors. *Advanced drug delivery reviews*. 2010;62(13):1257-1264.

52. Rigalli JP, Tocchetti GN, Weiss J. Modulation of ABC transporters by nuclear receptors: Physiological, pathological and pharmacological aspects. *Current medicinal chemistry*. 2019;26(7):1079-1112.

53. Toporova L, Balaguer P. Nuclear receptors are the major targets of endocrine disrupting chemicals. *Molecular and Cellular Endocrinology*. 2020;502:110665.

54. Zhang Z, Burch PE, Cooney AJ, Lanz RB, Pereira FA, Wu J, Gibbs RA, Weinstock G, Wheeler DA. Genomic analysis of the nuclear receptor family: new insights into structure, regulation, and evolution from the rat genome. *Genome research*. 2004;14(4):580-590.

55. Howard-Ashby M, Materna SC, Brown CT, Chen L, Cameron RA, Davidson EH. Gene families encoding transcription factors expressed in early development of Strongylocentrotus purpuratus. *Developmental biology*. 2006;300(1):90-107.

56. Miglioli A, Canesi L, Gomes ID, Schubert M, Dumollard R. Nuclear receptors and development of marine invertebrates. *Genes*. 2021;12(1):83.

57. Gomes ID, Gazo I, Besnardeau L, Hebras C, McDougall A, Dumollard R. Potential roles of nuclear receptors in mediating neurodevelopmental toxicity of known endocrine□ disrupting chemicals in ascidian embryos. *Molecular reproduction and development*. 2019;86(10):1333-1347.

58. Vogeler S, Galloway TS, Lyons BP, Bean TP. The nuclear receptor gene family in the Pacific oyster, Crassostrea gigas, contains a novel subfamily group. *BMC genomics*. 2014;15(1):1-15.

59. Huang W, Xu F, Li J, Li L, Que H, Zhang G. Evolution of a novel nuclear receptor subfamily with emphasis on the member from the Pacific oyster Crassostrea gigas. *Gene*. 2015;567(2):164-172.

60. Fuchs B, Wang W, Graspeuntner S, Li Y, Insua S, Herbst EM, Dirksen P, Böhm AM, Hemmrich G, Sommer F, Domazet-Lošo T. Regulation of polyp-to-jellyfish transition in Aurelia aurita. *Current Biology*. 2014;24(3):263-273.

61. Brekhman V, Malik A, Haas B, Sher N, Lotan T. Transcriptome profiling of the dynamic life cycle of the scypohozoan jellyfish Aurelia aurita. *BMC genomics*. 2015;16(1):1-15.

62. Katsiadaki I. Are marine invertebrates really at risk from endocrine-disrupting chemicals? *Current Opinion in Environmental Science & Health*. 2019;11:37-42.

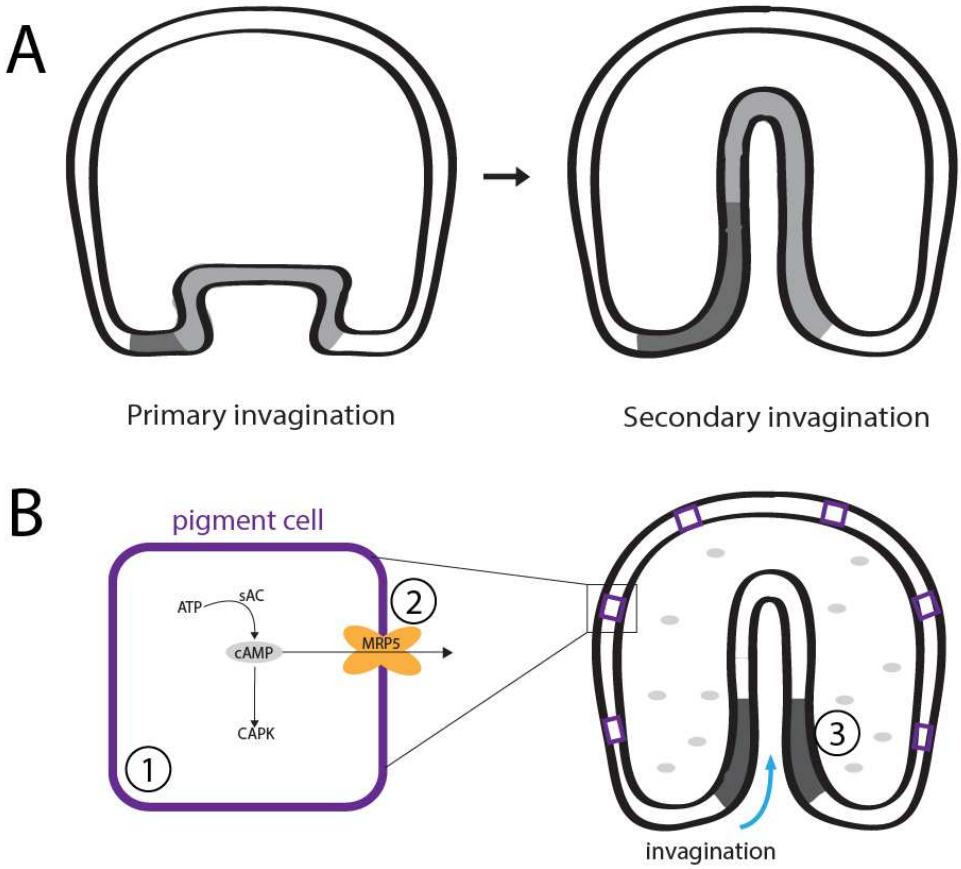

Figure 5.1. Conceptual model of cAMP signaling in sea urchin gastrulation. Adapted from Shipp *et al.* 2015). **A)** Gastrulation occurs in two phases, primary and secondary invagination. **B)** We propose that during secondary invagination, shown above, 1) Pigment cells (purple boxes) embedded into the ectoderm of the embryo generate a cAMP signal via sAC; 2) sAC-derived cAMP is secreted from pigment cells via the ABCC5a transporter into the blastocoel of the embryo; and 3) receptors located on the surface of cells in the hindgut of the embryo (grey shaded region) receive the signal and invagination progresses via a currently unknown mechanism.

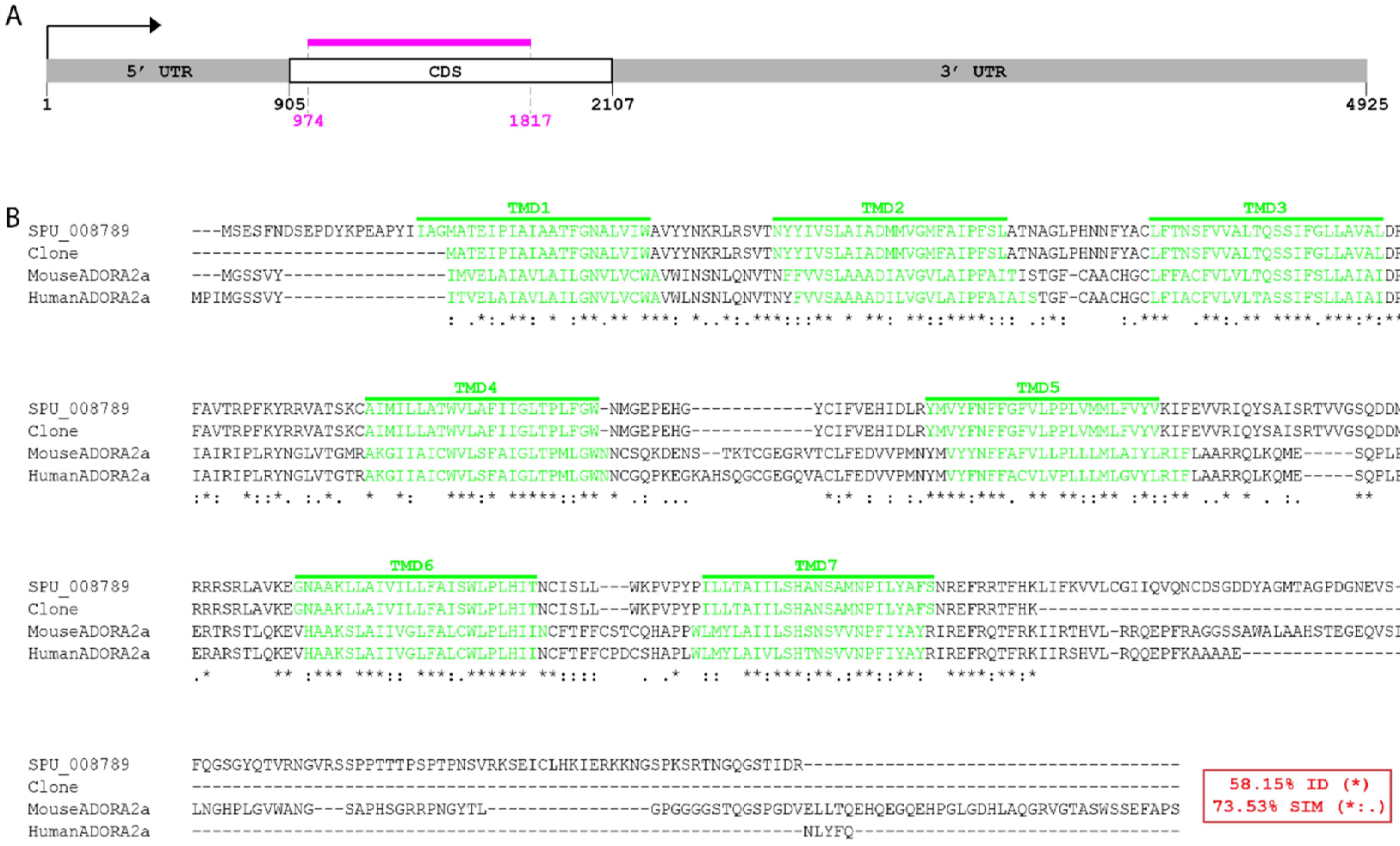

Figure 5.2. Gene structure of sea urchin A2a and alignment with known adenosine receptors. A) Gene structure of SPU_008789, the sea urchin A2a receptor candidate is 1 exon long (4925 bp long). The gene model is located on the + strand. Number indicates the base pair position. The magenta line and corresponding numbers indicate the section in the gene that matches the *in situ* probe for localization. **B)** The sea urchin A2a candidate has seven transmembrane domains (marked in green), a characteristic of GPCRs, that align well with the placement of TMDs (also in green) in known A2a sequences from mammalian models (Mouse: NCBI NP_001318024.1; Human: NCBI 4UHR_A). Identical amino acids are marked with a "*", highly similar residues are marked with ":", and similar residues are marked with ".". The sea urchin candidate has 58.15% identity to the homologous sequences, and 73.53% similarity. Identity and similarity within the identified TMDs are greater than overall peptide sequence homology.

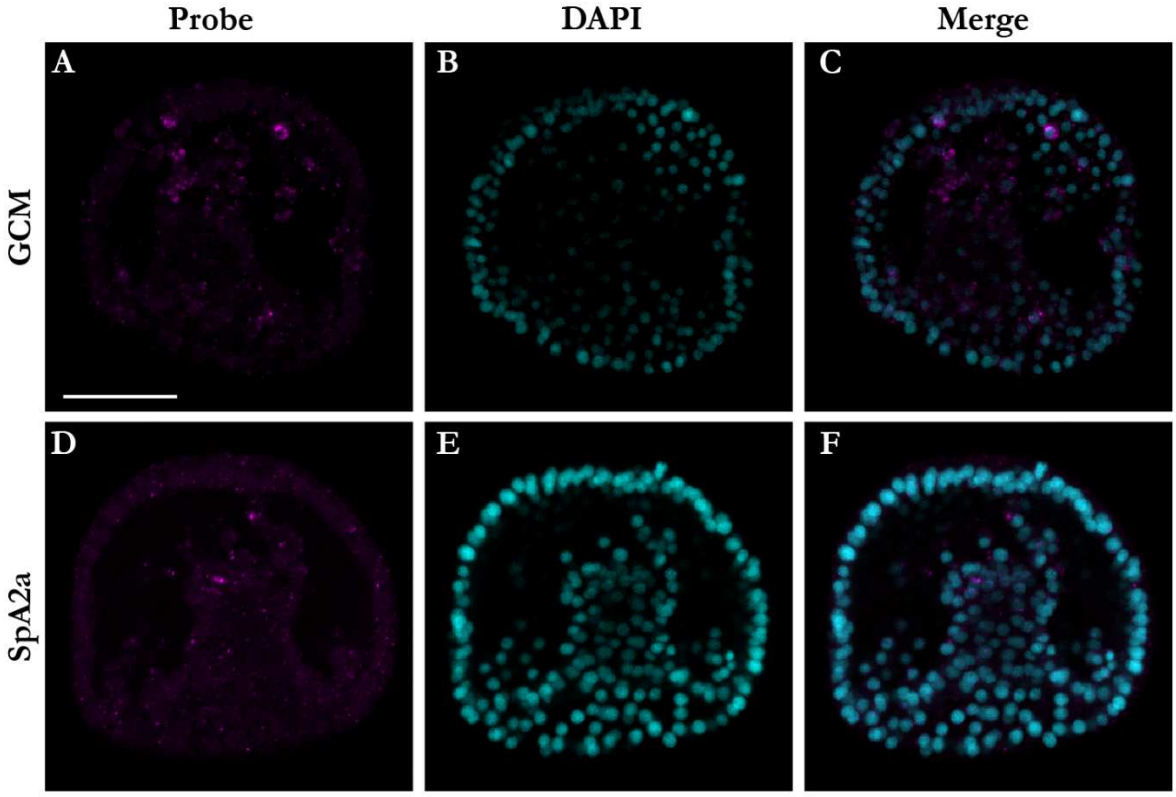

Figure 5.3. Preliminary localization of the sea urchin adenosine receptor. Embryo orientation depicts the vegetal pole pointing down. Scale bar is 50 microns and applies to all panels. **A)** Control embryos at 36 hpf labeled with an antisense probe for *gcm* (which marks SMCs that eventually differentiate into pigment cells). This cell population is labelled at the tip of the archenteron in cells that are migrating through the blastocoel. **B)** Control embryo labelled with the nuclear stain, DAPI. **C)** Merge of the antisense probe and DAPI for control embryo. **D)** An embryo labelled with the antisense probe for sea urchin A2a shows distinct labelling in some cells on the archenteron (bright pink spots) as well as in other portions of the embryo – namely in the ectoderm and some cells that appear to be secondary mesenchymal cells migrating off the tip of the archenteron. **E)** DAPI labelling for the antisense adenosine receptor probe. **F)** Merge of the antisense probe and DAPI for the experimental embryo group.

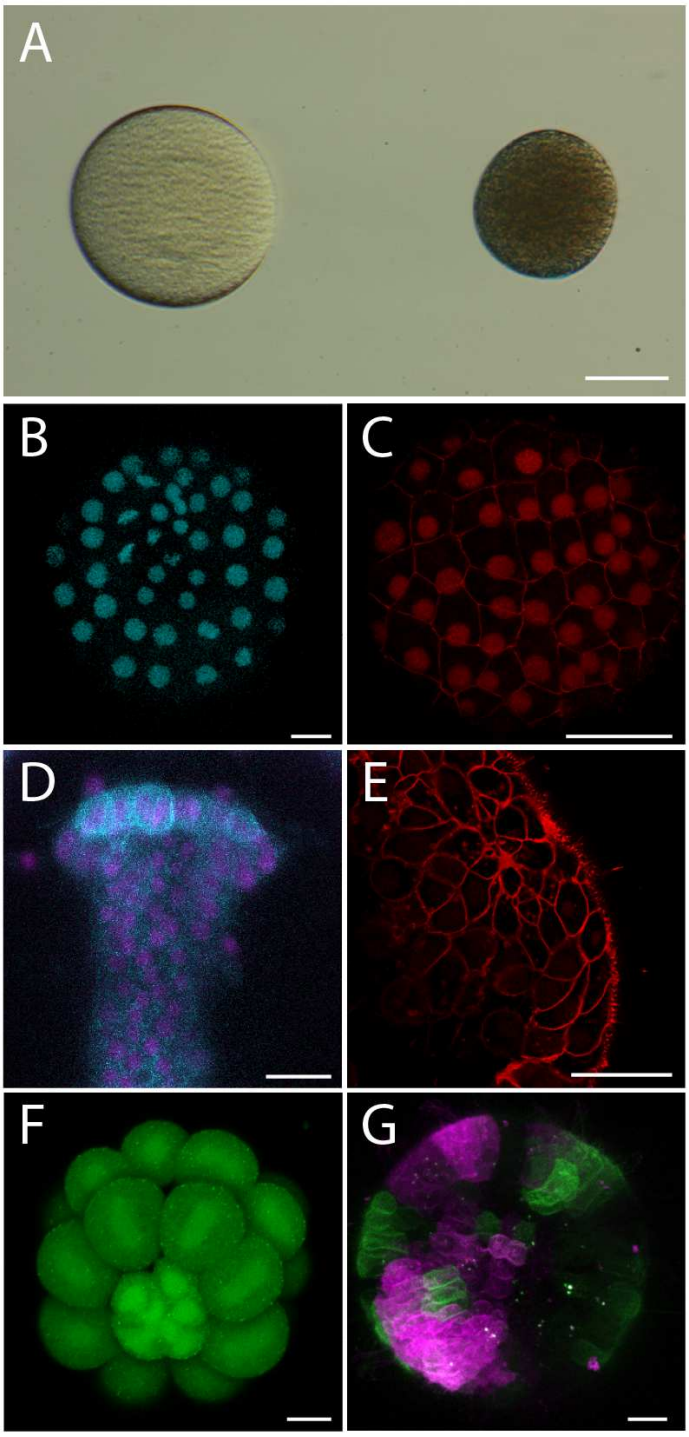

Figure 5.4. Imaging approaches adapted for utilization in *Lytechinus pictus*. Scale bar = 50µm for A and 20µm for B-G. **A)** Oocytes from *L. pictus* (left) and *S. purpuratus* (right) reveal striking differences in egg pigmentation. mRNA overexpression of cellular markers: **B)** Cerulean-H2b (50ng/µl), **C)** RFP-H2b (50ng/µl) and RFP-TJP (100ng/µl); **D)** Citrine-PH Domain (in cyan, 125ng/µl) and RFP-H2b (in magenta, 25ng/µl), and **E)** mCherry-LCK (100ng/µl). In addition to overexpressed mRNAs, small molecules such as **F)** calcein-AM (CAM) (250nM) and lipophilic carbocyanine dyes like **G)** DiI (green, 2µM) and DiO (magenta, 2µM) can be used to label cells. B-G are maximum intensity projections of Z-stacks through the whole embryo (B, F, G), portions of the ectoderm (C, E), or the archenteron (D).

A

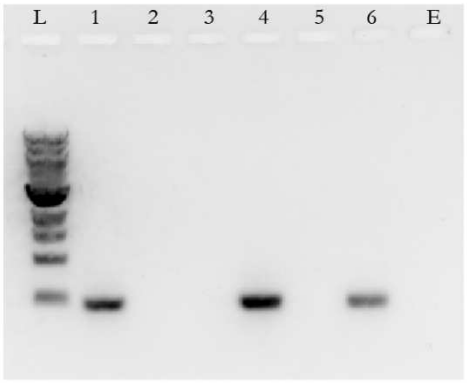

B

Sample	Top Hit Accession No.	E-value
Colony 1	JN964598.1 (*M. musculus*)	2E-06
Colony 4	MF3277707.1 (*V. diazotrophicus*)	0
Colony 6	MK9754859.1 (*V. diazotrophicus*)	0

C

```
Vd_16S    ------ATGCAGCCATGCCGCGTGTGTGAAGAAGGCCTTCGGGTTGTAAAGCACTTTCAG
Colony4   -AGCNNATGCAGCCNTGCCGCGTGTGTG-AGAAGGCCTTCGGGTTGTAAAGCACTTTCAG
Colony6   CAGCNGATGCAGCCNTGCCGCGTGTGTGAAGAAGGCCTTCGGGTTGTAAAGCACTTTCAG
                 ******** ************* ******************************

Vd_16S    TCGTGAGGAAGGTGGTGTTGTTAATAGCACCATCATTTGACGTTAGCGACAGAAGAAGCA
Colony4   TCGTGAGGAAGGTGGTGTTGTTAATAGCACCATCATTTGACGTTAGCGACAGAAGAAGCA
Colony6   TCGTGAGGAAGGTGGTGTTGTTAATAGCANCATCATTTGACGTTAGCGACAGAAGAAGCA
          ****************************** ******************************

Vd_16S    CCGGCTAACTCCGTGCCAGCAGCCGCGGTAATACGGAGGGTGCGAGCGTTAATCGGAATT
Colony4   CCGGCTAACTCCGTGCCAGCAGCCGCGGTAATACGGAGGGTGCGAGCGTTAATCGGAATT
Colony6   CCGGCTAACTCCGTGCCAGCAGCCGCGGTAATACGGAGGGTGCGAGCGTTAATCGGAATT
          ************************************************************

Vd_16S    ACTGGGCGTAAAGCGCATGCAGGTGGTTTGTTAAGTCAGATGTGAAAGCCCGGGGCTCAA
Colony4   ACTGGGCGTAAAGCGCATGCAGGTGGTTTGTTAAGTCAGATGTGAAAGCCCGGGGCTCAA
Colony6   ACTGGGCGTAAAGCGCATGCAGGTGGTTTGTTAAGTCAGATGTGAAAGCCCGGGGCTCAA
          ************************************************************

Vd_16S    CCTCGGAATAGCATTTGAAACTGGCAAGCTAGAGTACTGTAGAGGGGGGTAGAATTTCAG
Colony4   CCTCGGAATAGCATTTGAAACTGGCAAGCTAGAGTACTGTAGAGGGGGGTAGAATTTCAG
Colony6   CCTCGGAATAGCATTTGAAACTGGCAAGCTAGAGTACTGTAGAGGGGGGTAGAATTTCAG
          ************************************************************
```

Figure 5.5. Validation of antibiotic resistant bacteria through 16S sequence amplification. A) PCR amplification of the 16S region of colonies grown on antibiotic plates yielded bands for three colonies. Lane assignments: L - 1KB ladder; 1 - Colony 1; 2 - Colony 2; 3 - Colony 3; 4 - Colony 4; 5 - Colony 5; 6 - Colony 6; E - empty lane. **B)** BLAST of the sequences amplified from colonies with bands showed that sequences from Colony 4 and Colony 6 were likely *Vibrio* with antibiotic resistance. **C)** Alignment of the sequences from Colony 4 and Colony 6 with a references 16S sequence from *Vibrio diazotrophicus* showed that sequences from Colony 4 and 6 were 99.5% and 99% identical respectively to the reference sequencing at this locus. A "*" denotes identical residues, "N" indicates an ambiguous residue from the sequencing.

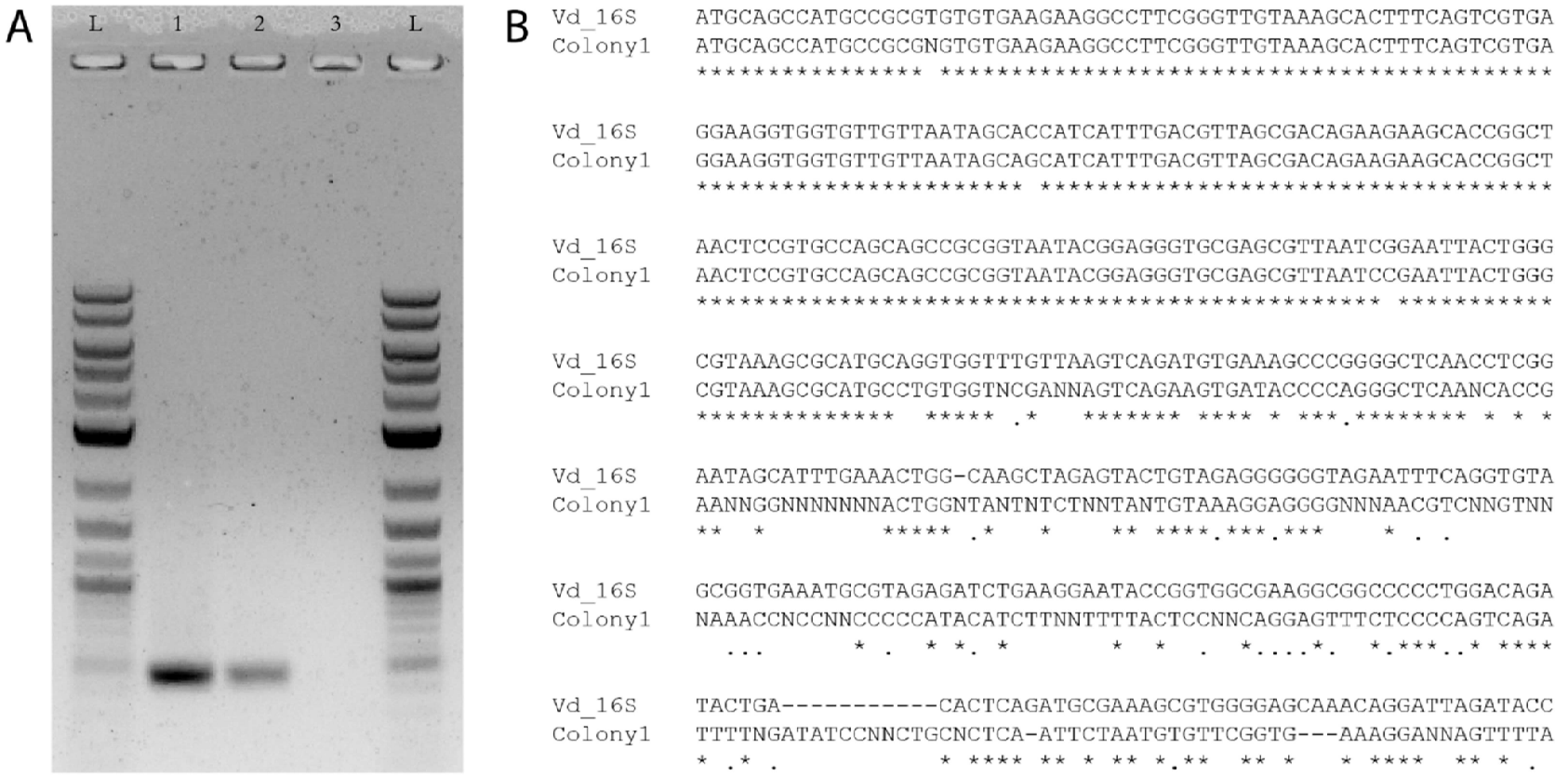

Figure 5.6. Validation of DNA-restriction deficient *Vibrio*. A) A single colony was selected out of screened colonies and used for 16S PCR amplification. Lane Assignments: L – 1KB ladder; 1 – Colony 1 Replicate 1; 2 – Colony 1 Replicate 2; 3 – No template control. **B)** Alignment of the sequence from Colony 1 with a reference 16S sequence from *Vibrio diazotrophicus* shows 72% identity to the reference sequence. A "*" denotes identical residues, "N" indicates an ambiguous residue from the sequencing.

Table 5.1. The candidate ADORA2a receptor in the purple sea urchin *Strongylocentrotus purpuratus*. The top hit (SPU_008789) is the only plausible putative ADORA2a candidate from the reciprocal blast search, and is likely a true A2a full length peptide. Hit numbers listed in order by E-value. Annotation type (M for manual) and the most likely gene and length of the resulting peptide (AA) is listed.

Hit	SPU_ID	E-value	Annotation	(AA)
1	SPU_008789	4e-53	M; GPCR, adenosine	400
2	SPU_028351	5e-27	M; GPCR, dopamine D1	461
3	SPU_009766	3e-26	M; GPCR, histamine H2	413
4	SPU_013107	3e-26	M; GPCR, histamine H2	413
5	SPU_011320	4e-26	M; GPCR, dopamine D1	434

Table 5.2. Expression of the sea urchin adenosine receptor and reference genes. Table is based off the quantitative developmental transcriptome (Echinobase). Numbers are expressed as transcripts per embryo. Colors indicate a range of expression levels from low (tan) to high (dark purple) for a heat-map visualization. Reference genes are *glial cells missing* (*gcm*) and *ABCC5a*. These genes were selected as known pigment cell markers during mid-gastrulation (36 hpf).

Targets		Time (hpf)									
Gene Name	SPU_ID	0	10	18	24	30	40	48	56	64	72
GCM	SPU_006462	2	177	5817	7909	8947	5609	2871	3265	2142	1916
ABCC5a	SPU_023723	3	5	72	551	345	344	179	220	66	81
SpA2a	SPU_008789	14	32	0	55	44	262	292	280	259	296

Table 5.3. Concentration ranges for mRNA overexpression in *Lytechinus pictus* and *Strongylocentrotus purpuratus*. The reduced pigmentation of the oocytes of *L. pictus* enable injection of overexpression markers at lower concentrations (e.g., PH Domain and TJP). Markers with abbreviations listed are: RFP-H2b (red fluorescent protein histone 2b), Citrine-PH Domain (citrine pleckstrin homology domain), Citrine-LCK (citrine lymphocyte tyrosine kinase membrane anchoring domain), mCherry-LCK (mCherry lymphocyte tyrosine kinase membrane anchoring domain), and mCherry-TJP (mCherry tight junction protein).

Marker	Labels	Lp [ng/μl]	Sp [ng/μl]
RFP-H2b	Histone (nuclear)	25-50	25-50
Cerulean H2b	Histone (nuclear)	25-50	25-50
Citrine-LifeAct	Membrane	25-50	25-50
Citrine-PH Domain	Membrane/PGCs	75-125	100-250
Citrine-LCK	Membrane	25-50	25-50
mCherry-LCK	Membrane	25-50	25-50
mCherry-TJP	Tight Junctions	50-100	>500

Table 5.4 Putative nuclear hormone receptor candidates identified in the *Lytechinus pictus* genome.

Lytechinus pictus NHR Candidate Genes											
Subfamily	LPI ID	Length (AA)	NCBI Top Hit	E-value	Identity	Coverage	Echinobase Top Hit	SPU ID	E-value	Identity	Genomic Coordinates
Ahr	LPI_026082	77	Ahr (Rabbit); O02747	4.15E-24	70.30%	83.12%	Sp-Ahr	SPU_005022	1.00E-28	88%	ScPm3Vo_193_HRSCAF_276:36,856,221-36,887,903 (F)
	LPI_026086	1199	Ahr (Beluga); Q95LD9	2.36E-39	41.90%	13.84%	Sp-Ahr_1	SPU_013788	E-109	60%	ScPm3Vo_193_HRSCAF_276:9,804,893-9,816,096 (R)
	LPI_032614	749	Ahr (Rabbit); O02747	1.41E-27	28.30%	34.05%	Sp-Ahrl	SPU_012296	0	83%	ScPm3Vo_1273_HRSCAF_4448:24,038,494-24,040,104 (F)
Couptf	LPI_002603	264	N2F1A / COUPTF1 (Zebrafish); Q06725	1.37E-50	64.40%	51.14%	Sp-Couptf	SPU_023867	7.00E-42	100%	ScPm3Vo_1273_HRSCAF_4448:24,088,187-24,095,325 (R)
	LPI_002604	195	N2F1A / COUPTF1 (Zebrafish); Q06725	1.27E-106	81.90%	94.36%	Sp-Couptf	SPU_023867	5.00E-92	97%	ScPm3Vo_1273_HRSCAF_4448:36,529,485-36,545,611 (R)
E78	LPI_031711	377	---	---	---	---	Sp-E78a	SPU_003548	2.00E-79	93%	ScPm3Vo_247_HRSCAF_834:25,508,976-25,530,110 (F)
	LPI_031038	113	---	---	---	---	Sp-E78b	SPU_018366	2.00E-32	61%	ScPm3Vo_247_HRSCAF_834:25,415,652-25,418,812 (F)
	LPI_031044	368	---	---	---	---	Sp-E78b_1	SPU_001660	3.00E-87	80%	ScPm3Vo_1290_HRSCAF_4503:8,896,915-8,906,601 (R)
NR1H	LPI_020179	348	---	---	---	---	Sp-Nr1h6a	SPU_017404	9.00E-70	47%	ScPm3Vo_1290_HRSCAF_4503:39,468,840-39,486,410 (F)
	LPI_013046	897	NR1H3 / LXR1 (Bovine); Q5E9B6	3.74E-27	44.70%	13.71%	Sp-Nr1h6e	SPU_004526	0	68%	ScPm3Vo_478_HRSCAF_1922:82,430,672-82,457,107 (R)
	LPI_012913	352	NR1H4 / FXR1 (Bovine); Q3SZL0	5.91E-25	37.70%	46.02%	Sp-Nr1h6b	SPU_015456	E-151	88%	ScPm3Vo_473_HRSCAF_1904:22,940,232-22,947,451 (R)
Fax	LPI_044935	82	NR2E1 / TXL (Human); Q9Y466	8.52E-30	67.50%	90.24%	Sp-Fax1	SPU_012586	6.00E-48	100%	ScPm3Vo_215_HRSCAF_529:4,755,265-4,777,793 (R)
Fxr	LPI_047465	382	NR1H3 / LXR1 (Bovine); Q5E9B6	4.17E-86	38.90%	95.03%	Sp-Fxr	SPU_011348	E-137	69%	ScPm3Vo_478_HRSCAF_1922:66,768,654-66,795,843 (F)
	LPI_047466	477	NR1H3 / LXR1 (Bovine); Q5E9B6	1.19E-91	39.50%	82.18%	Sp-Fxr	SPU_011348	E-150	67%	ScPm3Vo_285_HRSCAF_1033:59,972,741-59,974,171 (F)
GCNF	LPI_038339	475	NR6A1 / GCNF (Zebrafish); Q9PU65	2.69E-119	44.60%	85.68%	Sp-Gcnf1_1	SPU_011061	E-146	81%	ScPm3Vo_285_HRSCAF_1033:59,983,395-59,987,054 (F)
GRF	LPI_038349	728	NHR-91 (C. elegans); Q9U2R6	1.47E-53	31.00%	60.30%	Sp-Grf	SPU_013305	0	75%	ScPm3Vo_215_HRSCAF_529:34,967,026-35,021,268 (F)
Hnf	LPI_010951	790	HNF1A / LFB1 (Rat); P15257	5.83E-58	52.80%	19.87%	Sp-Hnf1_1	SPU_010305	E-147	60%	ScPm3Vo_473_HRSCAF_1904:20,583,499-20,623,716 (F)
	LPI_008792	485	NR2A3 / HNF4B (Frog); P79926	2.96E-170	58.60%	82.27%	Sp-Hnf4	SPU_021192	0	88%	ScPm3Vo_473_HRSCAF_1904:21,747,300-21,765,330 (R)
Nr1m	LPI_015577	868	NR1D2 / Rev-erb (Human); Q14995	6.69E-31	34.30%	19.93%	Sp-Nr1m1	SPU_017491	0	82%	ScPm3Vo_473_HRSCAF_1904:10,921,824-10,967,561 (F)
	LPI_010816	564	NR1F4 / HR3 (Fruit fly); P31396	1.28E-41	27.90%	80.85%	Sp-Nr1m2	SPU_011576	0	80%	ScPm3Vo_473_HRSCAF_1904:22,881,671-22,922,126 (F)
	LPI_011744	393	NR1D3 / E75 (Shrimp); O77245	2.90E-57	36.20%	88.55%	Sp-Nr1m3	SPU_013178	0	97%	ScPm3Vo_478_HRSCAF_1922:64,203,106-64,227,826 (R)
	LPI_030696	457	RXR (Snail); Q5I7G2	1.12E-32	30.40%	66.52%	Sp-Nr1m4	SPU_018845	0	70%	ScPm3Vo_1088_HRSCAF_3292:42,364,490-42,380,543 (R)
Nr1x	LPI_015066	609	NR1D3 / E75 (Shrimp); O77245	1.77E-37	56.10%	20.20%	Sp-Nr1x	SPU_028255	0	85%	ScPm3Vo_1088_HRSCAF_3292:22,252,637-22,280,413 (R)
Nr2C	LPI_021709	442	NR2B1 / RXR 1 (Human); P19793	1.75E-52	29.70%	84.84%	Sp-Nr2C	SPU_013134	E-177	69%	ScPm3Vo_1246_HRSCAF_4187:29,182,154-29,196,792 (F)
	LPI_021704	130	NR6A2 / HR4 (Fruit fly); Q15637	2.38E-60	66.20%	100.00%	Sp-Nr2C	SPU_013134	9.00E-37	90%	ScPm3Vo_1246_HRSCAF_4187:29,169,802-29,178,419 (R)
NR2dbd	LPI_013888	988	NR1F4 / HR3 (Fruit fly); P31396	6.08E-28	45.30%	11.84%	Sp-Nr2dbd	SPU_018355	0	55%	ScPm3Vo_1088_HRSCAF_3292:18,813,424-19,056,967 (F)
Nr5a	LPI_015456	226	NR4A4 / HR38 (Silk worm); P49870	2.29E-69	77.80%	59.73%	Sp-Nr5a	SPU_013843	1.00E-88	98%	ScPm3Vo_478_HRSCAF_1922:21,885,540-21,918,797 (R)
	LPI_038338	321	NR5A2 / LHR (Human); O00482	7.33E-97	50.80%	94.70%	Sp-Nr5a	SPU_013843	E-163	87%	ScPm3Vo_193_HRSCAF_276:36,910,621-36,932,730 (F)
Onecut	LPI_028696	462	One cut2 / HNF6 (Human); O95948	1.17E-106	52.30%	81.39%	Sp-Onecut	SPU_016449	0	73%	ScPm3Vo_247_HRSCAF_834:18,745,563-18,776,116 (F)
Pnr	LPI_002360	353	NR2E3 (Human); Q9Y5X4	3.39E-91	49.00%	99.72%	Sp-Pnr	SPU_014405	E-142	74%	ScPm3Vo_1237_HRSCAF_4130:23,375,090-23,380,098 (F)
Ppar	LPI_034236	330	NR1C2 / PPARδ (Mouse); P35396	8.28E-41	52.90%	41.21%	Sp-Ppar1	SPU_019332	E-148	70%	ScPm3Vo_285_HRSCAF_1033:54,444,118-54,450,089 (R)
RAR	LPI_015533	499	NR1B1 / RAR (Newt); P18514	4.27E-81	46.40%	56.91%	Sp-Rar	SPU_016523	1.00E-81	88%	ScPm3Vo_473_HRSCAF_1904:19,908,065-19,913,971 (F)
Reverb	LPI_015576	358	NR1D3 / E75 (Shrimp); O77245	5.06E-71	37.50%	97.21%	Sp-Reverb	SPU_017492	0	95%	ScPm3Vo_215_HRSCAF_529:34,612,388-34,620,726 (R)
RXR	LPI_036784	474	GFI1B (Chick); O42409	4.20E-64	86.50%	23.42%	Sp-Rxr	SPU_028422	0	90%	ScPm3Vo_215_HRSCAF_529:34,691,101-34,725,438 (R)
	LPI_036774	401	RXR (Snail); Q5I7G2	3.74E-137	62.00%	70.82%	Sp-Rxr	SPU_028422	E-104	65%	ScPm3Vo_1245_HRSCAF_4185:25,182,160-25,232,513 (F)
Shr2	LPI_007618	237	SpSHR2 (Purple Urchin); Q26622	3.92E-169	96.60%	100.00%	Sp-Shr2	SPU_008117	E-121	91%	ScPm3Vo_1245_HRSCAF_4185:30,793,498-30,807,166 (F)
Thr	LPI_015490	373	NR1A2 / Thr (Bullfrog); Q02965	7.22E-107	46.10%	91.69%	Sp-Thr_1	SPU_018861	0	90%	ScPm3Vo_1273_HRSCAF_4448:17,415,984-17,432,987 (F)
Tll	LPI_025665	378	NR2E1 / TXL (Human); Q9Y466	2.40E-119	51.40%	88.89%	Sp-Tll	SPU_008936	E-157	80%	ScPm3Vo_215_HRSCAF_529:4,576,705-4,643,556 (R)
Zinc	LPI_014645	703	ZN253 (Human); O75346	5.06E-68	50.70%	30.58%	Sp-Z193	SPU_006637	0	78%	ScPm3Vo_1193_HRSCAF_3749:87,811,488-87,854,398 (F)
	LPI_028939	1315	ZN729 (Human); A6NN14	0	58.10%	77.72%	Sp-Z339	SPU_005035	0	65%	ScPm3Vo_473_HRSCAF_1904:1,984,992-1,999,391 (F)
	LPI_047500	1310	ZNF91 (Human); Q05481	0	56.50%	66.87%	Sp-Z339	SPU_005035	0	60%	ScPm3Vo_1245_HRSCAF_4185:30,417,962-30,432,885 (R)
	LPI_028957	881	PRDM9 (Mouse); Q96EQ9	0	42.80%	74.57%	Sp-Z386	SPU_013902	0	70%	ScPm3Vo_1246_HRSCAF_4187:29,627,600-29,640,873 (R)